DEPARTMENT of OCEANOGRAPHY

SCHOOL of SCIENCE

OREGON STATE UNIVERSITY

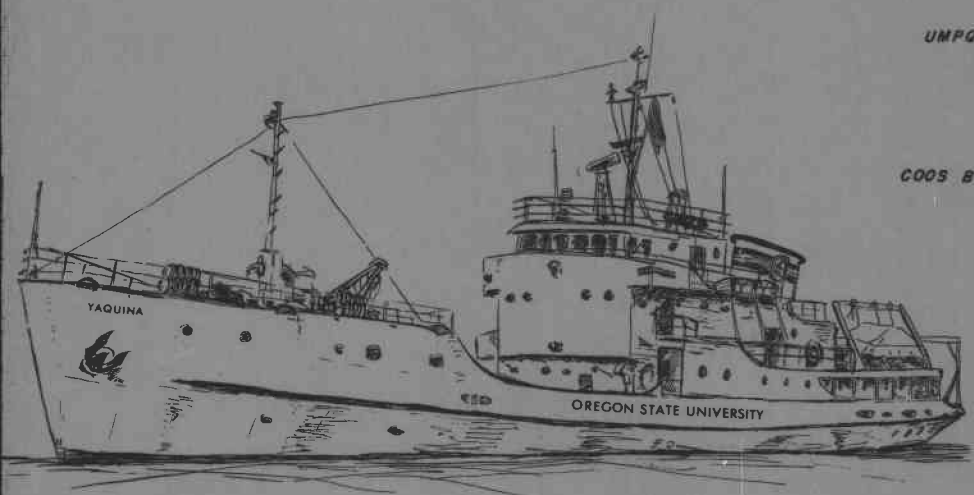

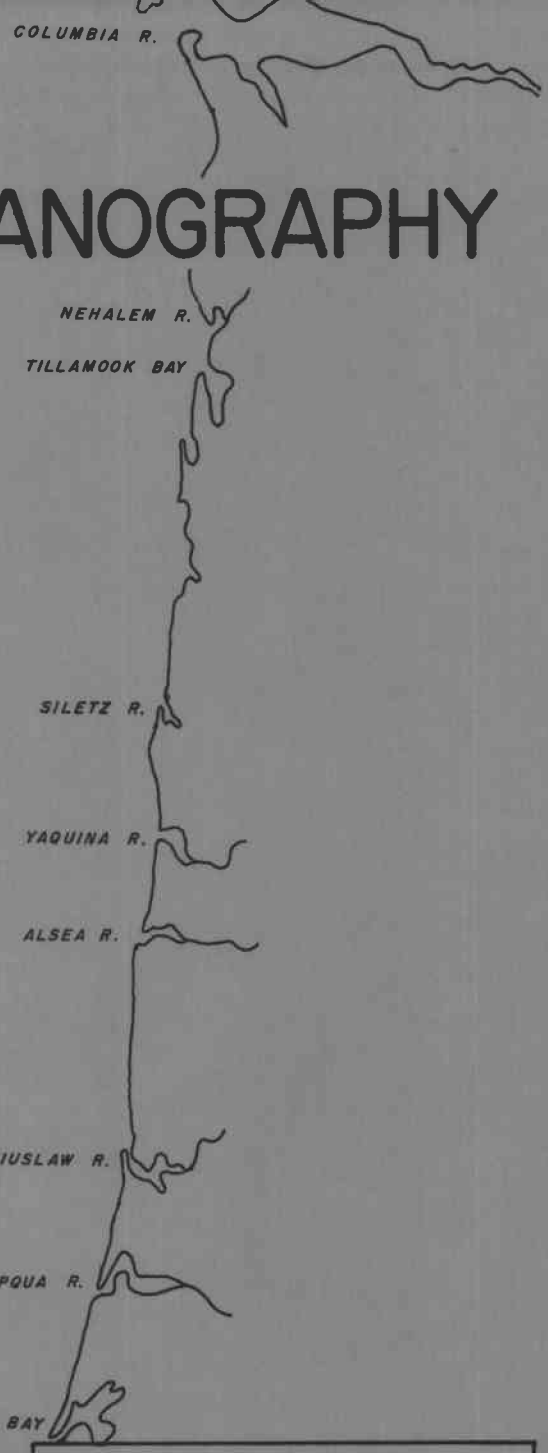

A Compilation of Observations From Moored Current Meters and Thermographs (and of Complementary Oceanographic and Atmospheric Data)

VOLUME II: OREGON CONTINENTAL SHELF, AUGUST-SEPTEMBER 1966

by

C. N. K. Mooers, L. M. Bogert, R. L. Smith, and J. G. Pattullo

National Science Foundation
Grant GA 331

Data Report No. 30 **Reference 68-5**

June 1968

DEPARTMENT OF OCEANOGRAPHY

SCHOOL OF SCIENCE

OREGON STATE UNIVERSITY

Corvallis, Oregon 97331

A COMPILATION OF OBSERVATIONS FROM MOORED CURRENT METERS AND THERMOGRAPHS (AND OF COMPLEMENTARY OCEANOGRAPHIC AND ATMOSPHERIC DATA)

VOLUME II: OREGON CONTINENTAL SHELF, AUGUST - SEPTEMBER 1966

by

C. N. K. Mooers,
L. M. Bogert,
R. L. Smith,
J. G. Pattullo

with the editorial assistance
in preparation of text and figures
of

S. M. Butschun,
D. L. Evans,
M. R. Baldwin,
W. E. Gilbert

Data Report No. 30

National Science Foundation
Grant GA 331

Reference 68-5
June 1968

John V. Byrne
Chairman

TABLE OF CONTENTS

ABSTRACT

A summary of one phase of a direct observational program conducted in the coastal region off Oregon is presented. The measurements were made primarily on the continental shelf in late coastal upwelling season (August and September 1966). The principal measurements were time series of horizontal current velocity and temperature fields; these observations were made with an array of moored, recording meters. Supplementary measurements of hydrographic variables, wind, atmospheric pressure, and mean sea level were also made.

The emphasis of this data report is on the graphical and tabular display of first-order statistics. Limited descriptive remarks are made in order to provide some interpretation for these initial results. More thorough analyses and discussions of the observations are expected to follow from this stage of analysis.

In brief, this set of measurements in the coastal upwelling frontal zone indicates the flow field:

i) is highly variable on the time scale of tidal-like motions to that of motions with several-day periods.

ii) has a southerly mean at a depth of 20 meters (in the "surface layer").

iii) has a northerly mean at a depth of 60 meters (at the base of the "permanent pycnocline").

iv) has a marked response to variations in the wind field on the time scale of several days.

Recommendations regarding future observations and analyses are made.

LIST OF FIGURES

LIST OF TABLES

LIST OF APPENDICES

INTRODUCTION

This is the second data report of a program designed to study physical processes in the Oregon coastal regime by means of moored arrays containing recording instrumentation and by use of complementary hydrographic and atmospheric data. Various first-order statistics and plots of error-corrected and numerically-tapered data are presented for time series of current velocity and of temperature. Supplemental data from hydrographic sections and anchor stations, and from sea level, atmospheric pressure, and wind velocity measurements, are shown. The data were collected in August and September 1966, principally on the Oregon continental shelf.

The data report of the first phase of this program was compiled in a similar format (Collins, Creech, and Pattullo, 1966). A comprehensive summary of the results from the first phase of this program has been given in a Ph. D. thesis by Collins (1968) from which formal papers are being prepared. Some preliminary results of the second phase of this program were described by Mooers and Smith (1967). A pair of papers is in preparation synthesizing some of the measurements and the interpretations of the first two phases (Part I, Collins, Mooers, Stevenson, Smith, and Pattullo; Part II, Mooers, Collins, Smith, and Pattullo).

After sets of data have been acquired, reduced, and processed to the extent that advanced statistical calculations or graphical descriptive discussions can commence, we have found it useful to present some of the data and first-order statistics. The principal objective is to "show the potential" of the data so that we and others will know what has been measured by available instruments, what exists oceanographically to be measured by these instruments, and what future measurements and analyses show appreciable promise. Most of the calculations presented can be considered in the category of "preliminary" or "initial" results; similarly, the descriptive remarks made in the text are limited in depth and scope. The determination of what constitutes an adequate set of presentations in a data report of this nature is a significant problem in itself; comments from the readers will be appreciated. As examples of the variety of approaches recently employed to achieve similar objectives, see Webster and Fofonoff (1967), Davidson and Birchfield (1967), Durham and Reid (1967), and Maloney (1967).

Rather than tabulate our "data bank," we think it is of greater interest to display our data records in graphical and tabular forms of first-order statistics. By pursuing this approach, we can provide feedback for subsequent measurements and calculations rather rapidly--months to years in advance of formal publication of only the principal results. A secondary objective is to indicate the need for "auxiliary data" of good quality by showing the utility of that which has actually been available. Since we think it is important to develop the descriptive art of time series and vertical profile presentation at an intermediate stage, i.e., preliminary to correlation and spectral analyses, we expect to continue to experiment with various graphical and tabular representations in the future, rather than to adhere to a rigid format. In a data report of this nature, it will

be necessary to record some items only once, others on all occasions. By exposing ourselves to internal and external review, we hope to stimulate constructive criticism. We believe it is also true that our work is most useful to a broad audience of oceanographers in this intermediate form; the subsequent, more sophisticated analyses are likely to be chiefly of interest to dynamical or theoretical physical oceanographers.

OBSERVATIONAL PROGRAM

The observational program can be divided into two phases: the moored-meter installations and the hydrographic sampling program. The latter can be further subdivided into two categories: vertical sections (primarily in the onshore-offshore direction) and anchor stations.

The main portion of the moored-meter installation consisted of three vertical strings of sensors, each composed of a current meter pair and a thermograph. One of the three sets was installed at each of the stations designated DB 5, DB 10, and DB 15 (Figures 1 and 2) for a period of 40 days; a fourth set, consisting of a single thermograph, was installed at DB 10B (Figure 2), but failed to function. Table I summarizes several pertinent facts about these installations.

The hydrographic cruises consisted chiefly of standard Nansen bottle and BT casts along tracks normal to the bottom topography off Depoe Bay and off Newport, Oregon; several anchor stations were taken for a lunar day at stations over the continental slope. Figure 2 gives the station locations for the three cruises, and Table II summarizes assorted facts about the cruises and the extent of the discussion of their results in this report. At certain anchor stations (Table II), vertical profiles of horizontal velocity were directly sampled with a Savonius rotor current meter, designated HPCM. On the Depoe Bay line, an effort was made to obtain a high definition of the complex vertical profiles of temperature and salinity by special bottle spacing, by dense station spacing, and by occupying anchor stations. This sampling procedure meant a departure from the Department's "standard" hydrographic sampling program but represented a considerable improvement in definition of coastal hydrographic features. "Real-time" data reduction, analysis, and interpretation were attempted in order to modify sampling procedures as the cruise proceeded and to enhance the educational aspect of each cruise. This effort was largely successful, but required excessive manual effort without an on-board computer.

MOORED-METER INSTALLATION

Array

An instrument string, consisting of recording current meters and thermographs, was installed at several positions (Figures 1 and 2) on the Oregon continental shelf with the following installation scheme. A schematic of a typical taut-wire, instrument string used in the array is given in Figure 3. (For a general discussion of several types of mooring schemes

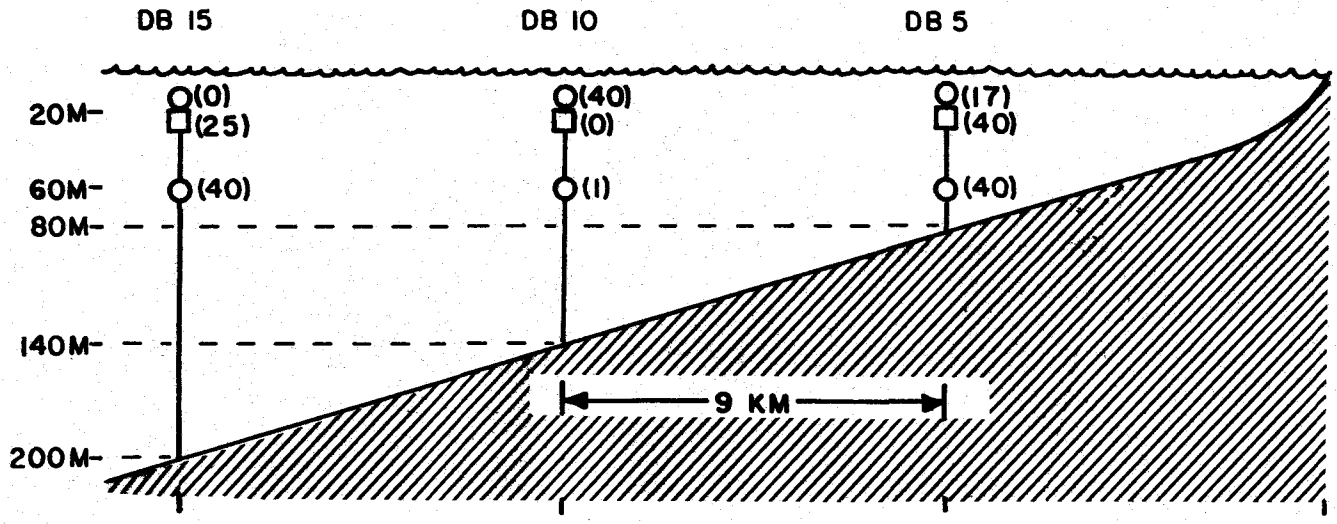

( ) Duration of useful data in days.

O Current meter

□ Thermograph

Figure 1. Vertical Section of Array Configuration and Sample Duration.

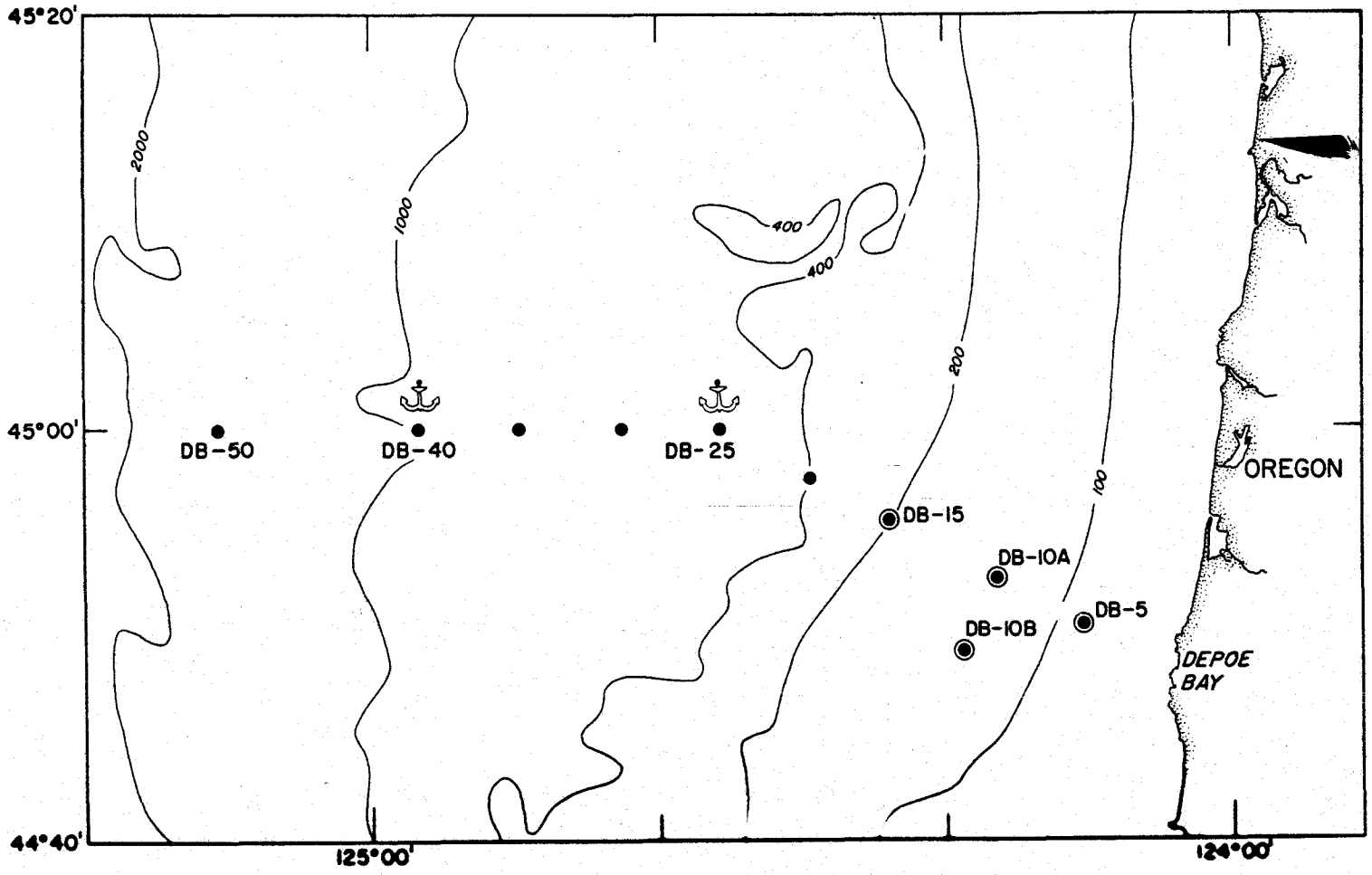

Figure 2. Locations of Array and Hydrographic Stations off Depoe Bay, Oregon, August-September 1966.
Legend: • Hydrographic Station ⚓ Anchor Station
● Instrument Installation DB Depoe Bay
Station numbers are given in nautical miles offshore and depth contours in meters.

TABLE I
ARRAY FACTS

Location	Installation Number	Water Depth (m)	Meter Identification (Serial Number)	Meter Depth (m)	Data Length (days)
DB 5	1	80	BRCM 1 (316-049)	20	17
			BRT 1 (146-087)	20	40
			BRCM 2 (316-054)	60	40
DB 10A	2	140	BRCM 3 (316-055)	20	40
			BRT 2 (146-088)	20	1/4
			BRCM 4 (316-088)	60	1
DB 15	3	200	BRCM 5 (316-089)	20	0
			BRT 3 (146-089)	20	25
			BRCM 6 (316-090)	60	40
DB 10B	4	140	BRT 4 (146-090)	20	0

LEGEND: BRCM - Braincon Current Meter; BRT - Braincon Thermograph
NOTE: % Data Recovery $\frac{(1 + 17 + 4 \times 40)}{10 \times 40} \times 100 = 50.75\%$

TABLE II
CRUISE FACTS

Cruise Designation (Year/Month)	Dates	Track (with Hydrographic and BT Data	Anchor Stations	Remarks
6608-A	15-16 August	DB installation		Discussed
6608-C	26-30 August	DB line		Discussed
6608-C	26-27 August		DB 25 (with HPCM)	Discussed
6608-C	28-29 August		DB 40 (with HPCM)	Discussed
6608-C	1-2 September	NH line		Not discussed
6608-C	30-31 August		NH 65	Discussed
6609-B	23-24 September	DB line and recovery (with HPCM)		Discussed
6609-B	27-28 September		DB 25 (with HPCM)	Discussed
6609-B	24-26 September	NH line		Not discussed

LEGEND: DB- Depoe Bay; NH - Newport; HPCM - Hydroproducts Current Meter Casts

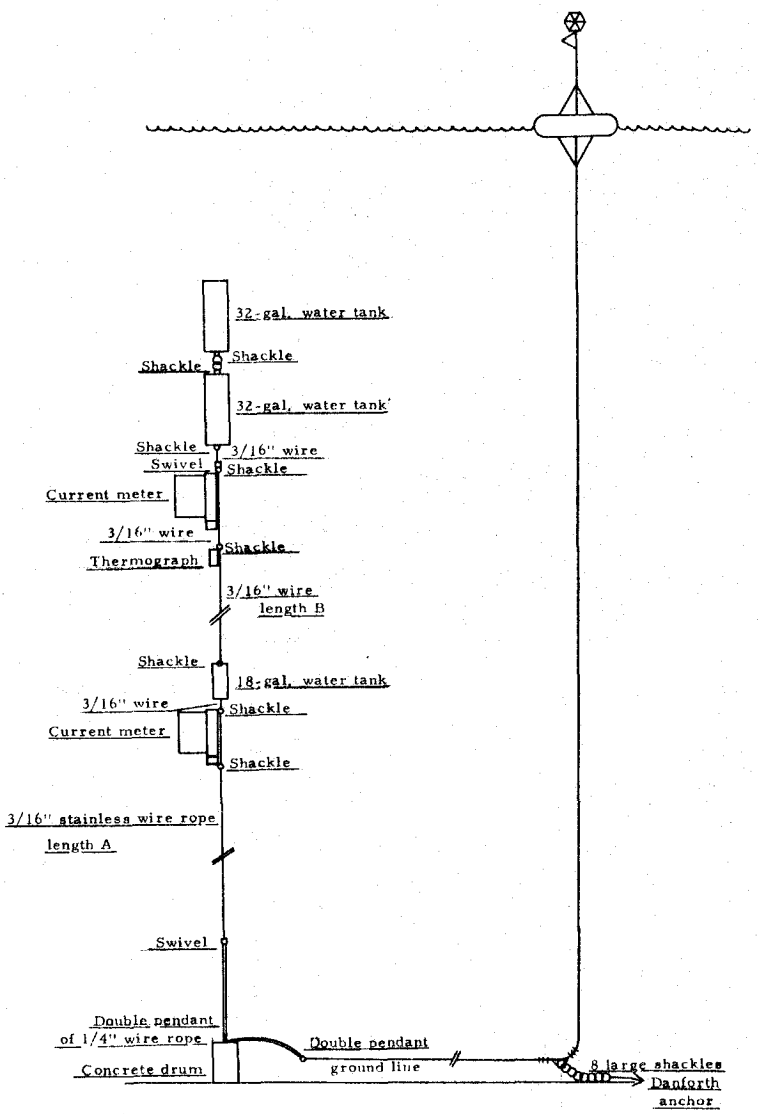

Figure 3. Instrument String Schematic.

and their relative merits, see Daugherty (1966); sensor performance under a variety of environmental conditions is also reported.) Details concerning the hardware are as follows:

Main Anchor--A 55-gallon drum filled with scrap steel and concrete; total weight in air of about 1300 lbs.

Ground Line--1/4-inch 7 x 19 preformed galvanized wire rope; 400-700 meters of wire were laid between the main anchor and the secondary anchor. The secondary anchor was attached to the ground line with 1/4-inch pendants and wire rope clips; the wire from the surface float to the main anchor was continuous.

Secondary Anchor--Seven 35-lb shackles and one 25-lb Danforth anchor.

Surface Float--A toroid, constructed of fiberglas over a urethane foam core; major diameter of 4 feet and minor diameter of 1 foot; this float had a positive flotation of 400 lbs and was equipped with a radar reflector and navigation light.

Subsurface Floats--Two 42-gallon hot water tanks were bridled by means of flat bar cages and pressurized with 50 lbs of air; when submerged, the depth of the top of the subsurface float was 15 meters.

A 3/16-inch 7 x 19 preformed stainless steel wire rope was used in the instrument string per se; components of the instrument string were fastened to it with 7/16-inch galvanized chain safety shackles. Half-inch swivels were used below the subsurface and surface floats and above the main anchor.

The sensors are launched first, and they float on the surface; they are then attached to the main anchor, which is lowered by the ground line. The ground line is payed-out until the secondary anchor and then the surface float are attached and launched. The instrument string is recovered by an operation inverse to the launch operation when the surface float remains attached. When the surface float is missing, a dragging operation is conducted to "snag" the ground line, and the recovery proceeds from there. It was necessary to drag for the gound line at DB15; though the operation was successful, it taxed the depth limits of the feasibility of the dragging procedure.

A linear array of instrument strings was installed on the continental shelf off Depoe Bay, Oregon, near 45° N. The bottom topography in this region is relatively smooth, and it is oriented approximately 020-200° T. Instrument strings were installed at 9-kilometer increments from 9 to 27 kilometers offshore, where the water depths at the installations were 80, 140, and 200 meters, respectively. The array configuration was designed to study internal tides and inertial motions, as well as some of the details of the mean and the time-varying flow at periods greater than a pendulum day (about 17 hours) in the coastal frontal region during the later stages of the nominal upwelling season. (A plan for an early upwelling season installation in 1966 was inhibited by the sudden appearance of a Russian fishing fleet in our coastal waters, whose trawling operations were

considered a potential hazard to our array. That particular experiment was eventually performed in the spring of 1967 and will be the subject of the next data report. The Russians remained in the region during our late summer installation; but, having been notified of our intentions, they did not interfere with our work.) Current meters were set at the base of the surface layer and near the base of the permanent pycnocline, giving a sample at two depths of perhaps a multi-layered or vertically continuous flow regime. A thermograph was set in the lower portion of the thermocline to estimate the vertical scale of motion, e.g., the vertical motion associated with upwelling or internal tides. (We have never set recording meters at depths shallower than 20 meters, hoping to avoid significant mooring motions and direct data contamination from surface waves.) In order to detect the directionality and to test the longcrestedness of the wave-fronts of internal tides and inertial motions, a single thermograph was positioned 9 kilometers to the south of the 18-kilometer offshore station, DB 10B (Figure 2), but that sensor never functioned.

Instruments

Current velocity in the sensor array was measured by Braincon Type 316 Histogram Current Meters (Braincon Corporation, 1965a; Sunblad, 1965). Current observations were made continuously over a 10-minute period and recorded on photographic film; actually, one minute of the sampling period was used for film advance so only nine minutes of data were recorded at the 10-minute sampling rate. Current speed was integrated by the meter over this period (note: it is possible to obtain a 10-minute speed sample by taking the difference between the "arc-value" at the beginning of the speed arc on successive film frames), and current direction was sampled by the meter as a quasi-frequency curve such as to serve as a low quality histogram which is usually sufficient to identify the extremes and the mode of direction. The mode of direction is taken to be the "mean direction." The "mean direction" and the speed are then combined in a polar coordinate format to give the mean velocity in an observational interval, since a true vector mean is impossible to achieve with the present recording procedure. The implicit hypothesis in this procedure is that the combined speed and direction variability was sufficiently small on a time scale less than ten minutes so that the vector formed from separately-determined speed and "mean direction" is not significantly different from the mean vector velocity. This hypothesis can only be tested qualitatively by checking the consistency of the resultant time series pattern of velocity and by examining the statistics of the direction variability. The hypothesis would be untenable if the flow actually had a zero mean velocity on a time scale of the order of ten minutes; because even if the actual current direction was highly variable (in the extreme, uniformly distributed over all values), if the measured speed was significantly large, we would record a non-zero velocity.

The operational characteristics of the Type 316 Histogram current meter are summarized below (see Braincon Corporation, 1965a):

speed sensor: (Savonius rotor)

i) calibration threshold: 2.6 cm/sec (minimum starting velocity is 0.6 cm/sec)

ii) sensitivity: 0.55° of film arc//1 cm/sec for a 10-minute cycle

iii) precision of film readout: ± 2 cm/sec for a 10-minute cycle

iv) accuracy: in excess of readout precision

v) operating range: 2.6 to 260 cm/sec

direction sensor: (3 foot-by-3 foot vane)

i) threshold: ± 5° at 2.6 cm/sec

ii) sensitivity: ± 5° at current speed of 2.6 cm/sec

iii) precision of film readout: ± 3°

iv) accuracy: ± 1°, again in excess of readout precision

v) operating range: 0 to 360° magnetic

Compasses were checked and found to be free from detectable deviation.

The current meter rotors were post-calibrated at the Division Hydraulic Laboratory of the Corps of Engineers, U. S. Army, Bonneville, Oregon. (For a thorough discussion of the calibration facility at Bonneville and of general considerations in current meter calibration, see Johnson (1966).) Revolutions of the rotor were sensed through the current meter's pressure casing by a magnetic reed switch. The resultant pulses were fed into a time-distance recorder provided by the Laboratory. Current speed was observed to be linear with respect to rotor pulses/sec/rev for all of the rotors at current speeds of 6 to 25 cm/sec. As expected from the manufacturer's specifications, a slightly non-linear relationship was observed for current speeds in the range 25 to 40 cm/sec. (This non-linear response is incorporated in our data conversion procedure.) The current speed calibration of our meters is consistent with the manufacturer's calibration curve; the examination of the calibration consistency is the principal purpose of our calibration work at Bonneville. (For more comprehensive analyses of Savonius Rotor performance in general, see Gaul, Snodgrass, and Cretzler (1963), Sexton (1964), and Fofonoff and Ercan (1967).)

Velocity measurements have not been corrected for mooring motions. Motions of the instrument array were minimized by the use of subsurface floats and do not appear to seriously contaminate velocity data: the effects of array motions have been examined by comparing data sampled under different wave and wind conditions and by examining the tilt variations.

In general, tilt was very small; substantiation of this statement is given below.

TILT MAGNITUDE
(Per Cent of Samples)

Meter Identification	Number of Samples	0°	≤ 1°	≤ 3°	≥ 5°	Note: 1° of tilt is equivalent to the horizontal displacement listed below for each sensor (meters)*
BRCM1	5734	6.4	28.3	86.1	4.0	1.0
BRCM2	2078	3.7	46.0	90.6	6.4	0.3
BRCM3	5229	57.7	95.2	100.0	0.0	2.1
BRCM6	5340	12.2	73.3	99.8	0.0	2.4

*The assumption is made that an instrument string tilts as would a rigid body, which we would not expect to be strictly true.

Water temperature was measured by Braincon Type 146 Recording Thermographs (Braincon Corporation, 1965b; Brainard, 1964). These were fitted with -2° C to +25° C thermometers. (The two rapid response thermographs, fitted with +5° C to +15° C thermometers and installed at DB 10A and DB 10B failed to function and are not evaluated here.) The thermometer was placed between a phosphorescent source and photographic film; temperature was recorded as a thick dark line where the mercury did not prevent film exposure. The thermographs were set to advance every ten minutes; our laboratory tests indicate that their 63% response time is about 10 minutes, which checks the manufacturer's specifications. Thermometer readout accuracy is ± 0.1C° (Brainard, 1964). Thermograph calibration tests were conducted in a constant temperature bath which was cycled through temperature variations as a consistency check. The absolute temperature values checked within the limits of the resolution of the readout.

Numerous tests have been run in the laboratory on the stability of the clocks which govern the film advance mechanisms. Pre- and post-installation laboratory tests were run to establish clock-error estimates. For sensors which ran throughout the installation period, or those current meters which had Timex watches photographed on each frame, logbook entries for installation and recovery times could be compared with film frame counts to further check clock-error. The results of these tests are tabulated below for those sensors which ran usefully long:

Meter Identification	Lab Pre-test (sec/day)	Lab Post-test (sec/day)	Actual Frame Count vs Equivalent Frames ("Time in Place")
BRT 1	+6	0	5627 vs 5629
BRT 3	no data	0	indeterminate*
BRCM 1	-7	no data	indeterminate
BRCM 2	-22	no data	indeterminate
BRCM 3	+30	no data	indeterminate
BRCM 6#	+2	no data	5734 vs 5730

*Indeterminate means sensor was not operating upon recovery.

#Only Timex which was readable on each frame; though the watch gained 20 minutes over the duration of the installation, it was quite useful in the data reduction phase, especially for "starting" the film readout and for verifying the frame count; the other five Timex watches ran from 2 to 30 minutes fast.

In summary, the greatest clock-error is of the order of plus 30 sec/day, or 2 frames in 40 days, i. e. clock stability was approximately 1 part in 3,000. Instrument depths are referenced to mean sea level and are accurate to ± 1 meter, as determined by wire lengths and water depth from fathometer records and charted depths. One limitation in positional accuracy is imposed by the nature of our installation procedure: the launch is made with reference to the main anchor, but the recovery is made with reference to the surface float. Consequently, it is difficult to determine whether or not the main anchor has dragged. Our navigational data suggest an upper bound of about one kilometer of drag to the south.

Despite their simple modular construction and our systematic checkout procedures, these instruments continue to require considerable care and preparation if they are to record worthwhile data; the instrument recovery rate (100%) has been superb, but the data recovery rate (51% for this installation) has been disappointingly low.

HYDROGRAPHIC SAMPLING PROGRAM

The hydrographic sampling program was essentially split into two sections: the Newport and the Depoe Bay hydrographic lines. The Newport line is sampled routinely by OSU: this line has ten-mile* station spacing inshore of 45 miles, and twenty-mile station spacing between 45 and 165 miles offshore, and Nansen bottles are set at "standard depths." The only modifications of the Newport line, in late Sugust, consisted of taking near-bottom samples at NH 65, of occupying an anchor station at NH 65 and of obtaining a deeper-than- ordinary sample at NH 47 rather than sampling at the usual, relatively shallow NH 45. Additional samples were taken inshore of NH 5, which had been the usual inshore terminus.

---

* We have attempted to use metric units throughout this data report, but the hydrographic stations are layed-out and designated in units of nautical miles.

On the Depoe Bay line, samples were taken generally at five-mile increments but no further than 50 miles offshore on three cruises. One set of samples commenced at 1 mile offshore; the other sets commenced at 5 miles offshore. Anchor stations were also occupied at DB 25 (in both late August and September) and DB 40 (only in late August). Special bottle spacing was employed on the Depoe Bay line in order to more precisely define the depth zone of a commonly occurring temperature inversion. Bottles were generally spaced at five-meter vertical increments in the depth zone of the temperature inversion as the supply of bottles permitted. The maximum depth of casts was limited to 300 meters.

Table II lists the hydrographic stations occupied on each cruise. The data will be reported in the OSU Department of Oceanography's hydrographic data series, but selected plots of the data for the Depoe Bay line and the anchor stations have been included here. Since much of our thinking is based on the assumption that the hydrographic fields are essentially uniform in the alongshore direction, the only available alongshore BT section during this period of time is also presented (Figure 15).

A summary of available data records and details of recording meter data records are given in Table III.

DATA PROCESSING AND PRESENTATION

Time Series Data

For the recording sensors, the data processing operation is divided into several steps:

i) photographic film development (performed commercially)

ii) film reading and data entry into a data log book (performed by project personnel, with support from the OSU Work-Study Program; see Acknowledgments)

iii) data punching and verification (performed both by OSU Computer Center key punch personnel and by project personnel)

iv) data editing (performed by initial visual checks and then computerized error detection (Appendix II), followed by visual verification and correction of indicated errors with reference to data log books and/or film)

v) data conversion (performed by computer program (Appendix I) in order to convert from mechanical to oceanographic units, from polar to cartesian coordinates, etc.)

vi) time series data plots (performed by computer programs, either a time series of a scalar variable or a progressive vector diagram (PVD) for horizontal velocity)

vii) data histograms (computer-program-calculated(Appendix I) but hand-plotted)

TABLE III

SUMMARY OF AVAILABLE DATA RECORDS

A. Available Data Records

Data Series	Sampling Interval	Data on Cards/Tape # Data Points	Start Time/Date	Stop Time/Date	Low-passed Data # Data Points	Start Time/Date	Stop Time/Date	Hourly Averages Start Time/Date	Stop Time/Date
Recording Meter Data									
BRT 1	10 Min	5628	1230//8/15	1520//9/23	816	0100//8/16	0100//9/21	1300//8/15	1400//9/23
BRT 3*	10 Min	2894	1800//8/15	2010//9/4	360	0600//8/18	0600//9/2	1800//8/15	1000//9/8
BRCM 1	10 Min	2078	1230//8/15	2240//8/29	204	1030//8/18	2230//8/26	1300//8/15	2100//8/29
BRCM 2	10 Min	5229	1240//8/15	2000//9/20	726	1040//8/18	1040//9/17	1300//8/15	1900//9/20
BRCM 3	10 Min	5337	1430//8/15	1550//9/21	744	1230//8/18	1230//9/18	1500//8/15	1500//9/21
BRCM 6	10 Min	5734	1810//8/15	1340//9/24	810	1610//8/18	1010//9/21	0000//8/16	1200//9/24

*Due to erratic film advance, questionable data begins at 2010//9/4 and ends at 1810//9/7 and is not used in the main.

Complementary Data									
Atmospheric pressure	1 Hour	1464	0000//8/1	2300//9/30	1344	1200//8/3	1200//9/28		
Sea Level**	1 Hour	900	1200//8/24	2300//9/30	786	1200//8/27	1200//9/28		
Bluewater Winds	1 Hour	1464	0000//8/1	2300//9/30	---	-----	-----		
Geostrophic Winds	6 Hours	241	0000//8/1	2300//9/30	---	----	-----		

** Gaps occurred in sea level record for: 0130//9/15-1100//9/15, 1500//9/16-0100//9/17, and 1500//9/17-1030//9/19. The gaps were filled by fitting predictions from tide tables to contiguous data and testing by error detection procedures until anomalous behavior of the data was reduced to an acceptable level.

B. Details of Recording Meter Data Records

Meter Identification	Time In Water	Time Out Water	Maximum Possible Frames	Estimate of Maximum Frame Error due to Clock Error (No. of Frames)	Time Main Anchor on Bottom	Time Array Broke Surface	Maximum Expected # of Usable Frames	Actual Usable Frame Count
BRT 1	1205//8/15	1536//9/23	5633	+0	1234//8/15	1525//9/23	5629	5627*
BRT 3	1713//8/15	1345//9/24	5738	0	1810//8/15	1317//9/24	5730	2894*
BRCM 1	1205//8/15	1536//9/23	5633	-0	1234//8/15	1525//9/23	5629	2078
BRCM 2	1218//8/15	1530//9/23	5630	-2	1234//8/15	1525//9/23	5629	5229
BRCM 3	1345//8/15	1734//9/23	5683	+2	1433//8/15	1724//9/23	5677	5337
BRCM 6	1716//8/15	1343//9/24	5738	+0	1810//8/15	1317//9/24	5730	5734#

* Total good data, i.e., prior to detectable, erratic film advance.

** Only meters running upon recovery; frame count discrepancy may in part be attributed to the total time taken for the meter to "settle down" upon installation and to be retrieved "after unsettling" upon recovery; from logbook entries, the best estimate is a total of 40 minutes (4 frames) in the case of BRT 1 and 80 minutes (8 frames) in the case of BRCM 6.

viii) other first-order statistics (by computer, Appendix I)

ix) weighted averages, i. e., numerical tapering (or filtering) of data (by computer, Appendix III).

In brief, the data processing phase consists of data reduction and first-order analyses designed to detect errors and to examine basic statistical-oceanographic features of the data. At the completion of this phase of the analysis, a data report can be prepared and higher-order time series analyses can commence.

In presenting the moored-meter data, we have followed the format used by Webster and Fofonoff (1965) as closely as feasible. Data are presented as follows:

i) Progressive vector diagrams (PVD's) (see Webster (1964) and definition below*)

ii) Current velocity time series

a) Histograms of speed, direction, U and V, and direction variability

b) Plots of smoothed, i. e., "low-passed," velocity components versus time

c) Daily kinetic energy

iii) Temperature time series

a) Histograms of temperature

b) Plots of smoothed, i. e., "low-passed," temperature versus time

c) One-half of daily-variances

iv) Histograms of meter tilt magnitude and direction.

Speed histograms give relative frequency for successive 2 cm/sec intervals; velocity component histograms are constructed for successive intervals of 5 cm/sec. Direction histograms are incremented in ten-degree intervals. Because reading bias distorted temperature histograms by

---

* A progressive vector diagram is simply a graphical vector addition of successive velocity vectors measured at a single spatial point in the Eulerian sense. It is not to be interpreted in the Lagrangian sense, i. e., it does not represent the trajectory of a water parcel. With a modicum of thought, many qualitative and quantitative results can be extracted from such diagrams.

favoring even-and half-degree values, the following averaging scheme has been used: 5.9°, 6.0°, and 6.1° constitute one class; 6.2° and 6.3°, the second class; 6.4°, 6.5°, and 6.6°, the third class; 6.7° and 6.8°, the fourth class; etc.

The available sea level, atmospheric pressure, geostrophic wind, and directly-measured wind data have been processed and presented in a similar manner.

Hydrographic Data

The hydrographic data processing has been by standard means. The OSU hydrographic group computer-edited and processed the data. Because we had intentionally used special bottle spacing for much of our work, we chose to work with data at observed depths. All vertical space and time sections have been plotted from smoothed vertical profiles of edited data at observed depths rather than by direct interpolation of data fields. The bulk of the effort has been invested in graphical representation of the scalar vertical profiles, vertical time and space sections, and T-S diagrams, and then in testing them for consistency. Some of the first-order statistics for the hydrographic data are presented. For the vector field of the vertical profiles of current velocity, first-order statistics on both the vertical profile and the individual time series at fixed depths have been computed. Only selected portions of this work are presented in this data report.

Since hydrographic samples were taken to complement the recording current meter and thermograph measurements, certain material has been chosen for explicit display in this data report in order to give our estimate of the hydrographic environment at the sensor array. An attempt at extensive oceanographic interpretation of the combined hydrographic and flow fields would be premature and inappropriate for a data report. As a consequence, the remarks will be confined to the identification of the key features in each figure.

DISCUSSION OF DATA PRESENTED

Hydrographic Data

Certain portions of the hydrographic data have been tabulated and plotted to convey some idea of the "hydrographic setting" of our time series measurements; only the data which appear in the plots have been tabulated. (For general background on the hydrography of the coastal upwelling region, see Collins, 1964.)

Table IV lists the sigma-t data at observed depths for the Depoe Bay hydrographic line (see Figure 2) for 26-29 August and 23-27 September 1966. These data were used for the construction of the vertical sections of sigma-t shown in Figures 4 and 5; the sections extend from the surface to a depth of 150 meters. The locations of the recording meters are indicated on the figures. The current meters and the thermographs located at a depth of 20 meters were situated near the 25.0 isopycnal and at the base of the near-surface or seasonal pycnocline (governed principally by the thermocline and secondarily by a halocline). The current meters at a depth of 60 meters were

TABLE IV

SIGMA-t DATA, DEPOE BAY LINE

(Date: 26-29 August 1966)

Depth(m)	DB 5	DB 10A	DB 15	DB 20	DB 25-1	DB 30	DB 35	DB 40-1	DB 50
0	24.98	24.10	23.74	23.73	23.65	23.58	23.62	23.44	23.24
10	25.08	24.38	23.93	23.74	24.41	24.36	23.87	24.03	23.51
20	25.69	25.33	25.25	25.15	25.16	25.23	24.77	23.93	24.28
30	25.96	25.49	25.42	25.34	25.30	25.36	25.04	25.22	24.89
50	26.19	25.84	25.74	25.60	25.47	25.55	25.37	25.47	25.35
75		26.25	26.15	25.99	25.80	25.93	25.90	25.93	25.77
100		26.42	26.33	26.28	26.18	26.24	26.28	26.21	26.18
150			26.56	26.54	26.53	26.53	26.55	26.52	26.45
200				26.64	26.65	26.63	26.66	26.65	26.60
250				26.72	26.74	26.71	26.72	26.71	26.70
300				26.77	26.79	26.76	26.76	26.76	26.76
Date	26	26	27	27	27	28	28	28	29
Time	2155	2330	0121	0423	0624	0800	0933	1250	1537

(Date: 23-27 September 1966)

Depth(m)	DB 5	DB 10A	DB 15	DB 20	DB 25-1	DB 30
0	24.36	23.70	23.67	23.55	23.42	23.55
10	24.41	24.68	23.69	23.55	23.51	23.55
20	25.07	25.32	24.89	24.82	23.59	24.69
30	25.78	25.56	25.29	25.28	24.85	25.11
50	26.14	25.94	25.45	25.53	25.38	25.39
75		26.25	26.03	25.93	25.72	26.82
100		26.41	26.25	26.30	26.26	26.23
150				26.52	26.50	26.48
200				26.57	26.54	26.60
250				26.62	26.61	26.68
300				26.68	26.70	26.75
Date	23	23	24	24	27	24
Time	2255	0627	0820	1022	0635	1242

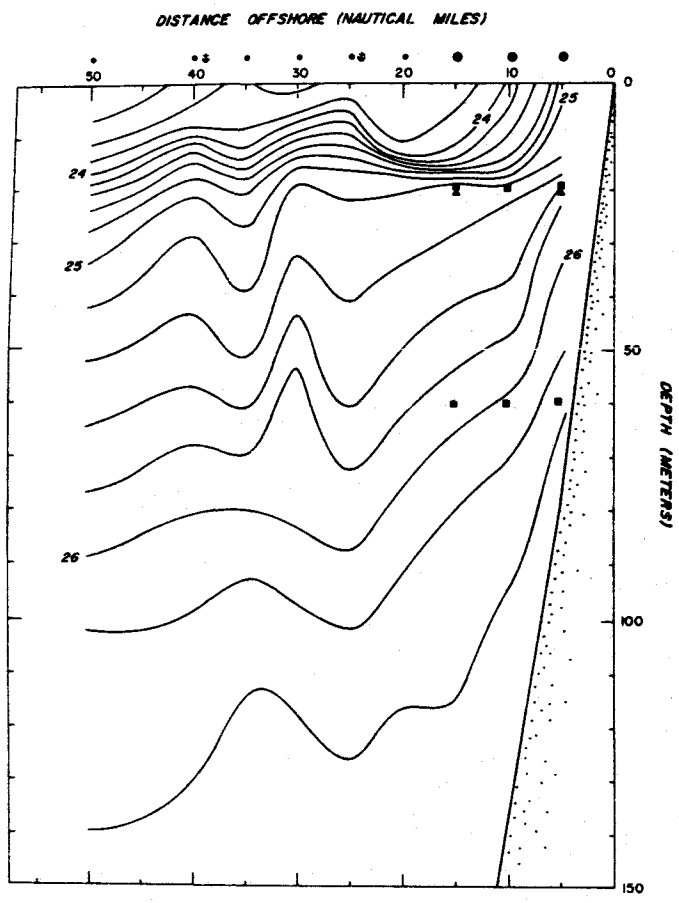

Figure 4. August 1966.

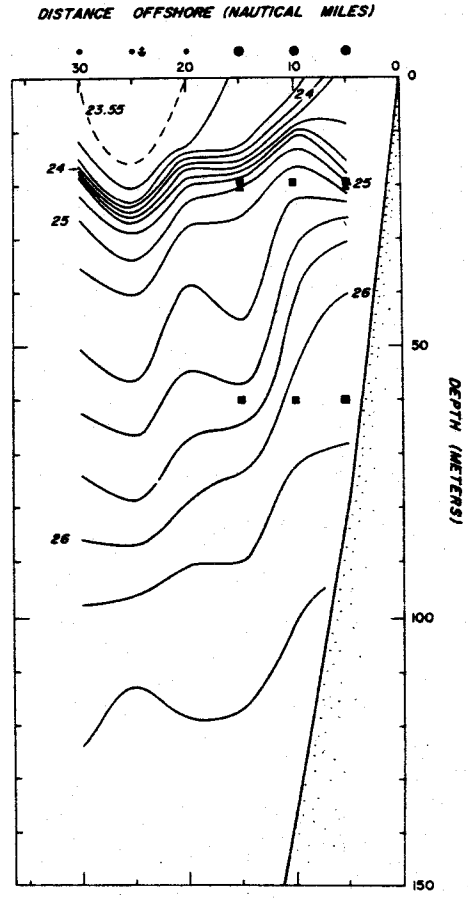

Figure 5. September 1966.

Vertical Sigma-t Sections (Depoe Bay Line)

▪ Current Meter
▲ Thermograph
• Hydrographic Station
● Instrument Installation
•⚓ Anchor Station

situated near the 26.0 isopycnal. The meter locations relative to the basic hydrography were similar in both August and September. Those at 20 meters we consider to be in the "surface layer," with the thermograph just above the base of the thermocline, and those at 60 meters to be at the base of the permanent pycnocline (governed by a halocline).

The permanent pycnocline is deeper at the anchor station DB 25 than at the array, and the seasonal pycnocline is deeper there only in the September vertical section; these facts are important in comparing velocities determined at the anchor station vis-a-vis those measured at the sensor sites.

The vertical density structure has several characteristic features:

i) The permanent pycnocline rises from 40 to 100 meters at 45 kilometers offshore to 20 to 60 meters at 10 kilometers offshore; this inshore rise of the permanent pycnocline is a key indication of coastal upwelling.

ii) The near-surface, seasonal pycnocline tends to break the surface at 10 to 20 kilometers offshore, rising from a depth of 10 to 20 meters at 30 kilometers offshore; in September, the seasonal pycnocline "splits" inshore, with downwarping in its lower half indicative of strong mixing.

iii) There are 10- to 20-meter vertical "kinks" in the permanent pycnocline centered about 35 to 50 kilometers offshore; they may be manifestations of standing or progressive internal waves, or their associated downwarping may be a geostrophic indication of northward flow in the "lower layer."

iv) The low values of sigma-t visible in the upper 10 meters offshore are probably associated with the Columbia River plume.

Table V lists the mean and the standard deviation of the temperature, salinity, and sigma-t data at the August and September DB 25 anchor stations and at the August DB 40 and NH 65 anchor stations, which were each occupied for a lunar day. Figures 6 and 7 were plotted from Table V. No attempt has been made to remove temporal variability from Figures 4 and 5, such as that due to the internal tides, though Figures 6 and 7 give an indication of such variability at the anchor station DB 25. (To estimate the standard error of the mean profile, divide the standard deviation by the square root of the sample size given in Table V.) The temperature profiles are remarkably similar in August and September, especially the depth and the temperature maxima and minima of the temperature inversion; the greatest differences are in the warming of both the surface and the lower layer between late August and late September. The average salinity and density profiles are also very similar in kind, though the September profiles show more variability. The surface sigma-t decreased from late August to late September by 0.3 of a sigma-t unit due to surface warming (+1.7C°) and freshening (-0.09‰).

Figures 8, 9, and 10 display the temperature, salinity, and density vertical profiles, respectively, sampled adjacent to the sensor arrays upon array installation, midway in the sampling period, and upon array recovery; they are based on the data listed in Table VI. A temperature inversion generally appeared beneath the surface thermocline and the depth of the

TABLE V

TEMPERATURE, SALINITY, AND SIGMA-T MEANS AND

STANDARD DEVIATIONS AT ANCHOR STATIONS

Anchor Station DB-25

(no. casts=14) (Date: 27-28 August 1966)

Depth (m)	TEMPERATURE (°C) mean	std. dev.	SALINITY (o/oo) mean	std. dev.	SIGMA-t mean	std. dev.
0	14.52	0.38	31.94	0.07	23.74	0.08
10	11.93	1.11	32.17	0.26	24.42	0.34
20	9.30	0.32	32.44	0.02	25.09	0.06
30	8.45	0.19	32.49	0.02	25.26	0.04
40	7.86	0.10	32.55	0.03	25.40	0.04
50	7.64	0.04	32.67	0.05	25.52	0.04
60	7.58	0.02	32.83	0.05	25.65	0.04
70	7.62	0.05	33.05	0.05	25.82	0.04
80	7.86	0.06	33.33	0.08	26.00	0.06
100	7.75	0.04	33.60	0.05	26.23	0.04
125	7.49	0.05	33.77	0.02	26.40	0.02
150	7.22	0.06	33.88	0.02	26.53	0.02
200	6.73	0.05	33.95	0.01	26.65	0.01
300	6.04	0.06	34.02	0.01	26.80	0.01
	(no. casts=18)				(Date: 27-28 September 1966)	
0	16.22	0.35	31.85	0.02	23.48	0.10
10	15.72	0.35	31.89	0.05	23.93	0.26
20	12.74	1.38	32.22	0.18	24.82	0.17
30	9.90	0.67	32.47	0.02	25.15	0.06
40	8.54	0.32	32.53	0.02	25.30	0.05
50	8.06	0.11	32.59	0.23	25.39	0.05
60	7.77	0.08	32.70	0.05	25.51	0.07
70	7.70	0.08	32.90	0.10	25.73	0.10
80	7.93	0.14	33.21	0.14	25.94	0.06
100	7.87	0.08	33.60	0.08	26.19	0.04
125	7.61	0.05	33.80	0.03	26.42	0.04
150	7.44	0.06	33.87	0.02	26.53	0.02
200	7.32	0.06	33.92	0.01	26.66	0.02
300	6.79	0.07	34.00	0.01	26.76	0.01

Anchor Station DB-40

(no. casts=14) (Date: 28-29 August 1966)

Depth (m)	TEMPERATURE (°C) mean	std. dev.	SALINITY (o/oo) mean	std. dev.	σ_t(x 10-3 gm cm-3) mean	std. dev.
0	15.86	0.38	31.98	0.06	23.48	0.10
10	14.15	0.89	32.09	0.10	23.93	0.26
20	10.87	0.78	32.43	0.05	24.82	0.17
30	9.12	0.32	32.48	0.02	25.15	0.06
40	8.44	0.20	32.54	0.03	25.30	0.05
50	8.07	0.17	32.59	0.03	25.39	0.05
60	7.79	0.13	32.68	0.07	25.51	0.07
70	7.69	0.03	32.95	0.12	25.73	0.10
80	7.75	0.02	33.23	0.08	25.94	0.06
100	7.81	0.03	33.56	0.05	26.19	0.04
125	7.48	0.12	33.79	0.02	26.42	0.04
150	7.15	0.06	33.87	0.02	26.53	0.02
200	6.77	0.09	33.97	0.02	26.66	0.02
300	6.32	0.03	34.02	0.01	26.76	0.01

Anchor Station NH-65

(no. casts=12) (Date: 30-31 August 1966)

0	16.29	0.34	31.98	0.61	23.25	0.12
10	15.30	0.85	32.06	0.60	23.54	0.24
20	11.98	1.02	32.28	0.19	24.55	0.26
30	10.19	0.74	32.42	0.18	25.05	0.29
50	8.39	0.27	32.54	0.06	25.32	0.07
75	7.88	0.06	32.84	0.14	25.65	0.06
100	7.96	0.07	33.30	0.25	26.04	0.05
150	7.52	0.05	33.74	0.26	26.44	0.03
200	7.01	0.22	33.88	0.13	26.59	0.03
250	6.42	0.29	33.93	0.04	26.69	0.03
300	5.91	0.33	33.96	0.03	26.77	0.04

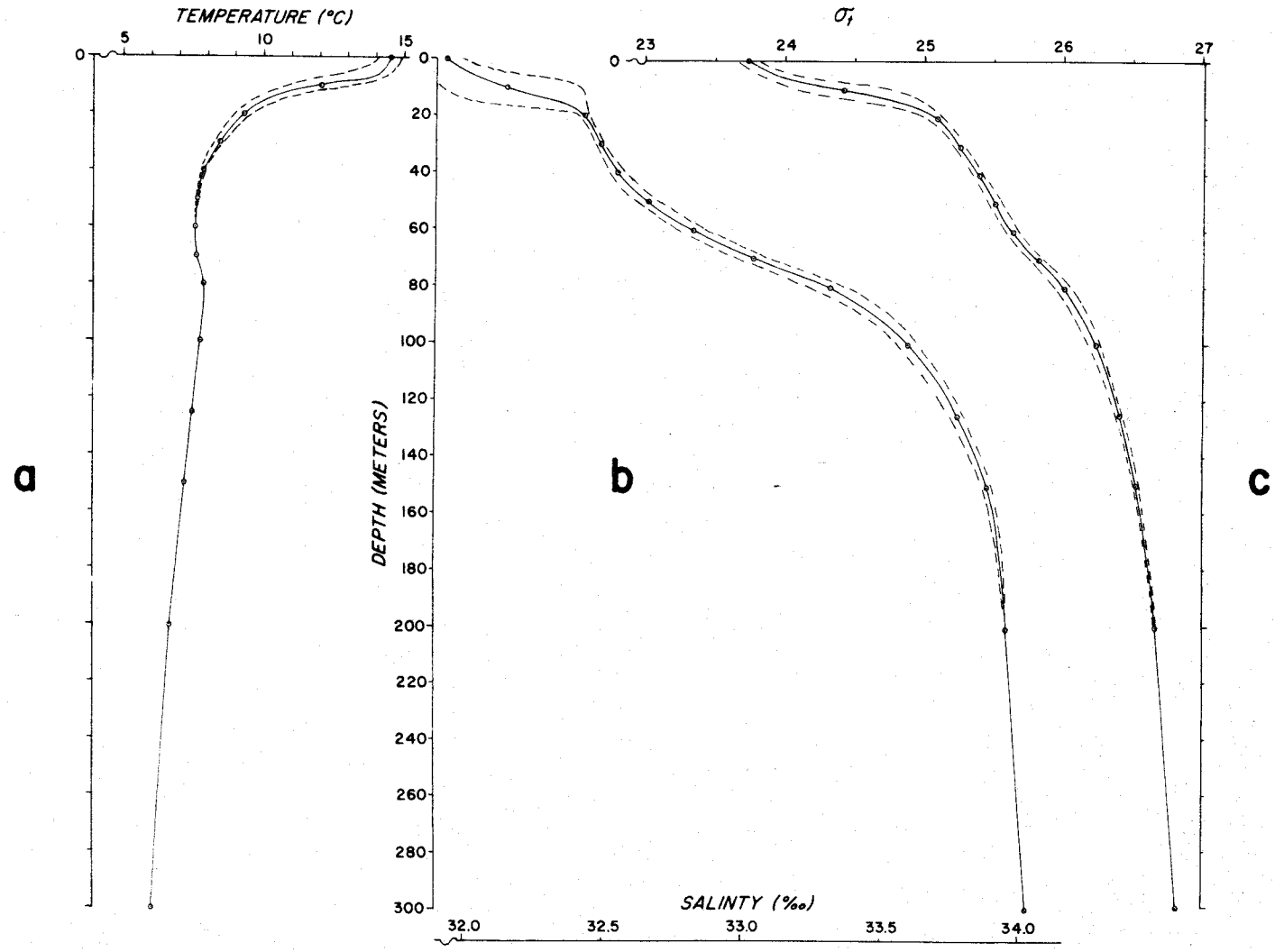

Figure 6. Mean and Standard Deviation of Hydrographic Profiles, Anchor Station DB 25, August 1966: a) Temperature b) Salinity c) Sigma-t.

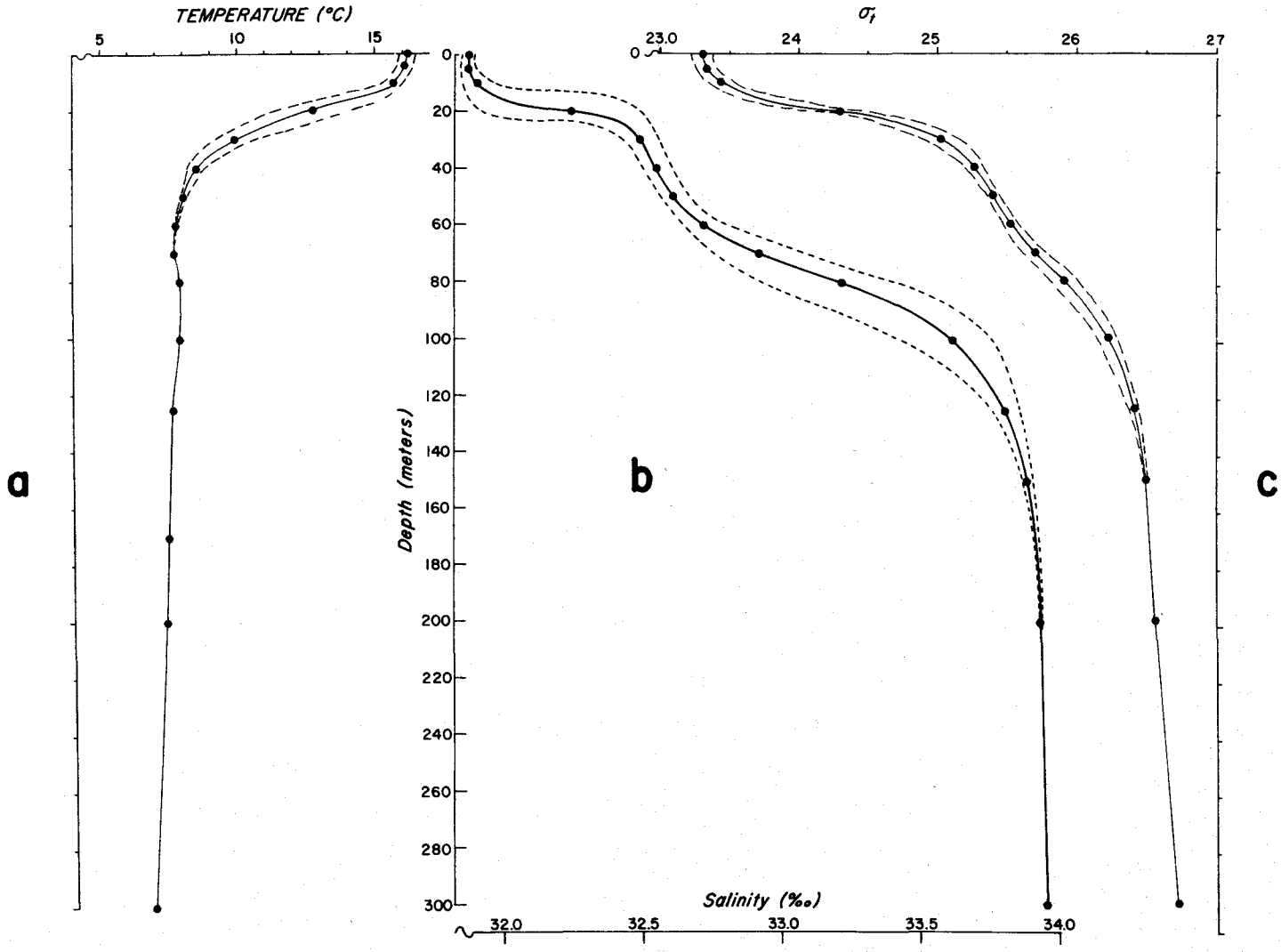

Figure 7. Mean and Standard Deviation of Hydrographic Profiles, Anchor Station DB 25, September 1966: a) Temperature b) Salinity c) Sigma-t.

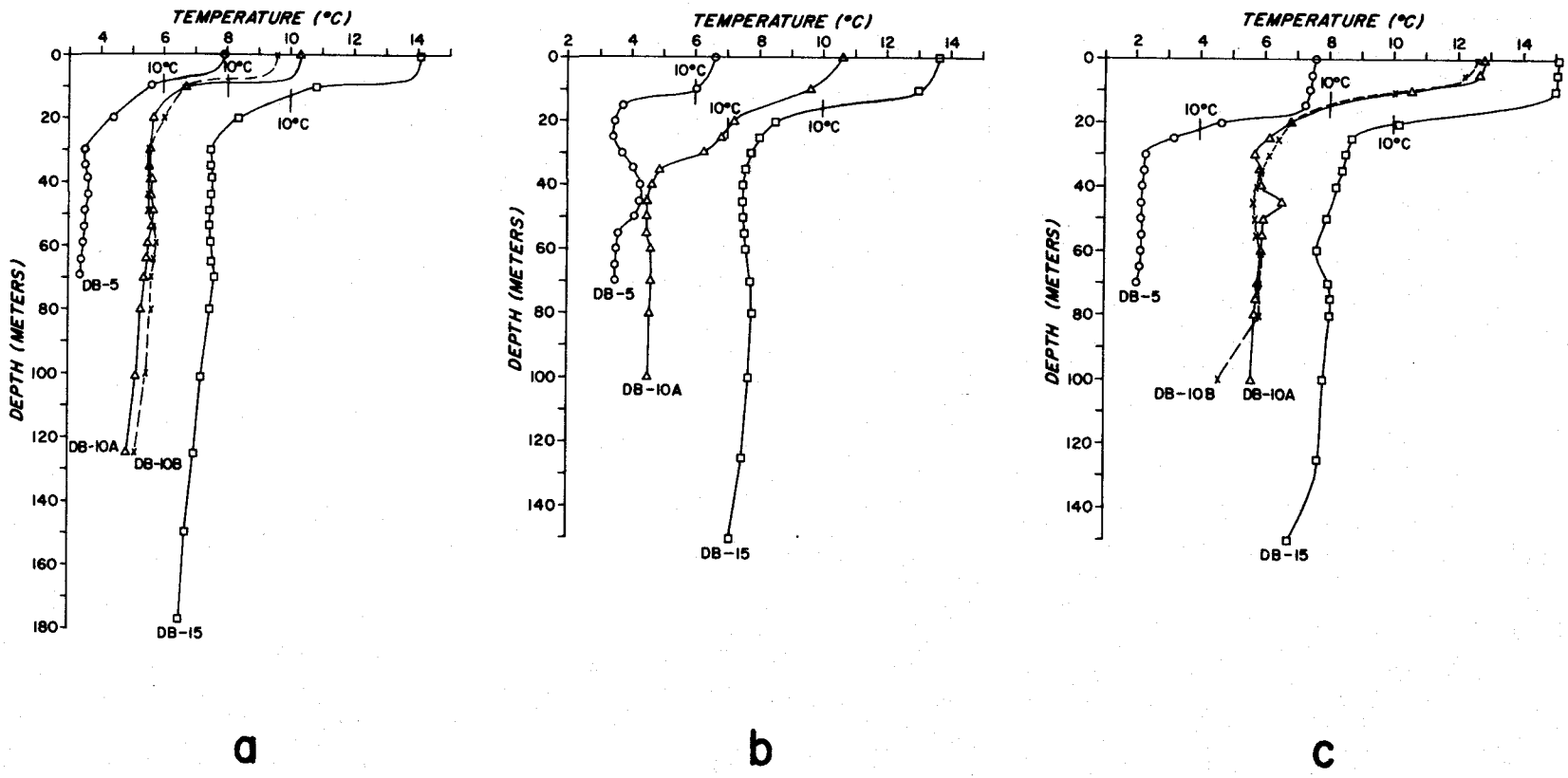

Figure 8. Vertical Profiles of Temperature at Sensor Sites:
a) 15-16 August 1966 b) 26-27 August 1966
c) 23-24 September 1966.

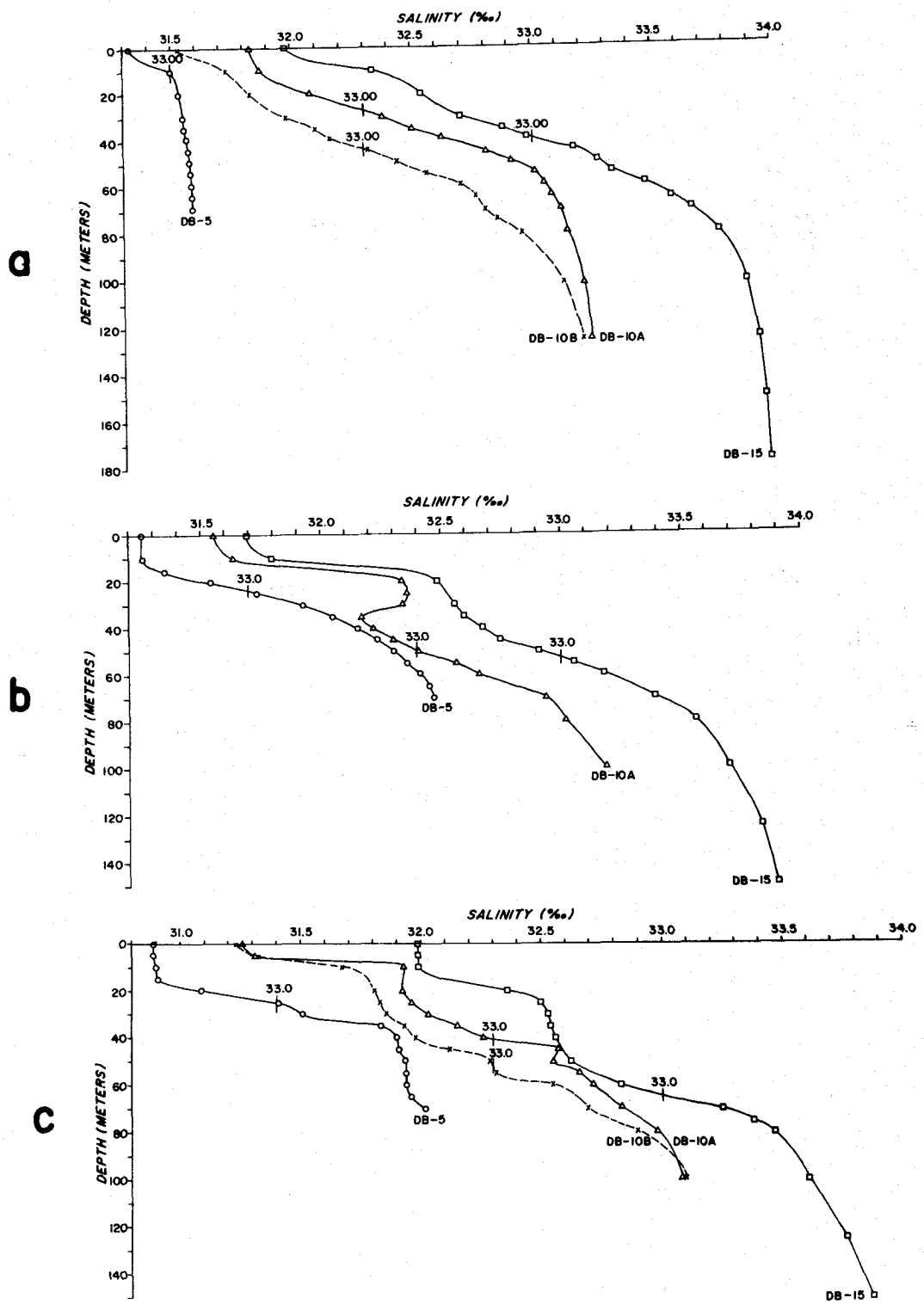

Figure 9. Vertical Profiles of Salinity at Sensor Sites: a) 15-16 August 1966 b) 26-27 August 1966 c) 23-24 September 1966.

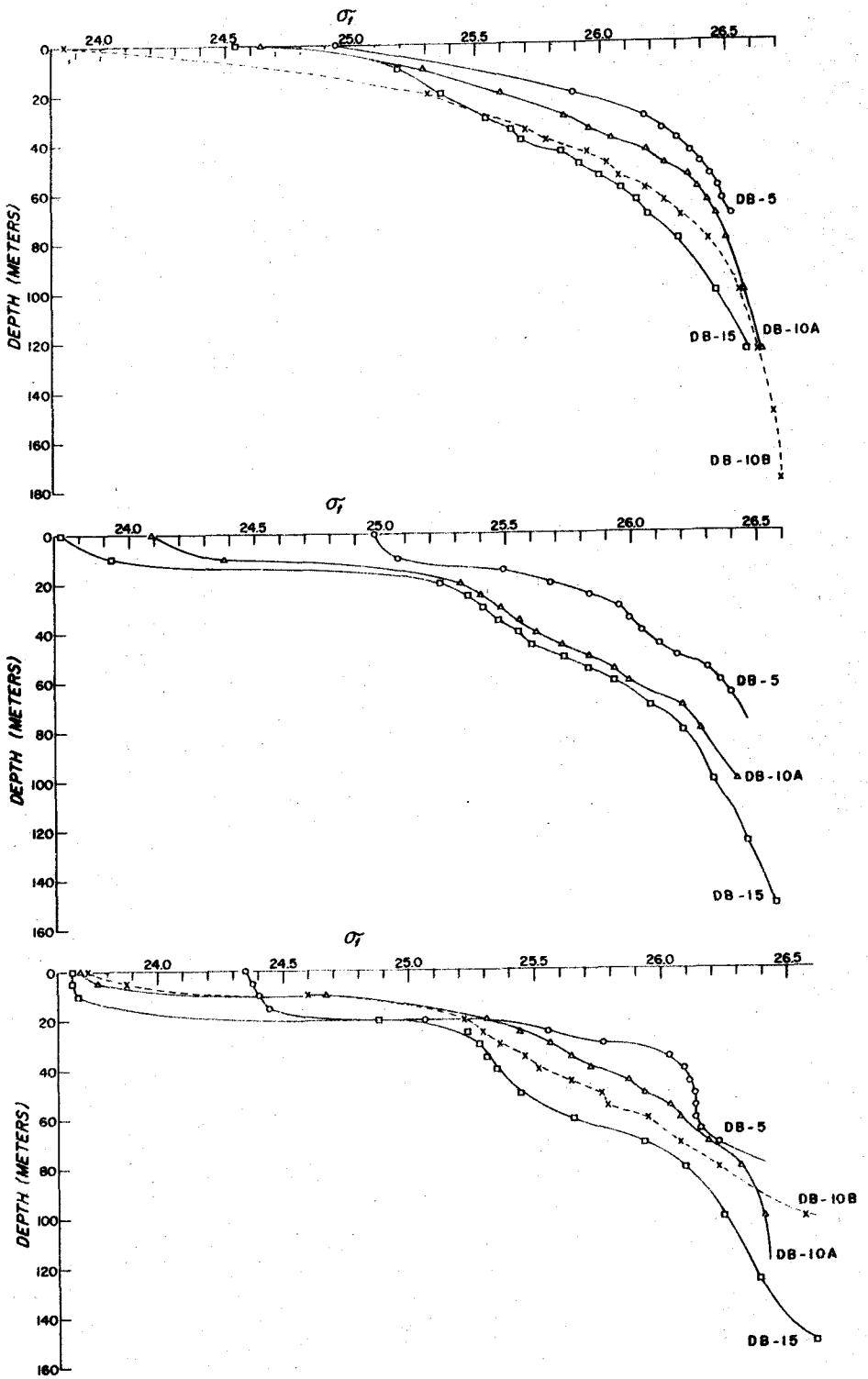

Figure 10. Vertical Profiles of Sigma-t at Sensor Sites: a) 15-16 August 1966 b) 26-27 August 1966 c) 23-24 September 1966.

TABLE VI

TEMPERATURE, SALINITY, AND SIGMA-t DATA AT SENSOR SITES

LEGEND: TEMPERATURE, T; SALINITY, S; SIGMA-t, σ_t

(Date: 15-16 August 1966)

	DB 5			DB 10A			DB 10B			DB 15		
Depth (m)	T(°C)	S(‰)	σ_t	T(°C)	S(‰)	σ_t	T(°C)	S(‰)	σ_t	T(°C)	S(‰)	σ_t
0	11.89	32.824	24.94	12.27	32.528	24.64	14.11	31.977	23.85	11.55	32.230	24.54
10	9.60	33.031	25.50	8.66	32.573	25.29	10.82	32.342	24.76	8.61	32.434	25.19
20	8.42	33.284	25.89	7.64	32.778	25.60	8.35	32.540	25.31	8.00	32.529	25.36
30	7.52	33.474	26.17	7.58	33.080	25.85	7.50	32.701	25.56	7.53	32.678	25.54
35	7.53	33.566	26.24	7.51	33.197	25.95	7.50	32.878	25.70	7.52	32.800	25.64
39	7.63	33.659	26.30	7.61	33.326	26.04	7.51	32.978	25.78	7.56	32.857	25.68
44	7.62	33.722	26.35	7.62	33.507	26.18	7.49	33.174	25.94	7.49	33.018	25.81
49	7.52	33.762	26.39	7.66	33.608	26.25	7.45	33.270	26.02	7.49	33.136	25.91
54	7.47	33.806	26.43	7.59	33.708	26.34	7.45	33.333	26.07	7.66	33.258	25.98
59	7.44	33.832	26.46	7.51	33.748	26.38	7.47	33.466	26.17	7.74	33.398	26.08
64	7.40	33.853	26.48	7.46	33.780	26.42	7.50	33.577	26.25	7.65	33.458	26.14
70	7.36	33.876	26.51	7.39	33.816	26.45	7.57	33.659	26.31	7.60	33.500	26.18
80				7.30	33.844	26.49	7.44	33.776	26.42	7.60	33.652	26.30
101				7.16	33.908	26.56	7.20	33.891	26.54	7.47	33.825	26.45
125				6.85	33.945	26.63	6.97	33.940	26.61	7.12	33.910	26.57
150							6.69	33.964	26.67			
177							6.53	33.980	26.70			

(Date: 26-27 August 1966)

0	10.55	32.558	24.98	13.66	32.162	24.09				13.67	31.697	23.73
10	10.03	32.563	25.07	12.66	32.279	24.38				13.07	31.801	23.93
15	7.73	32.652	25.49									
20	7.48	32.846	25.68	10.25	32.935	25.32				8.54	32.481	25.24
25	7.44	33.034	25.83	9.88	32.954	25.40				8.02	32.519	25.35
30	7.73	33.232	25.95	9.28	32.933	25.48				7.77	32.557	25.41
35	8.12	33.355	25.99	7.96	32.768	25.55				7.57	32.591	25.47
40	8.33	33.458	26.04	7.69	32.813	25.62				7.47	32.676	25.55
45	8.27	33.537	26.11	7.52	32.902	25.72				7.46	32.746	25.60
50	8.12	33.607	26.18	7.50	33.041	25.83				7.52	32.913	25.73
55	7.63	33.663	26.30	7.51	33.165	25.93				7.54	33.054	25.83
60	7.56	33.716	26.35	7.59	33.259	25.99				7.57	33.180	25.93
65	7.48	33.756	26.39									
70				7.64	33.541	26.20				7.75	33.396	26.07
80				7.63	33.616	26.26				7.75	33.562	26.20
100				7.54	33.787	26.41				7.67	33.697	26.32
125										7.47	33.827	26.45
150										7.10	33.894	26.56

(Date: 23-24 September 1966)

0	13.63	32.491	24.35	14.82	31.960	23.69	14.60	31.933	23.72	15.05	31.986	23.66
5	13.48	32.491	24.38	14.66	32.007	23.76	14.18	32.025	23.88	15.06	31.987	23.66
10	13.37	32.495	24.40	12.54	32.627	24.67	12.04	32.372	24.56	14.97	31.986	23.68
15	13.24	32.513	24.44									
20	10.64	32.686	25.06	8.79	32.622	25.31	8.80	32.506	25.22	10.19	32.357	24.88
25	9.21	33.007	25.55	8.12	32.658	25.44	8.43	32.528	25.29	8.71	32.502	25.23
30	8.31	33.114	25.77	7.70	32.728	25.56	8.15	32.555	25.36	8.51	32.525	25.28
35	8.24	33.435	26.03	7.81	32.849	25.64	7.86	32.630	25.46	8.37	32.537	25.31
40	8.19	33.498	26.09	7.84	32.967	25.72	7.72	32.676	25.51	8.21	32.559	25.35
45	8.16	33.514	26.11	8.45	33.269	25.87	7.61	32.815	25.64			
50	8.13	33.538	26.13	7.93	33.245	25.93	7.66	32.984	25.76	7.92	32.616	25.44
55	8.13	33.542	26.13	7.87	33.362	26.03	7.71	33.009	25.78			
60	8.12	33.543	26.13	7.84	33.413	26.07	7.84	33.244	25.94	7.62	32.828	25.65
65	8.10	33.555	26.15									
70	7.98	33.624	26.22	7.79	33.536	26.18	7.77	33.391	26.07	7.97	33.252	25.93
80				7.67	33.680	26.31	7.82	33.598	26.22	8.03	33.470	26.09
100				7.57	33.782	26.40	6.51	33.796	26.56	7.80	33.619	26.24
125										7.65	33.769	26.38
150										6.68	33.874	26.60

thermograph. In the late August period, the temperature gradient was non-uniform at the thermograph depth. The salinity profiles generally show a shallow, strong halocline and a deeper halocline, but a strong salinity inversion is indicated at DB 10 in late August. The density profiles generally show:

i) t he shoreward increase of density at any given depth

ii) a decrease in the density of the "surface layer" (about 20 meters deep) from mid-August to late-September due to warming and freshening

iii) a degradation in the "regularity" of the vertical profile patterns from mid-August to late-September, particularly in the permanent pycnocline.

In Figure 8, the vertical temperature profiles at the sensor sites can be characterized by a shallow thermocline from the surface to about 30 meters, a temperature inversion with a maximum value in the depth range of 40 to 80 meters and an intensity of 0.2 to 1.0C°, and a nearly uniform gradient below the temperature inversion. The thermographs (at 20 meters depth) were near the base of the shallow thermocline. The meter at DB 15 was in a nearly linear region of the thermocline, though the gradient was not constant throughout the installation period; the meter at DB 5 was in a more variable regime which was quite non-linear, especially in late-August. Estimates of the corresponding temperature gradients (C°/m) are:

	15-16 August	26-27 August	23-24 September
DB 5	0.1	0.03	0.4
DB 15	0.1	0.1	0.3

One point to be emphasized is the difficulty of converting temperature variation, as observed in time series, to equivalent vertical displacements with gradients as variable as these in general and as non-linear as those at DB 5 in particular. Typical semidiurnal temperature variations observed at the thermographs and the corresponding estimates of peak-to-peak vertical displacements are:

	15-16 August	26-29 August	27-28 September
DB 5	1C°, 20 m	3C°, 20 m	4C°, 15 m
DB 15	1.5C°, 15 m	2C°, 15 m	no data .

Resonable results for conversion of temperature variations to vertical displacements probably could be achieved from BT traces sampled at time intervals of the order of a few days; this is an argument for the efficacy of hydrographically monitoring an array site at least weekly.

In Figure 9, the vertical salinity profiles at the sensor sites can be characterized by a strong halocline in which the salinity generally increases by 1‰ from the surface to a depth of 40 or 80 meters. The DB 5 profiles are exceptional in the first and third cases, being nearly isohaline below 10 meters

and 40 meters, respectively. Even though there are inversions and kinks in the salinity profiles as well as in the temperature profiles, in late August and late September, the salinity gradient is essentially constant over a depth range large enough to give a linear response to large vertical motions on a salinograph set in the halocline.

In contrast to Figures 8 and 9, the sigma-t profiles of Figure 10 have not been offset (a beneficial, graphical by-product of coastal upwelling!). The rise of the permanent pycnocline inshore is obvious, as is the breakdown of the regularity of profile patterns from mid-August to late-September. In general, a decrease of 2 sigma-t units occurs in the upper 60 meters, i. e. across the seasonal and the permanent pycnoclines.

Figure 11 depicts the T-S diagrams for the inshore hydrographic stations adjacent to sensor strings on the Depoe Bay line; it is also based on the data listed in Table VI. The principal features are the variations of the T-S curves within the permanent pycnocline, which is generally isothermal except for the frequent presence of a temperature inversion near the base of the permanent pycnocline, and for warming on the permanent pycnocline's upper side, where it approaches the surface inshore.

The T-S diagrams plotted from the average temperature and salinity profiles (see Table V), measured over a lunar day, at the four anchor stations of August and September 1966 are shown in Figures 12a and b. Figure 12a contains the two T-S diagrams computed for DB 25, one in August and the other in September; they are remarkably similar, both indicating a temperature inversion at the base of the permanent pycnocline. The permanent pycnocline is about 5 meters deeper in September than in August. Figure 12b shows the T-S diagrams at DB 40 and NH 65 for August. The curve for DB 40 is very similar to the curve for DB 25 August, except that the permanent pycnocline is 5 meters deeper. The T-S curves for DB 40 and NH 65 are similar; they differ primarily in that the pycnocline is 15 meters deeper and the temperature inversion is less intense at NH 65.

The temperature and the salinity components of the static stability, E_T and E_S, respectively, are shown in Figure 13 based on the average profiles of temperature and salinity at anchor station DB 25 in September. These plots again show that the near-suface pycnocline is governed primarily by the thermocline, but that the shallow halocline also contributes, and that the permanent pycnocline is governed by a deeper halocline, with an intensity equal to that of the near-surface halocline, and which more than offsets the destabilizing effect (in the hydrostatic sense) of the temperature inversion.

In a similar fashion, the temperature and the salinity components of the sound speed gradient, $\nabla_T C$ and $\nabla_S C$, respectively, shown in Figure 14 are based on the same data as used in Figure 13. The salinity increase with depth causes a small positive sound speed gradient; its contribution is largest in the two haloclines. The temperature decrease with depth in the thermocline causes a large negative sound speed gradient, but the temperature inversion causes a positive sound speed gradient. The result is that the sound speed gradient due to both temperature and salinity is negative at all depths except in the temperature inversion at depths above the maximum temperature of the inversion. Since the sound speed gradient due to pressure is positive (equal to about $+0.018\ \text{sec}^{-1}$) the net result is that a sound speed maximum is found at the depth of the temperature inversion; thus, there is a narrow, weak sound speed minimum, or sound channel, above the depth of the maximum temperature of the inversion.

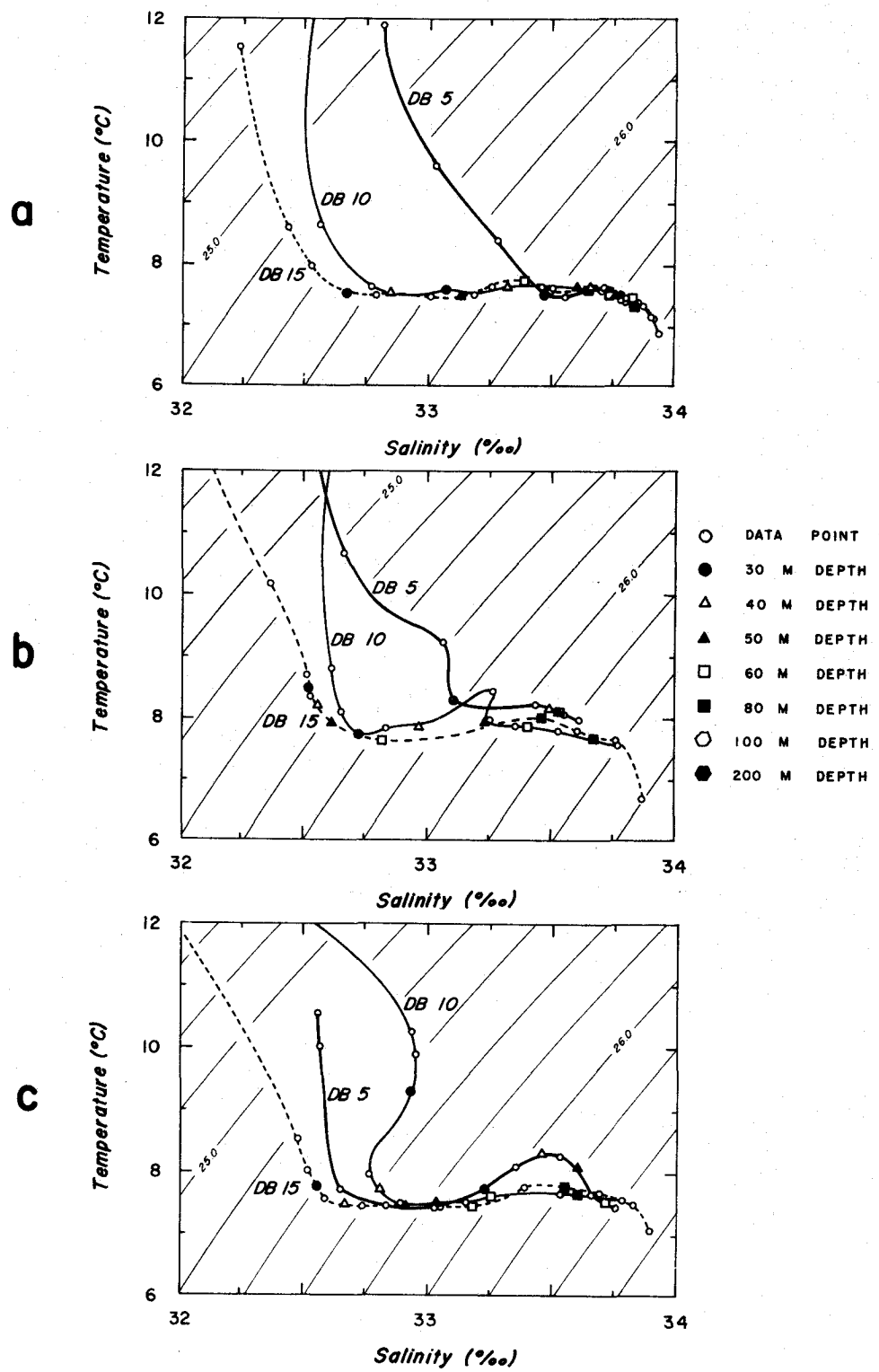

Figure 11. Temperature-Salinity Diagrams at Sensor Sites: a) 15-16 August 1966 b) 26-27 August 1966 c) 23-24 September 1966.

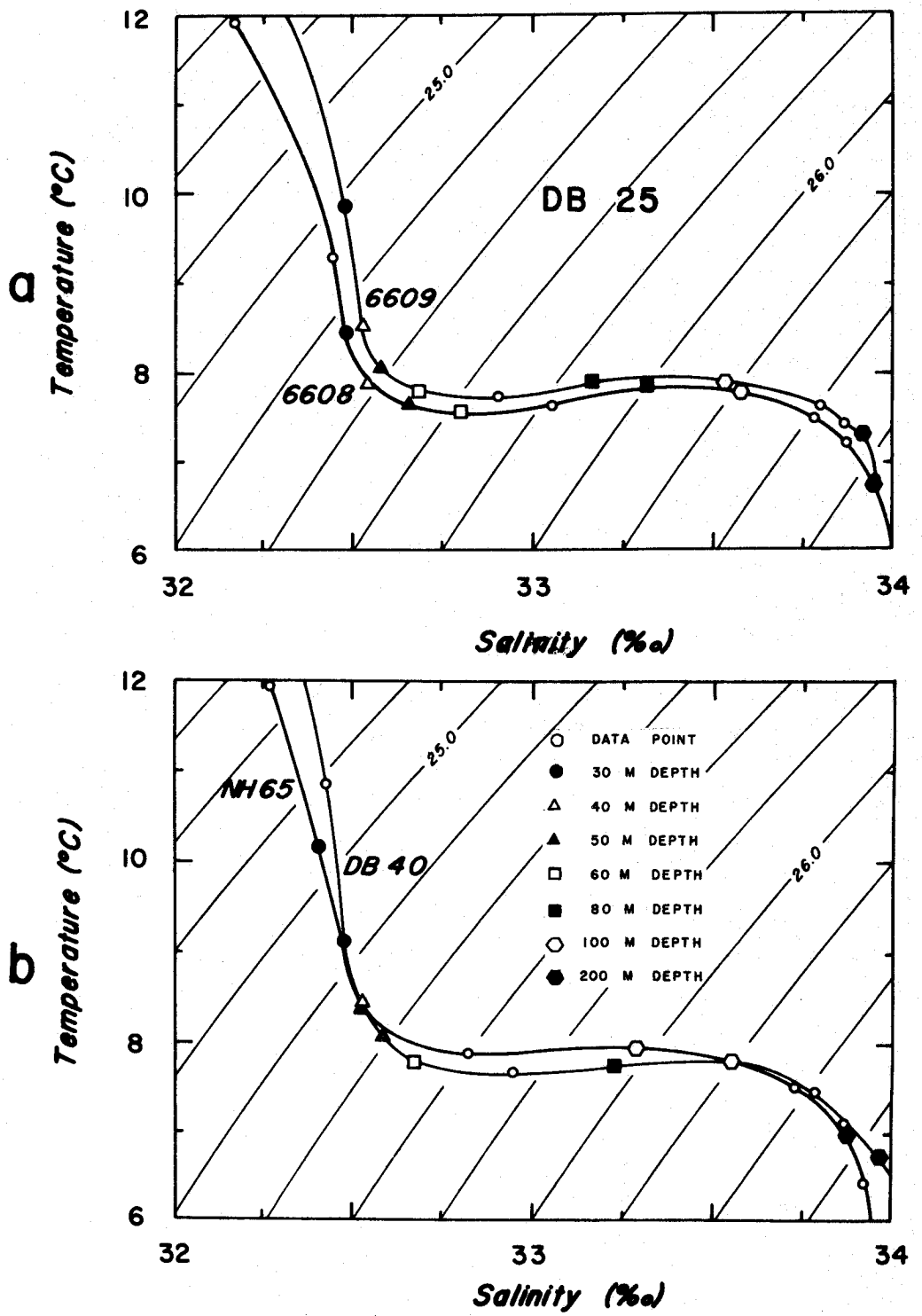

Figure 12. Temperature Salinity Diagrams at Anchor Stations: a) DB 25, 27-28 August and 26-27 September 1966 b) DB 40, 28-29 August 1966 and NH 65, 30-31 August 1966.

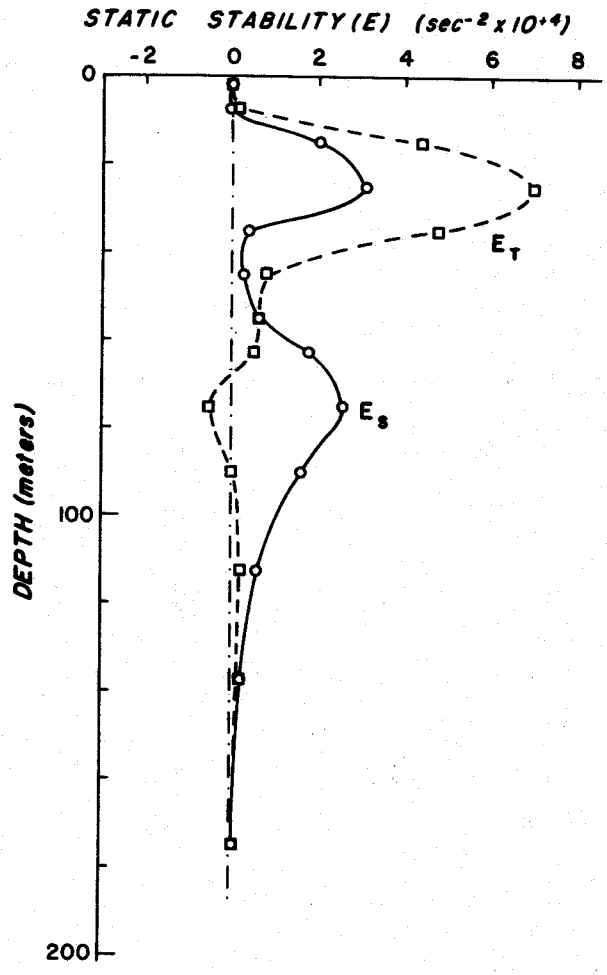

Figure 13. Static Stability, Anchor Station DB 25, 26-27 September 1966.

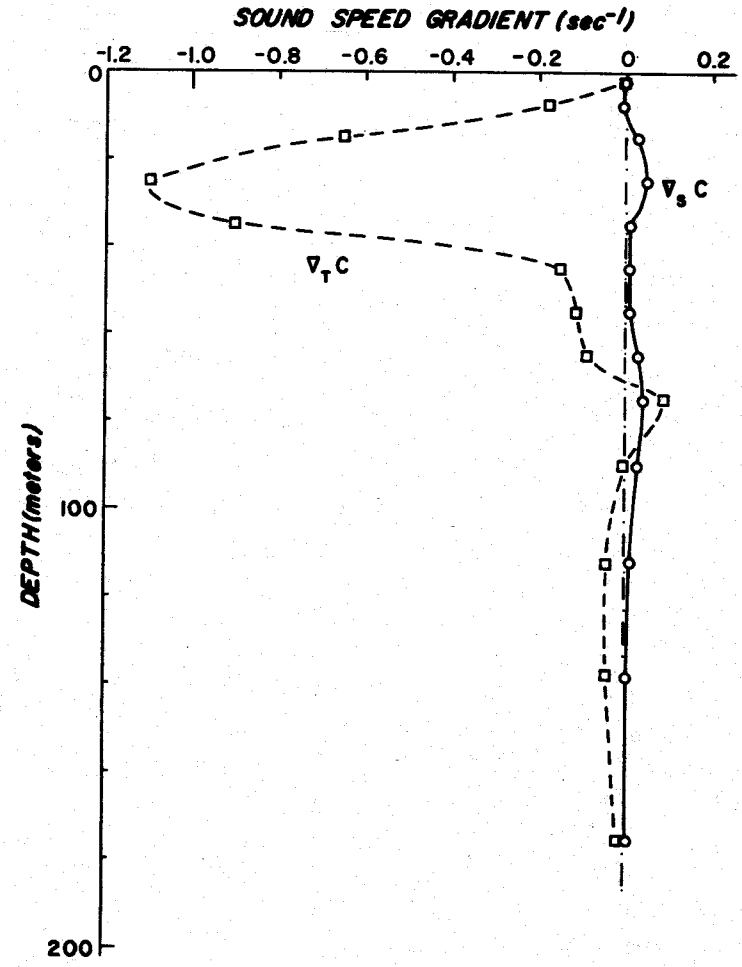

Figure 14. Sound Speed Gradient, Anchor Station DB 25, 26-27 September 1966.

Figure 15a shows an alongshore, vertical temperature section from near San Francisco to about 20 to 40 kilometers north of the Depoe Bay line. The depth zones and intensities of the inversions are indicated graphically. The figure shows that there is a sharp thermal front near 40° N((i. e., near the Mendocino Escarpment); more precisely, a sharp divergence (or upwelling) appears at 41°N. Otherwise, the temperature field is relatively uniform in the alongshore direction. The general but spasmodic occurrence of a subsurface temperature inversion is apparent. Figure 15b shows an onshore, vertical temperature section roughly parallel to the Depoe Bay line; its features are similar to those observed on the Depoe Bay and the Newport lines, viz. the inshore rise of isotherms in the upper 200 meters and an inshore shoaling of the subsurface temperature inversion. The table in Figure 15c records the positions, time, and surface temperatures of the BT casts used to plot Figures 15a and b.

Vertical Profiles of Current Speed

One of the inherent difficulties with a moored-meter system is the lack of available vertical detail in the vertical profile of horizontal velocity. In order to avoid developing erroneous notions about the flow field based on lengthy time series measurements at fixed depths, several vertical profiles of horizontal velocity were measured by a Savonius rotor current meter lowered from the YAQUINA in September 1966. Since the ship was anchored only at DB 25, the profiles sampled at the other locations can give values relative only to the surface flow. Nevertheless, this method was sufficient to detect and to locate an important recurring feature in the flow: a subsurface speed minimum and a deeper, relative maximum (see Figure 16). Direction data are not given because these data are based on a single profile and direction has been generally observed to vary considerably over a tidal cycle, and could thus be misleading. The speed curve at DB 5, in particular, suggests that samples at 5 to 10 meter vertical increments are necessary to detect and to define the subsurface, relative maximum in the speed. With the evidence to be shown in Figures 17 and 18 for DB 25, it can be concluded that this subsurface feature of the speed occurs in a zone at least 36 kilometers in width. The depth of the speed maximum is generally that of the temperature inversion in the lower portion of the pycnocline. The minimum in the current speed occurs near the depth of the base of the thermocline.

Because of its position with respect to the permanent pycnocline, the subsurface relative maximum in the speed can be thought of generally as a weak "pycnoclinic jet." Because the jet's depth is near the lower current meters (i. e., at 60 meters), the possibility that the depth of the jet oscillates vertically to alternately include and exclude the depth of the current meter must be considered. This jet has been detected on other occasions, but it is premature to state that it is a stationary feature. If it is dynamically linked to the upwelling front, its depth and intensity may vary with variations in the intensity of upwelling. As is made apparent in the profile of DB 5, a five-meter spacing was essential for proper definition of this feature at that location, while the moored meters had a 20-meter spacing.

Figure 17 shows the mean northward and eastward components of the velocity computed from the current meter casts at anchor station DB 25. The point we wish to make with these curves is that the mean flow was to the north

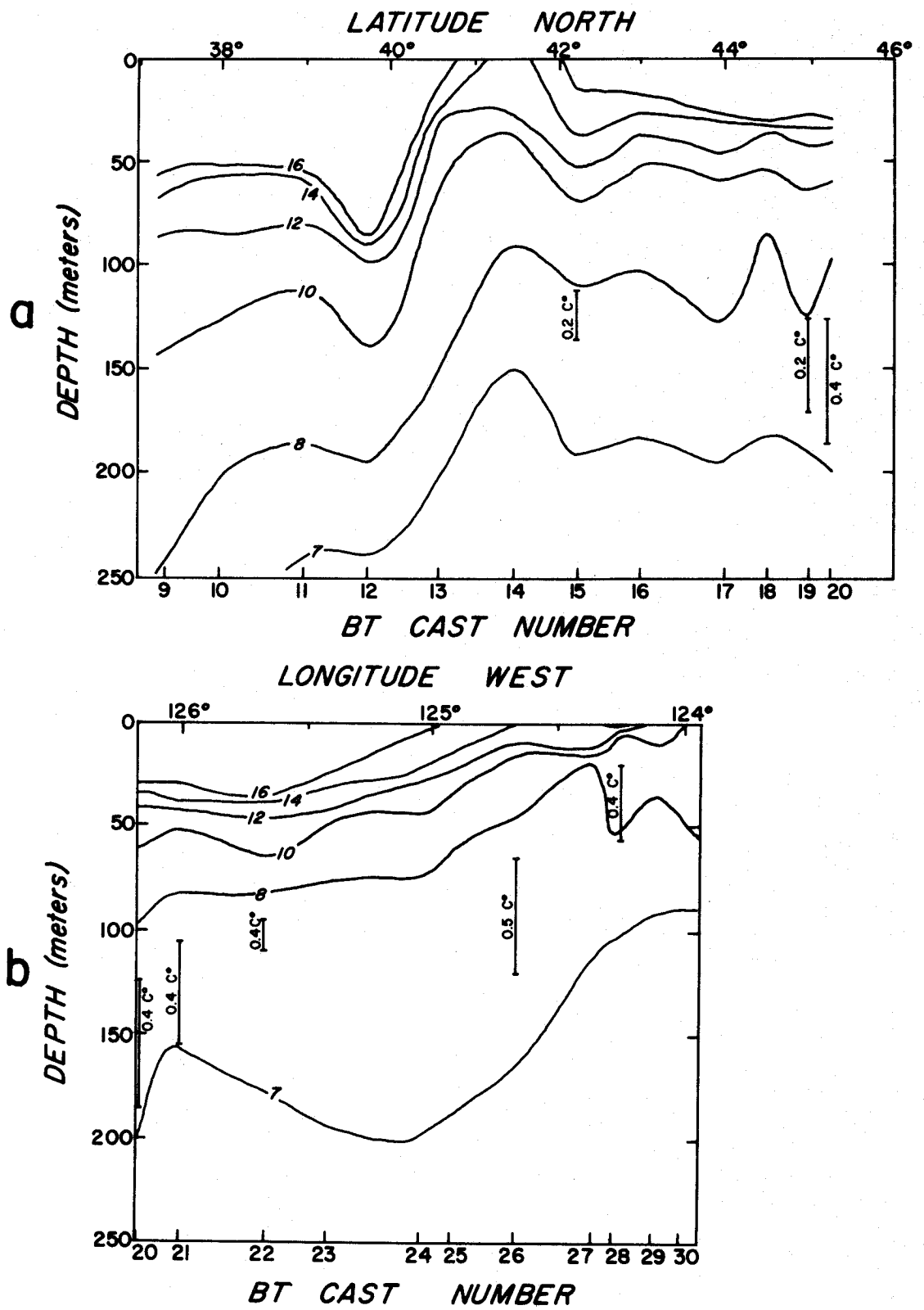

Figure 15. BT Vertical Sections, 21-24 August 1966: a) Alongshore b) Onshore.

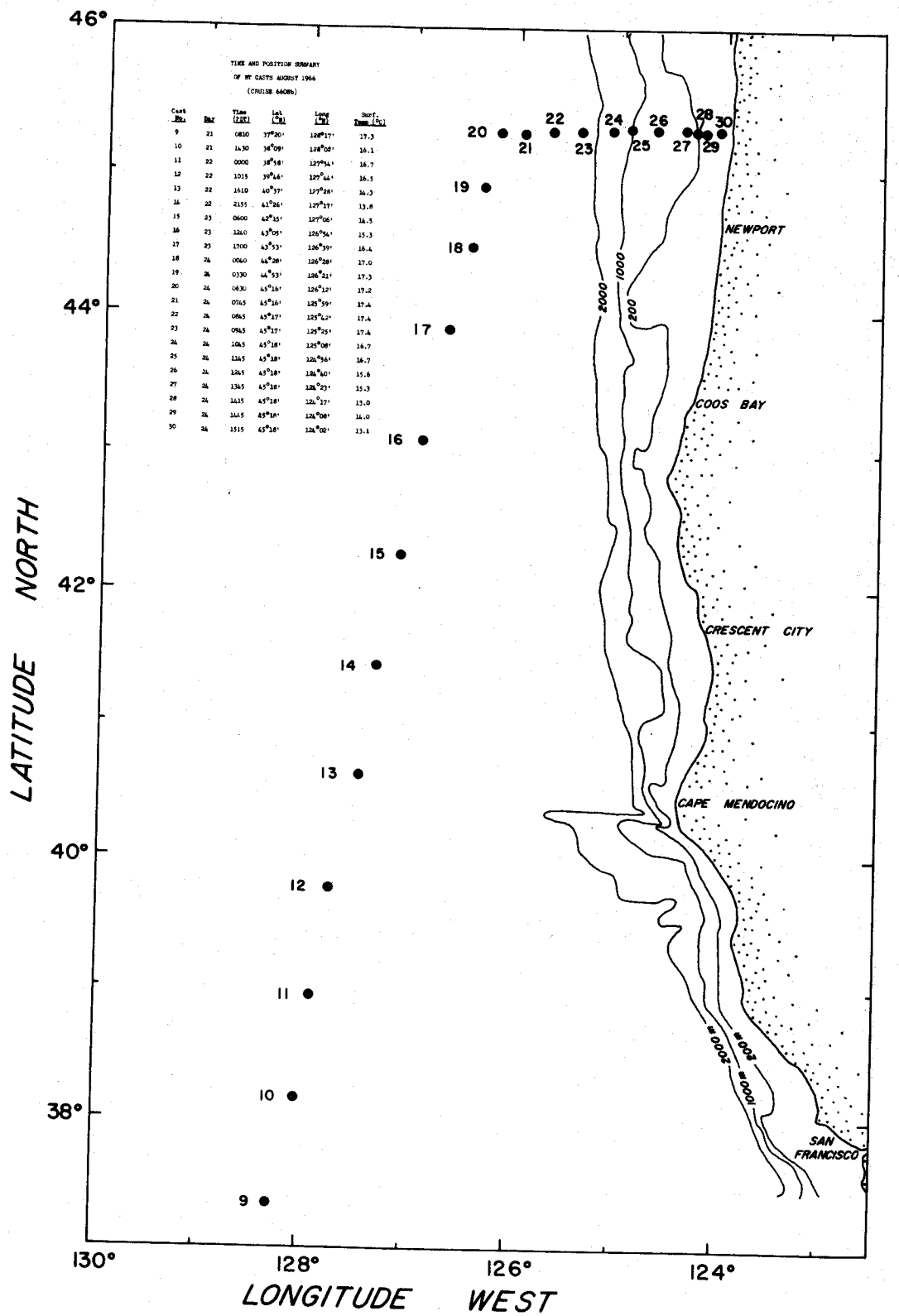

C

Figure 15c. Chart of BT positions.

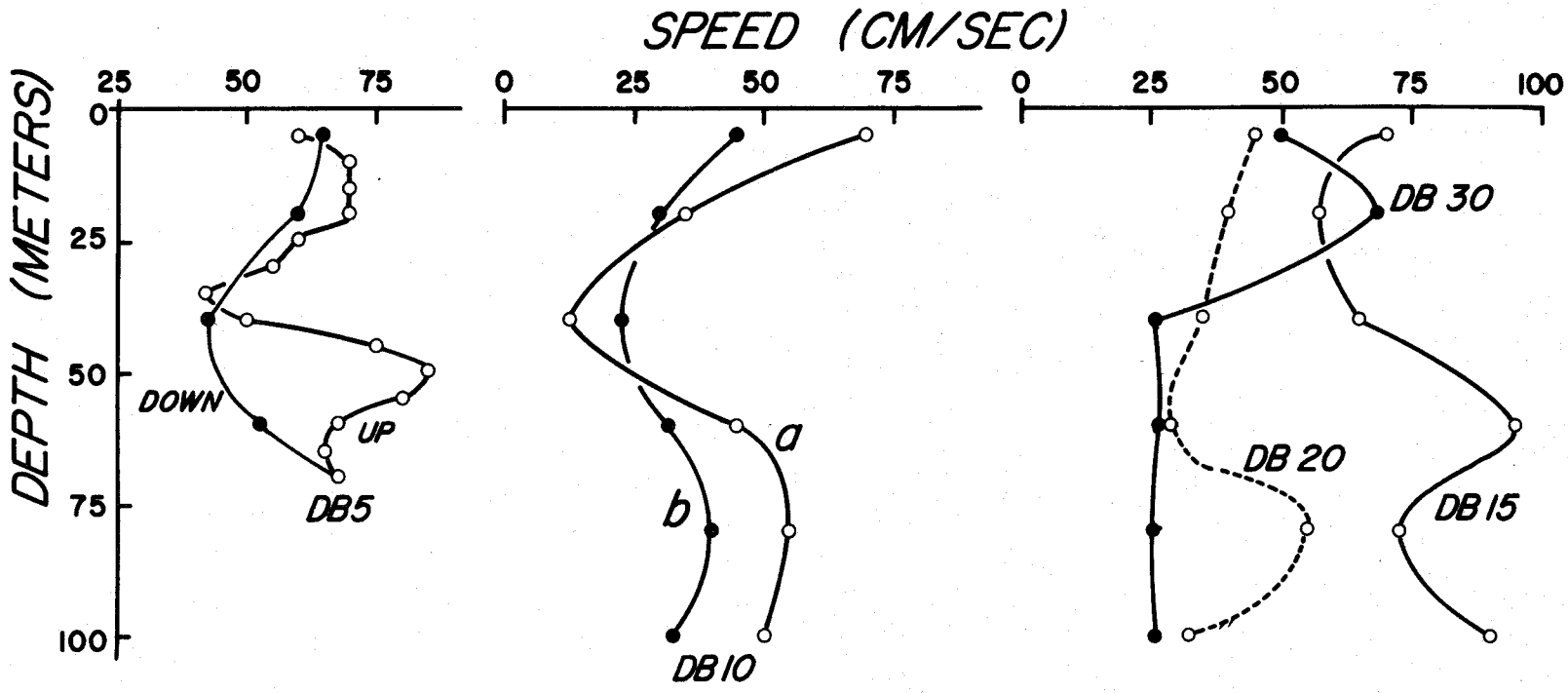

Figure 16. Current Speed Vertical Profiles, Depoe Bay Line, 23-24 September 1966.

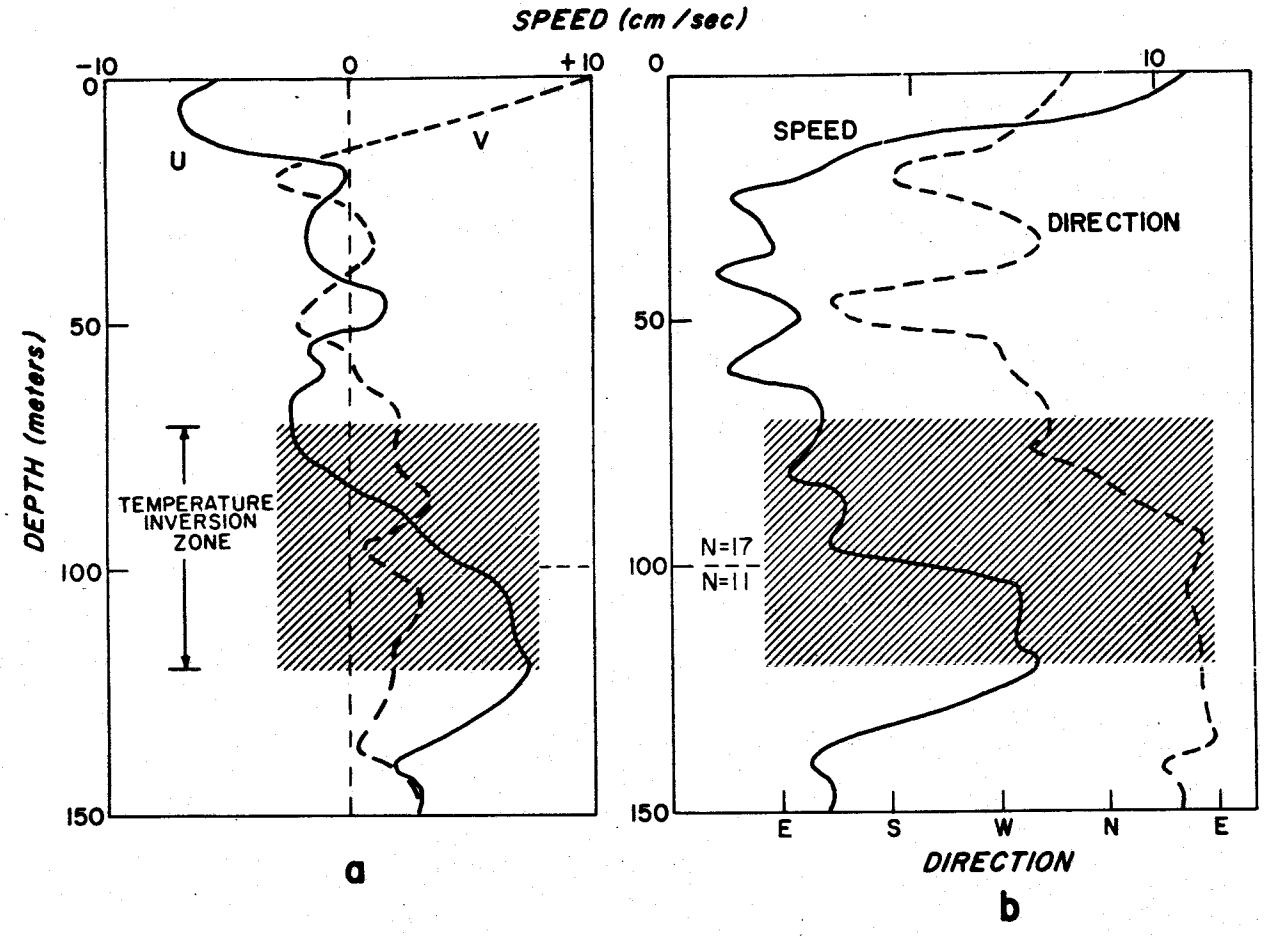

Figure 17. Vertical Profile of Mean Horizontal Velocity, Anchor Station DB 25, 27-28 September 1966: a) Velocity in cartesian components b) Velocity in polar components. N = no. of samples; curves are based on 17 samples above ---- and 11 samples below.

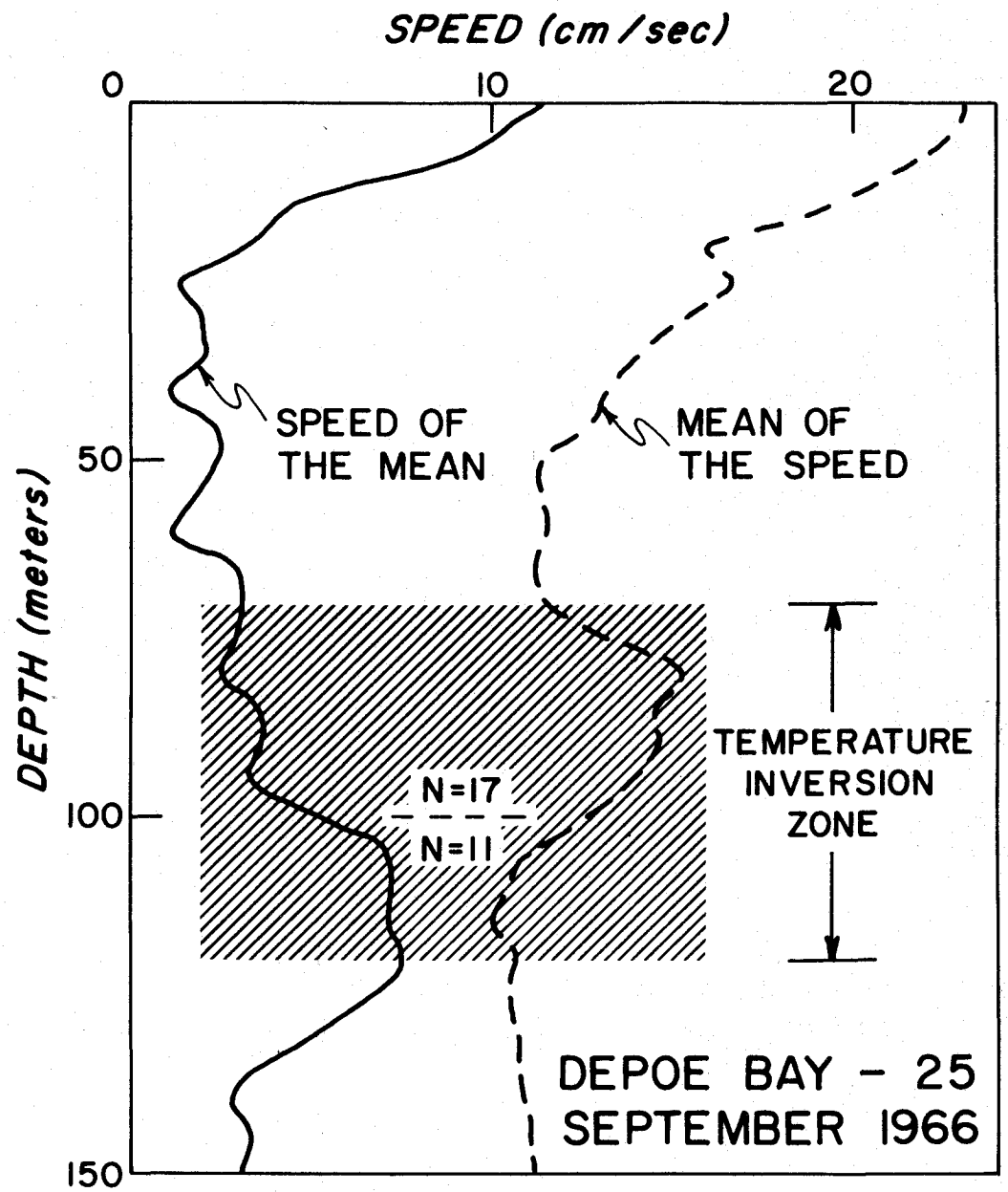

Figure 18. Vertical Profiles of the Mean of the Scalar Speed and Speed of the Vector Mean, Anchor Station DB 25, 27-28 September 1966. N = No. of Samples; Curves are Based on 17 Samples Above ---- and 11 Samples Below.

and east at the base of the permanent pycnocline and below; this fact should be used in comparison with results from the moored meters.

Figure 18 shows the mean of the scalar speed and the speed of the vector mean at the September, DB 25 anchor station as a function of depth. The mean scalar speed decreases nearly linearly from about 20 cm/sec at the surface to about 10 cm/sec at 50 meters, remains nearly constant from 50 to 70 meters, increases to about 15 cm/sec at 85 meters, decreases to 10 cm/sec again at 100 meters, and remains nearly constant to 150 meters. This is the strongest evidence available for the occurrence of the subsurface speed maximum at the base of the permanent pycnocline. And since the mean scalar speed is generally several times greater than the speed of the vector mean, especially at a depth of 85 meters and except at a depth of 125 meters, this is evidence for highly variable flow at 85 meters, near the base of the pycnocline, and for relatively steady flow at 125 meters. Further evidence for these features will be found in Collins, et. al. (in press).

Time Series of Current Velocity, Temperature, Wind, Atmospheric Pressure, and Sea Level

Figure 19 presents the progressive vector diagrams (PVD's) for the four current meters which ran usefully long. Midnight of every day is indicated; that of every fifth day is explicitly labelled. The first observation is that the flow is to the south at 20 meters, 9 and 18 kilometers offshore, and to the north at 60 meters, 9 and 27 kilometers offshore. The second observation is that the flow tends to follow the local topography, with the notable exception of DB 15, 60 meters; there a significant onshore component occurred, particularly in the latter portion of the observation period. The third observation is that there are frequent "wiggles" in the curves associated with tidal-like motions. The fourth observation is that time intervals of acceleration and deceleration of the flow can be detected visually, including an actual reversal in the flow at DB 5, 60 meters for four days, from the 17th to the 21st day. The flow was also to the south at this site for the initial three days of record, followed by a reversal to the north. Some of the statistics of the basic flow data are listed in section a of Table VII.

Figure 20 shows the PVD's for the geostrophic and the directly-measured surface wind fields from 1 August to 31 September. Again, midnight of every fifth day is labelled explicitly, but beginning from 1 August vice 15 August for the current data. The geostrophic wind is based on 6-hourly surface pressure charts; the surface geostrophic wind was determined for a point centered at 45°N, 125°W (about 50 kilometers seaward of the array site), by using the method of measuring isobar spacings and directions. The directly-measured wind is based on hourly observations taken from an anemometer located at a height of 10 meters above the sea surface on an oil-drilling platform (named Bluewater). The oil-drilling platform was located at the following points on the indicated dates:

1-25 August -- (46.0°N, 124.6°W), 30 miles off Astoria, Oregon
26-28 August -- undertow
29 August - 5 September -- inside mouth of Columbia River
6-7 September -- undertow
8-30 September -- (44.5° N, 124.4° W), 20 miles off Newport, Oregon.

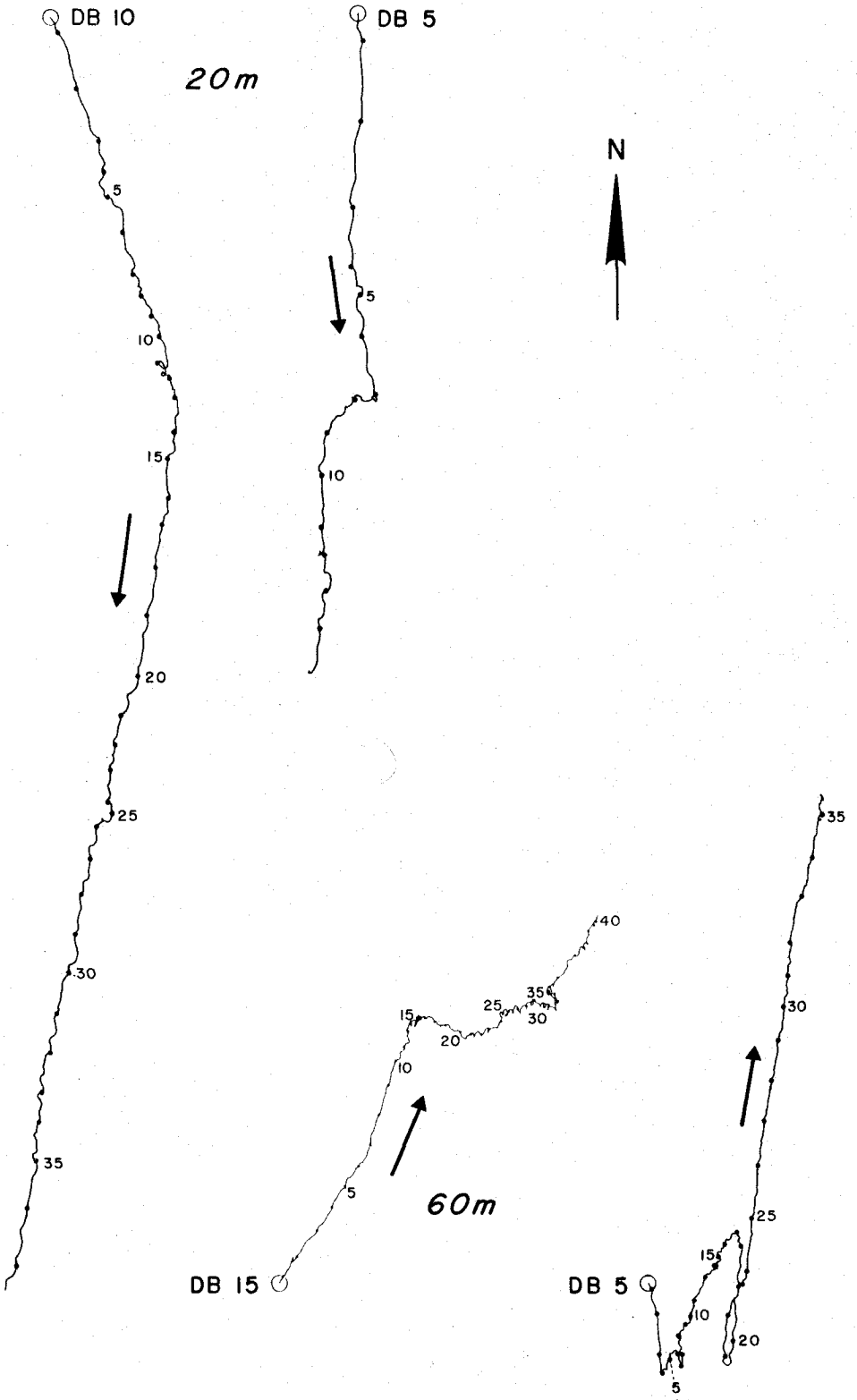

Figure 19. Progressive Vector Diagrams of Currents, Depoe Bay Array, 15 August - 24 September 1966.

TABLE VII

MEAN FLOW AND TEMPERATURE
(Based on 10-minute samples)

a. Mean Flow

Depoe Bay Station	Depth (meters)	N (No. of days)	U (cm/sec) Mean ± S. D. *	V (cm/sec) Mean ± S. D.	Scalar Speed (cm/sec) Mean ± S. D.	Vector Mean Speed (cm/sec)	Vector Mean Dir Deg True)
5	20	14.5	-2.1 ± 11.4	-17.9 ± 11.8	23.4 ± 7.0	18.0	187
	60	35.4	2.7 ± 6.7	5.1 ± 12.6	14.3 ± 5.8	5.8	028
10A	20	37.1	-0.8 ± 11.0	-13.6 ± 8.6	18.4 ± 6.3	13.6	183
	60	1	----------very little data----------				
15	20	0	----------no data----------				
	60	39.8	4.8 ± 7.6	3.9 ± 8.5	12.5 ± 3.4	6.1	051

b. Mean Temperature

Depoe Bay Station	Depth (meters)	N (No. of days)	Temperature (°C) Mean ± S. D.
5	20	38.1	8.9 ± 1.1
10A	20	0	no data
10B	20	0	no data
15	20	23.7	10.8 ± 1.6

*S. D. : Standard Deviation

The directly-measured wind is limited by direction resolution into 16 points of the compass; it leads to a generally lower estimate of the mean wind, but the patterns were basically similar for both wind measurements until the 35th day. Both curves indicate the breakdown of the predominantly northwesterly winds beginning on about the 23rd day. The directly-measured wind more dramatically indicates the oscillatory behavior of the alongshore winds in the latter six weeks of its plot; because of the limited direction resolution, the PVD makes the reversing pattern quite angular. The directly-measured wind from 8 to 24 September is particularly significant to us because it was sampled about 30 kilometers to the south of our array site. In summary, the winds were relatively steady from the northwest during the first two weeks of our sampling period, while they oscillated, primarily in the alongshore direction, during the latter four weeks with a period of the order of a week.

An interesting result, which is obtained from a casual comparison of data shown in Figures 19 and 20, is that when the steady northwesterly wind pattern "broke" on the 25th of August, the flow at DB 15, 60 meters, ceased running predominantly to the north and developed a strong set to the northeast. More careful comparison yields other, less dramatic, relationships between the winds and the currents. The above discussion is an argument for the efficacy of having PVD's of both winds and currents available for examination.

Figures 21a, b, c, and d are plots of the "low-passed" components of the horizontal velocity. The basic data have been numerically tapered, i. e. submitted to a weighted average, yielding time series with a half-power point of 40 hours. The details of the numerical taper are discussed in Appendix III, but the practical effect is that the tides and the higher frequencies have been suppressed and periods of two days or greater have been separated from the basic data to form the "low-passed" data. The solid and the dashed curves are the northward and the eastward components of the flow, respectively. From these curves, one can visually estimate the mean flow and the long-period variability about the mean. There appear to be significant oscillations with periods of the order of several days to a week; there also appears to be some coherency to these oscillations, which must be tested by spectral analysis. The dynamic range, i. e., the "peak-to-peak" amplitude of the "low-passed" flow is listed below:

	Eastward Component (cm/sec)	Northward Component (cm/sec)
DB 5, 20 m	30	30
DB 5, 60 m	15	40
DB 10, 20 m	15	20
DB 15, 60 m	10	20

In general, the dynamic range is greater in the alongshore (northward) component than the onshore-offshore (eastward) component; the largest values of the oscillations in the alongshore component are found inshore at DB 5. The results of these curves provide strong arguments for the necessity of the acquisition of lengthy time series, at least one hundred days long, in order to accurately resolve the low frequency periodic or quasi-periodic components.

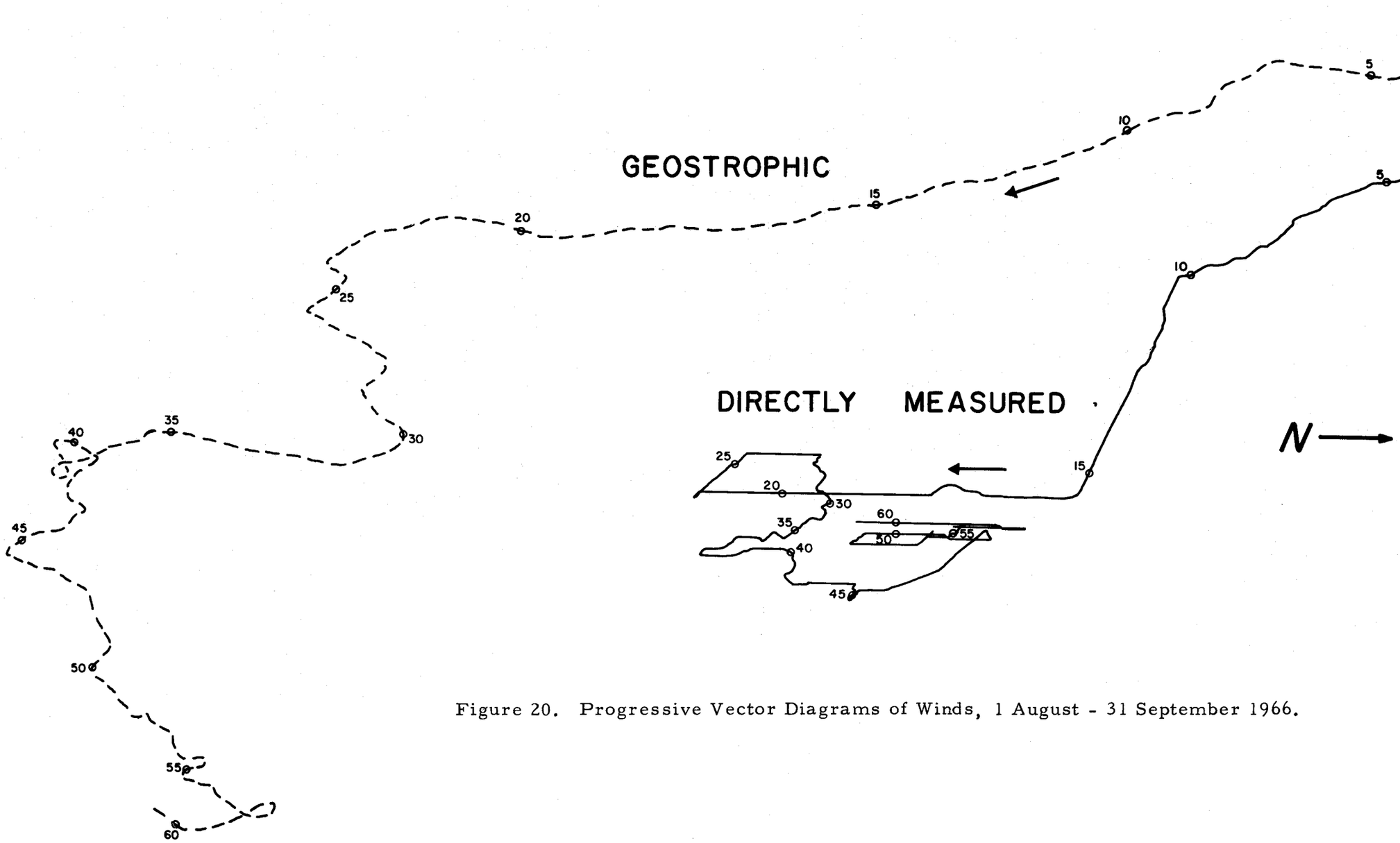

Figure 20. Progressive Vector Diagrams of Winds, 1 August - 31 September 1966.

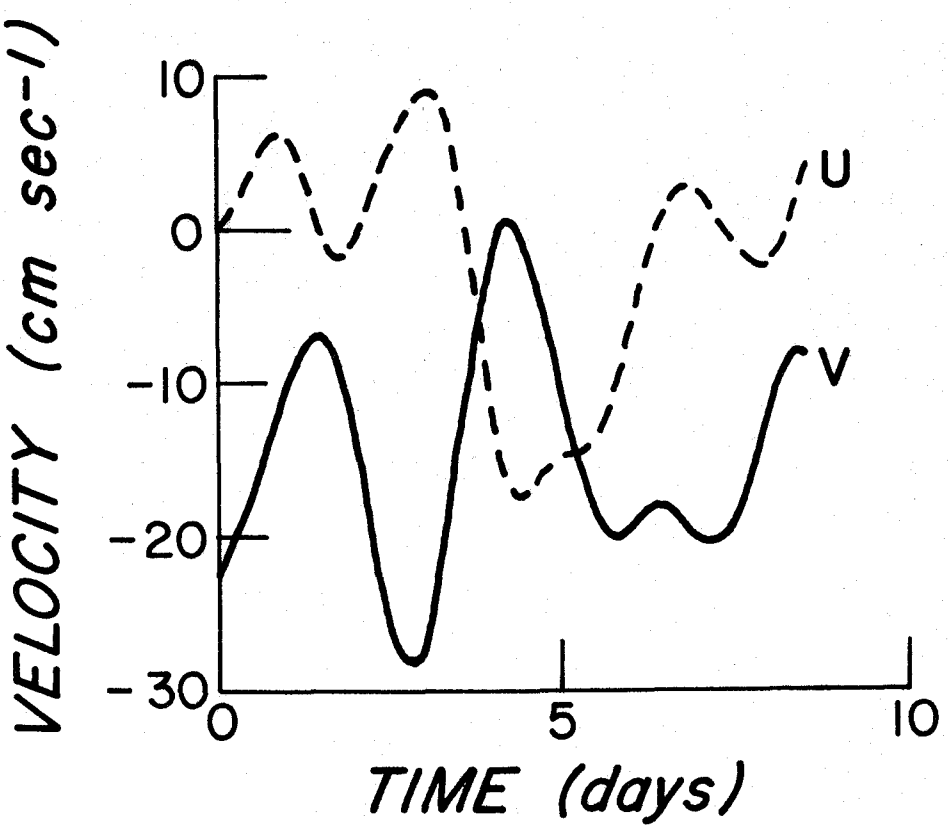

Figure 2la. Low-passed Horizontal Velocity Components Versus Time DB 5, 20 meters.

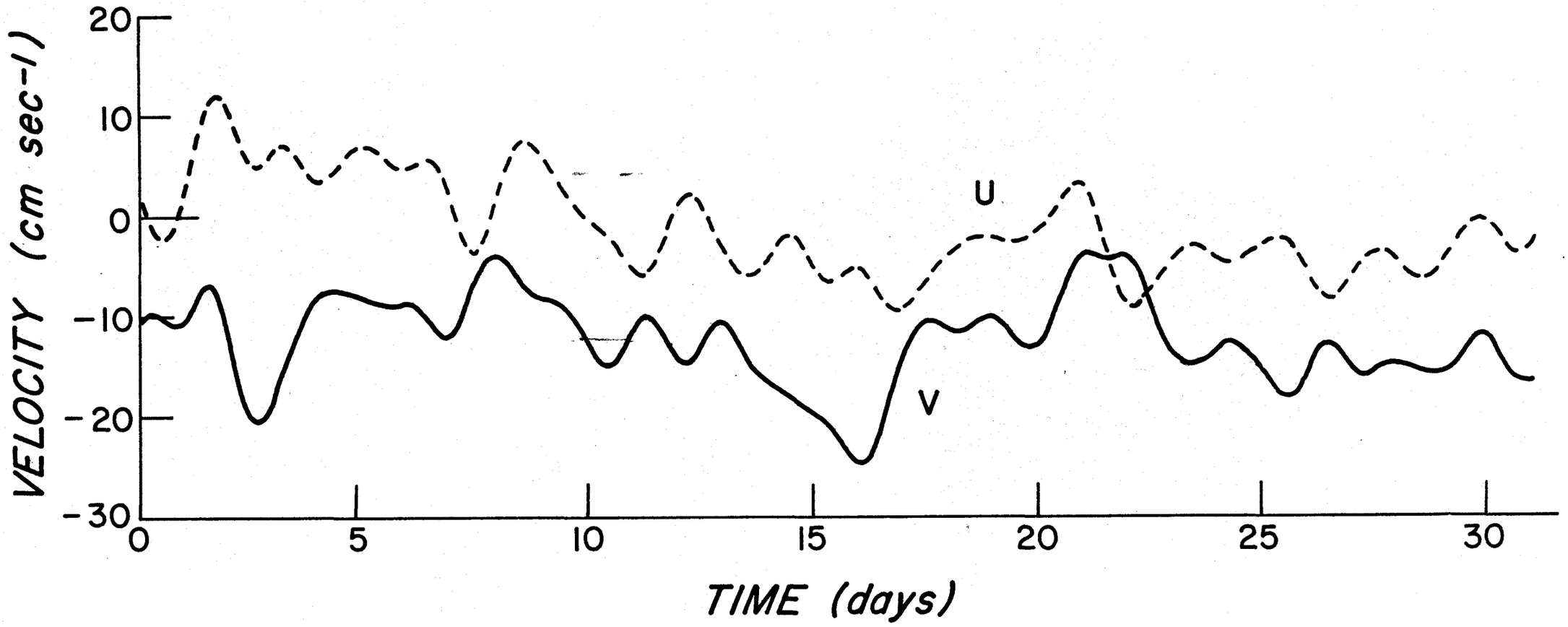

Figure 21b. Low-passed Horizontal Velocity Components Versus Time, DB 10, 20 meters.

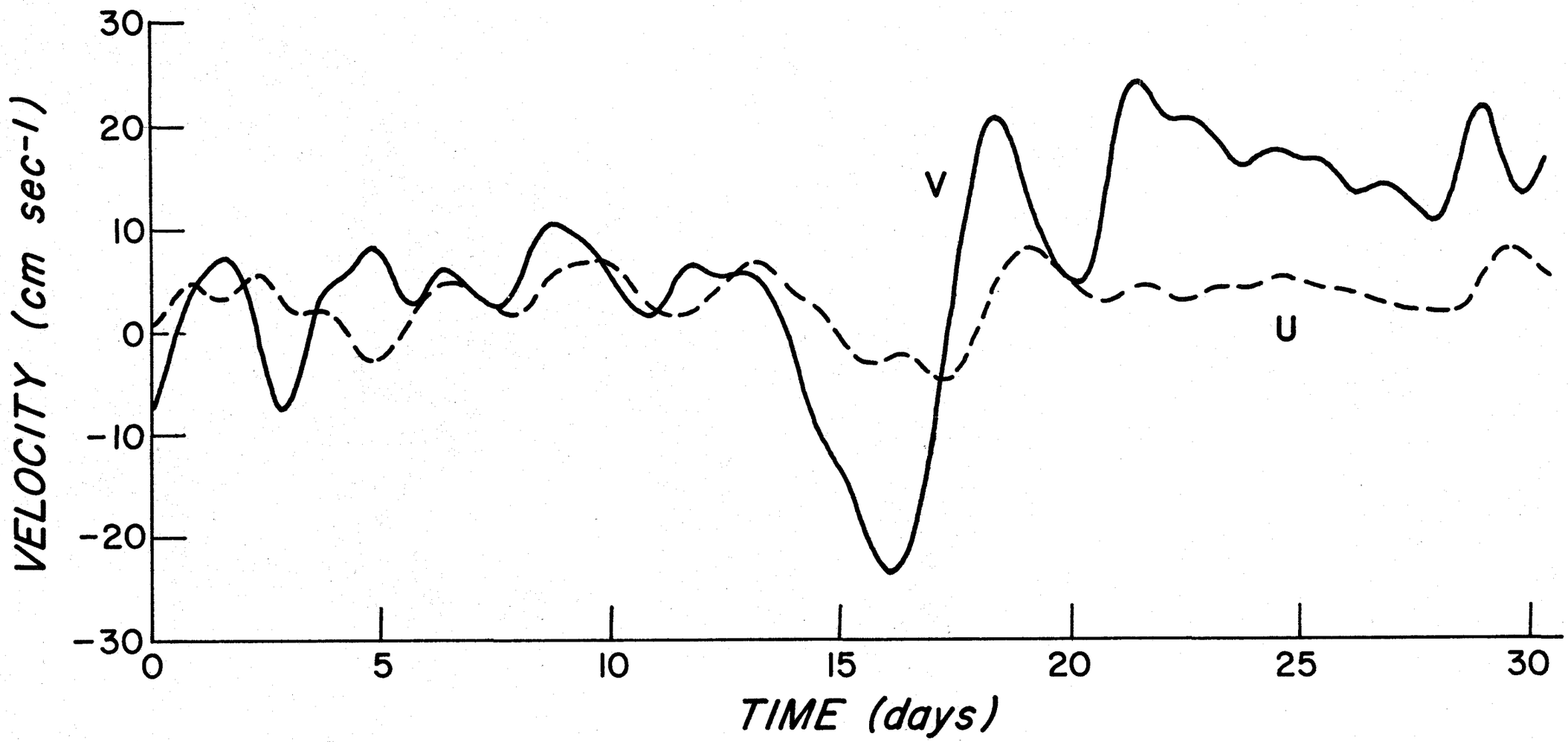

Figure 21c. Low-passed Horizontal Velocity Components Versus Time, DB 5, 60 meters.

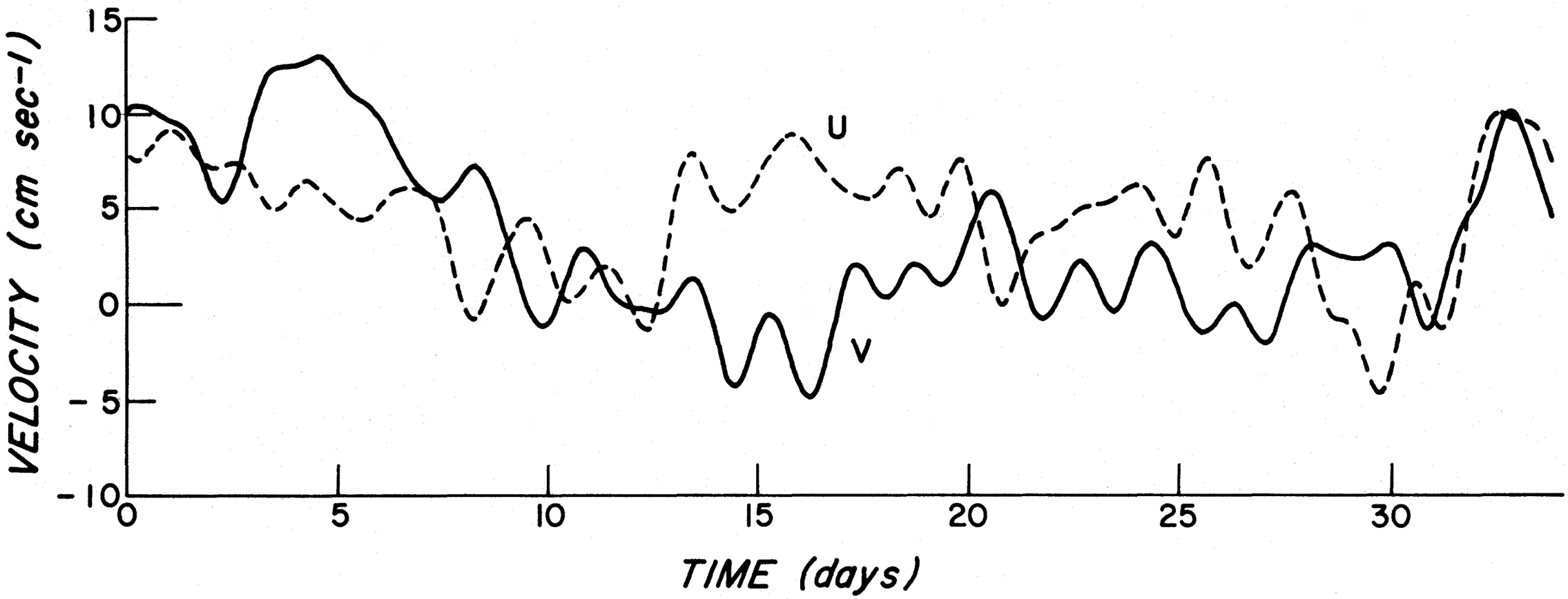

Figure 21d. Low-passed Horizontal Velocity Components Versus Time, DB 15, 60 meters.

In a similar fashion, the "low-passed" plots of temperature are shown in Figure 22. (The solid and the dashed curves correspond to DB 5 and DB 15 respectively, at 20 meters.) Again, the observer can estimate the mean and the long period variable components of the temperature field. The temperature was generally 2C° warmer at DB 15 than at DB 5. The dynamic range at both sites is of the order of 3C°. The most striking feature is the warming trend at the end of each record, which occurred over a period of about ten days and raised the temperature about 3C° at each site. The warming trend commenced about two weeks earlier at DB 15 than at DB 5. The warming trend occurred after the steady winds from the northwest shifted and weakened.

Figure 23 shows the "low-passed" plots of sea level and atmospheric pressure, beginning 23 August. Atmospheric pressure and sea level were not simply related; more precisely, sea level did not respond simply as an inverse barometer and had greater variability than atmospheric pressure. The diurnal variability in sea level is probably due to slight "leakage" of the diurnal tide through the numerical filter.

Figures 24a, b, c, and d show the histograms for the basic data of current speed, current direction, the northward component of velocity, and the eastward component of velocity for each recording current meter. The means, standard deviations, skewness, and kurtosis are listed in Table VIII. These graphs are quite self-explanatory; there are only two points which we wish to emphasize: most of the histograms are essentially unimodal and the extreme values of the speeds are generally of the order of 50 cm/sec while the means and the standard deviations of the velocity components are of the order of 0 to 20 cm/sec and 6 to 17 cm/sec, respectively.

Figure 25 displays the histograms of the velocity-differences (or essentially shears) of hourly averages for those records which ran usefully long. Figures 25a and b show the histograms of horizontal velocity-differences at 20 meters, between DB 5 and DB 10, and at 60 meters, between DB 5 and DB 15, respectively. Figure 25c shows the histogram of the vertical velocity-differences between DB 5, 20 meters, and DB 5, 60 meters. The means and the standard deviations are also tabulated in Table IX; note that the various sample sets of velocity-differences are of non-uniform size. The maximum value of mean shear occurs in the vertical shear of the northward component at DB 5, which is of the order of $-5 \times 10^{-3}\,\mathrm{sec}^{-1}$; a geostrophic estimate of the vertical shear of the northward component from Figures 4 and 5 and the so-called thermal wind equation ($\frac{\partial V}{\partial z} \cong E\, f^{-1} s$: E is static stability, f is Coriolis parameter, and s is slope of frontal surface, i.e., pycnocline) yields a value of about $-2.5 \times 10^{-3}\ \mathrm{sec}^{-1}$. The mean horizontal shear in the northward component is about $-6 \times 10^{-6}\ \mathrm{sec}^{-1}$ and $+1 \times 10^{-6}\ \mathrm{sec}^{-1}$ between DB 5 and DB 10 at 20 meters and between DB 5 and DB 15 at 60 meters, respectively; i.e., anticyclonic and cyclonic vorticity occurred at 20 and 60 meters, respectively. The mean horizontal divergence in the eastward component is about $-7 \times 10^{-6}\ \mathrm{sec}^{-1}$ and $-1 \times 10^{-6}\ \mathrm{sec}^{-1}$ between DB 5 and DB 10 at 20 meters and between DB 5 and DB 15 at 60 meters, respectively, i.e., convergence occurred at both 20 and 60 meters. The variability in the velocity-differences is strikingly large and, from other analyses (especially spectral), appears to be principally associated with tidal and inertial motions.

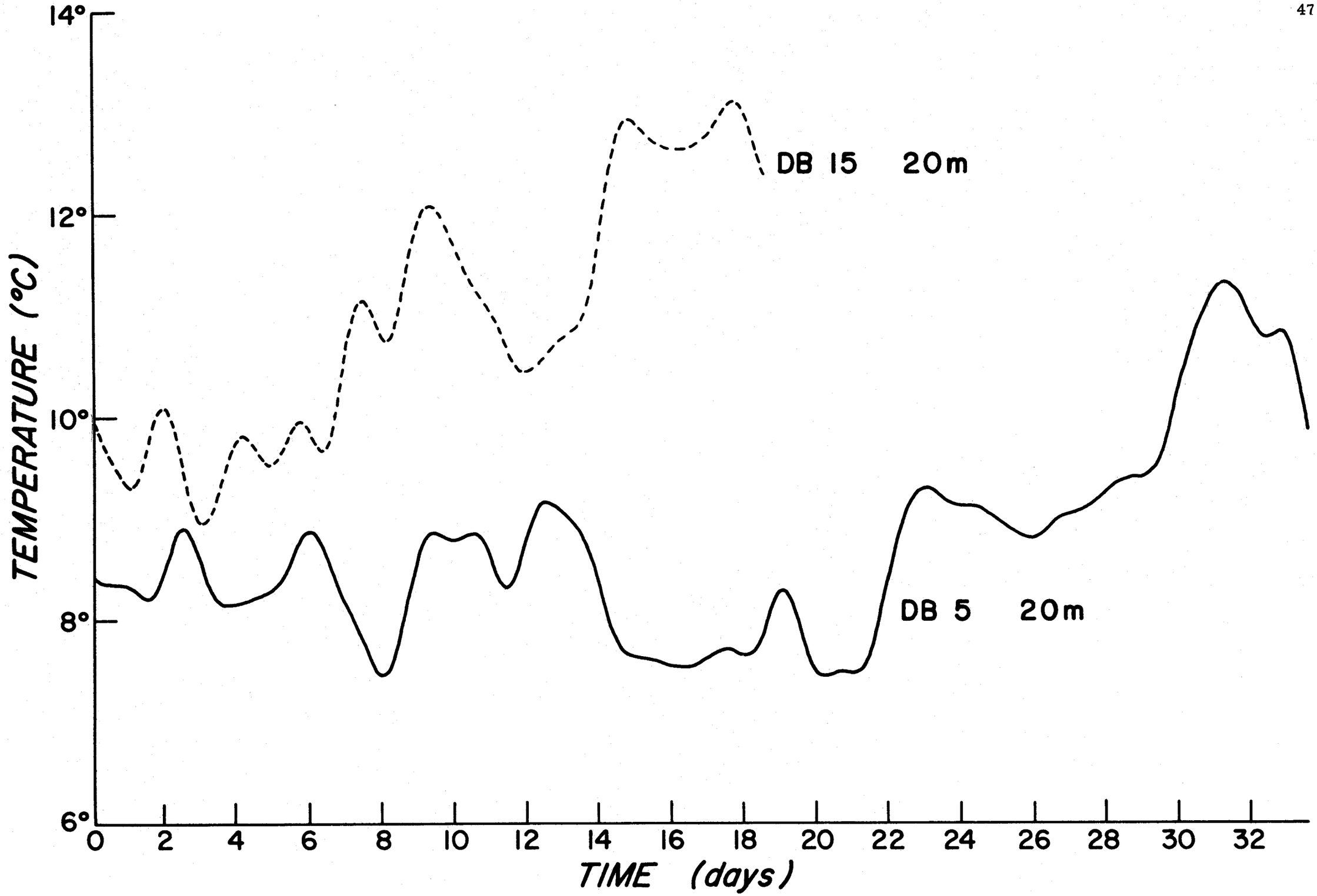

Figure 22. Low-passed Temperature Versus Time.

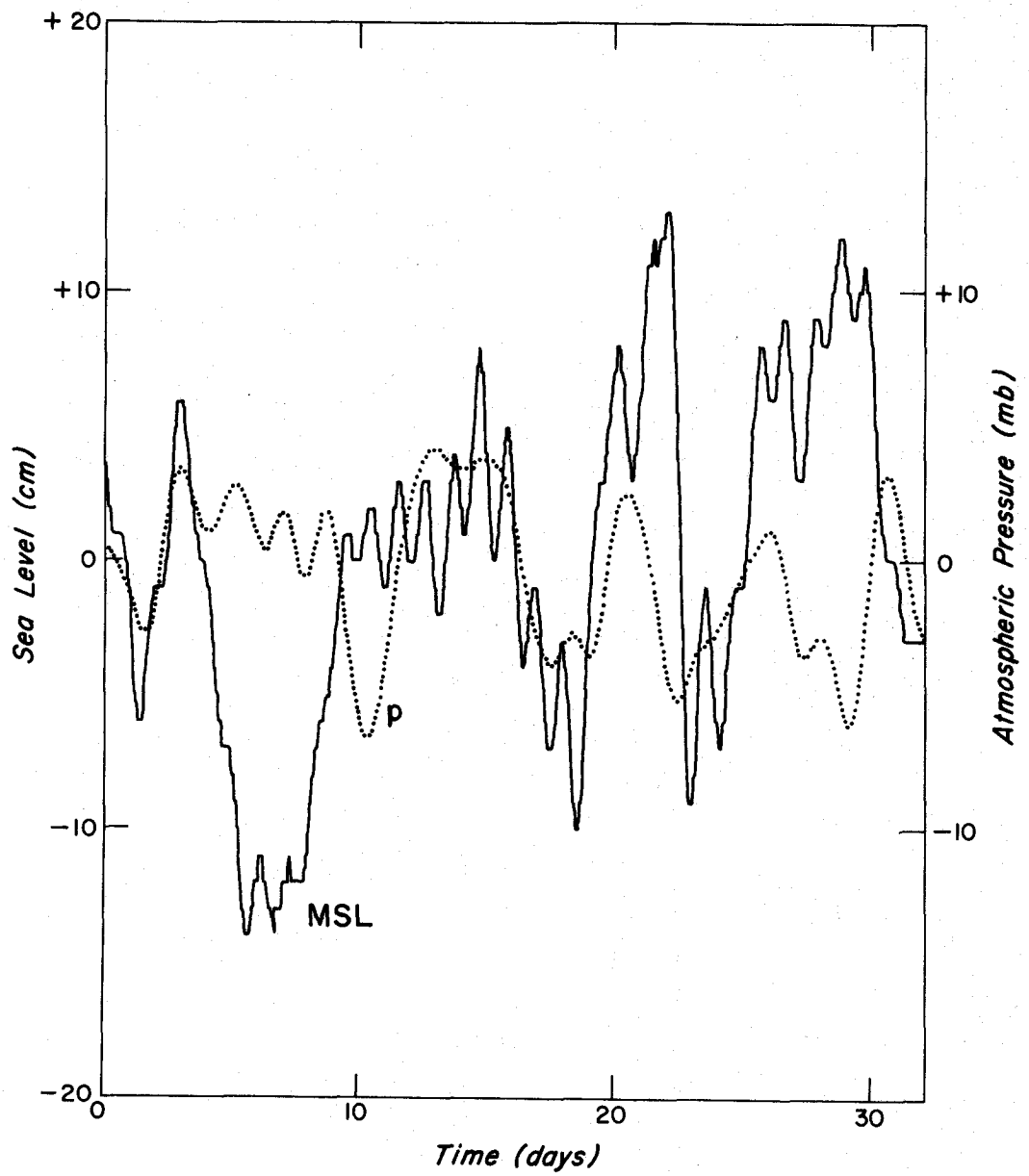

Figure 23. Low-passed Mean Sea Level (MSL) and Atmospheric Pressure (P) Versus Time.

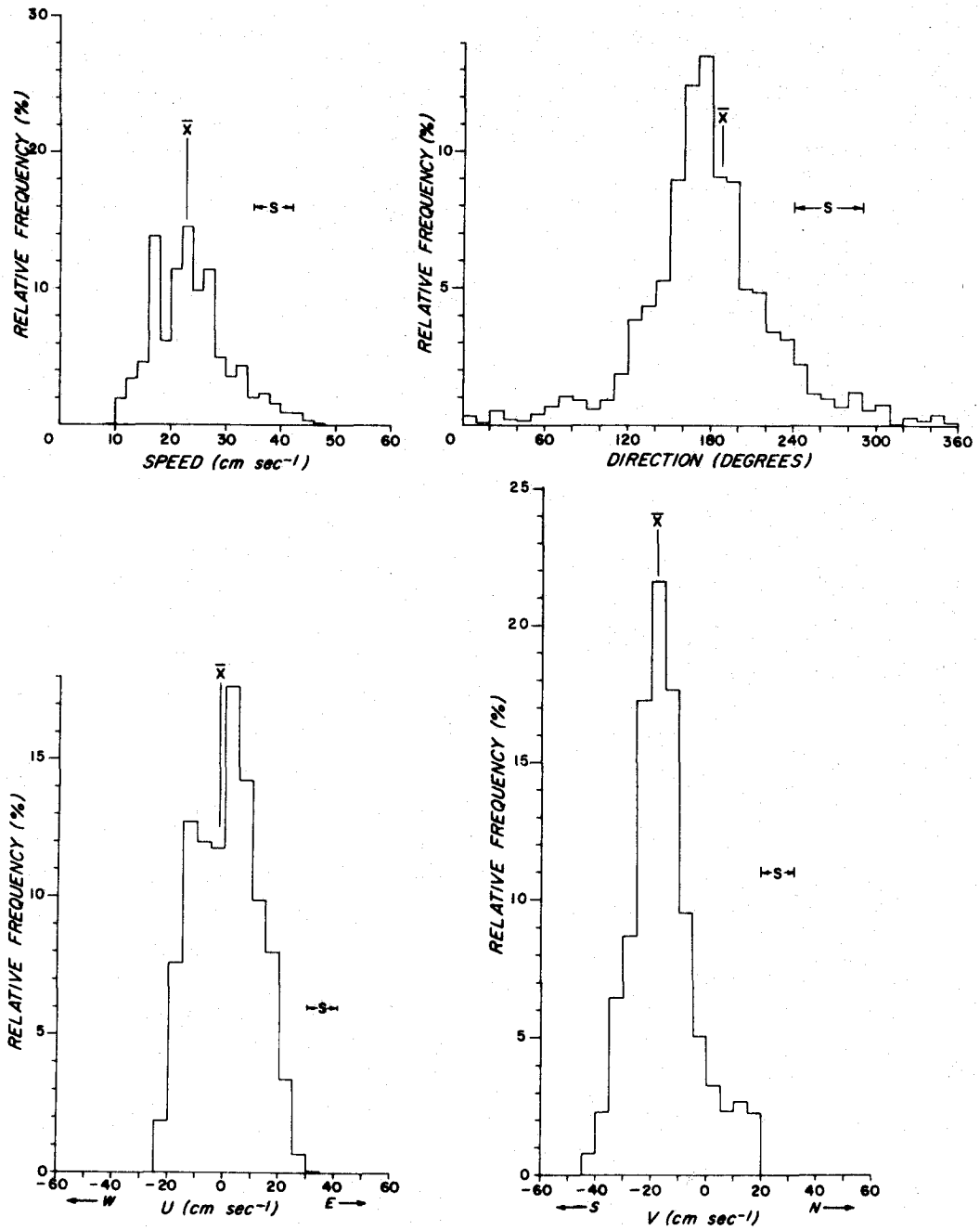

a

Figure 24a. Histograms of Speed, Direction, and Current Velocity Components, DB 5, 20 meters.

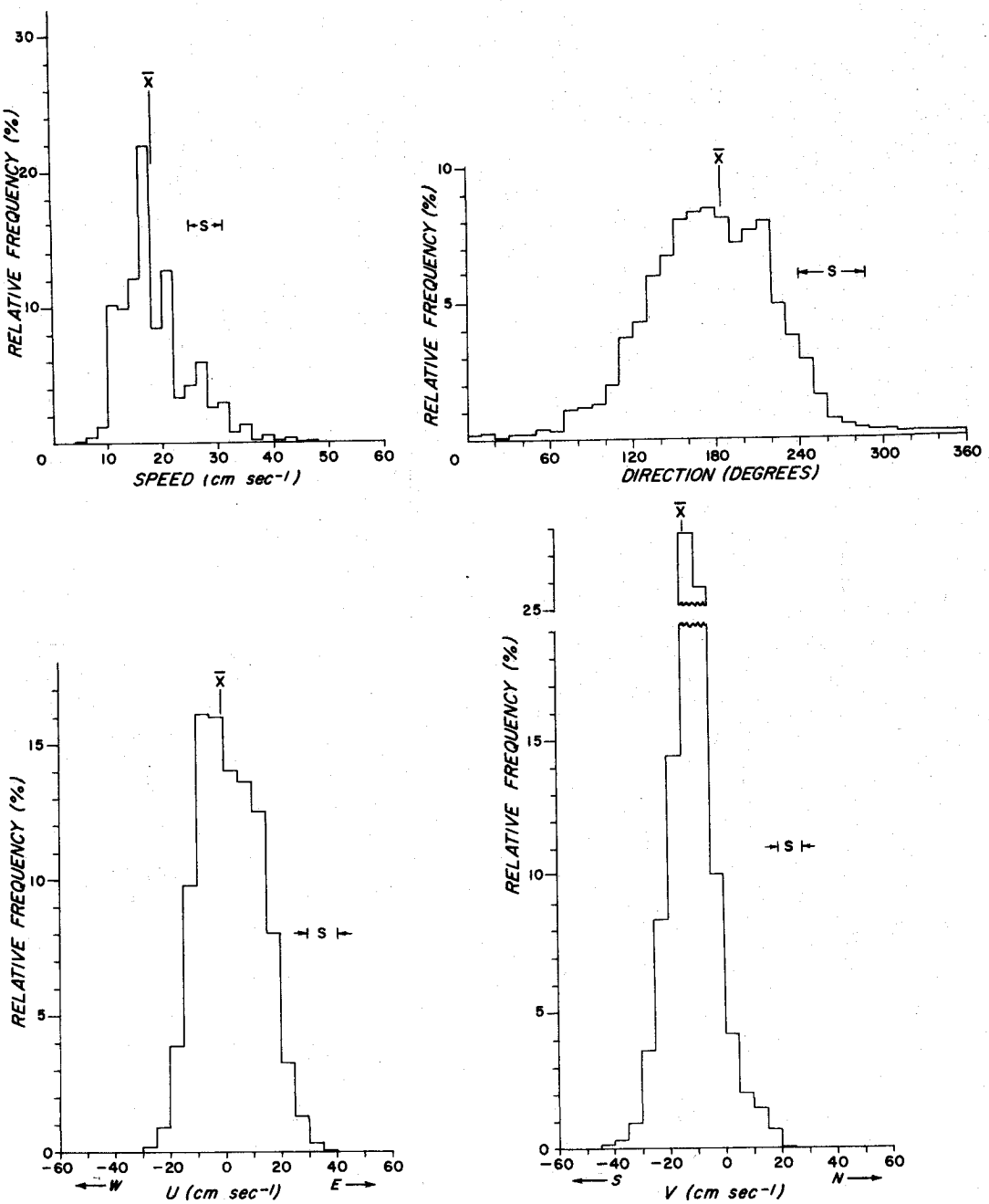

b

Figure 24b. Histograms of Speed, Direction, and Current Velocity Components, DB 10, 20 meters.

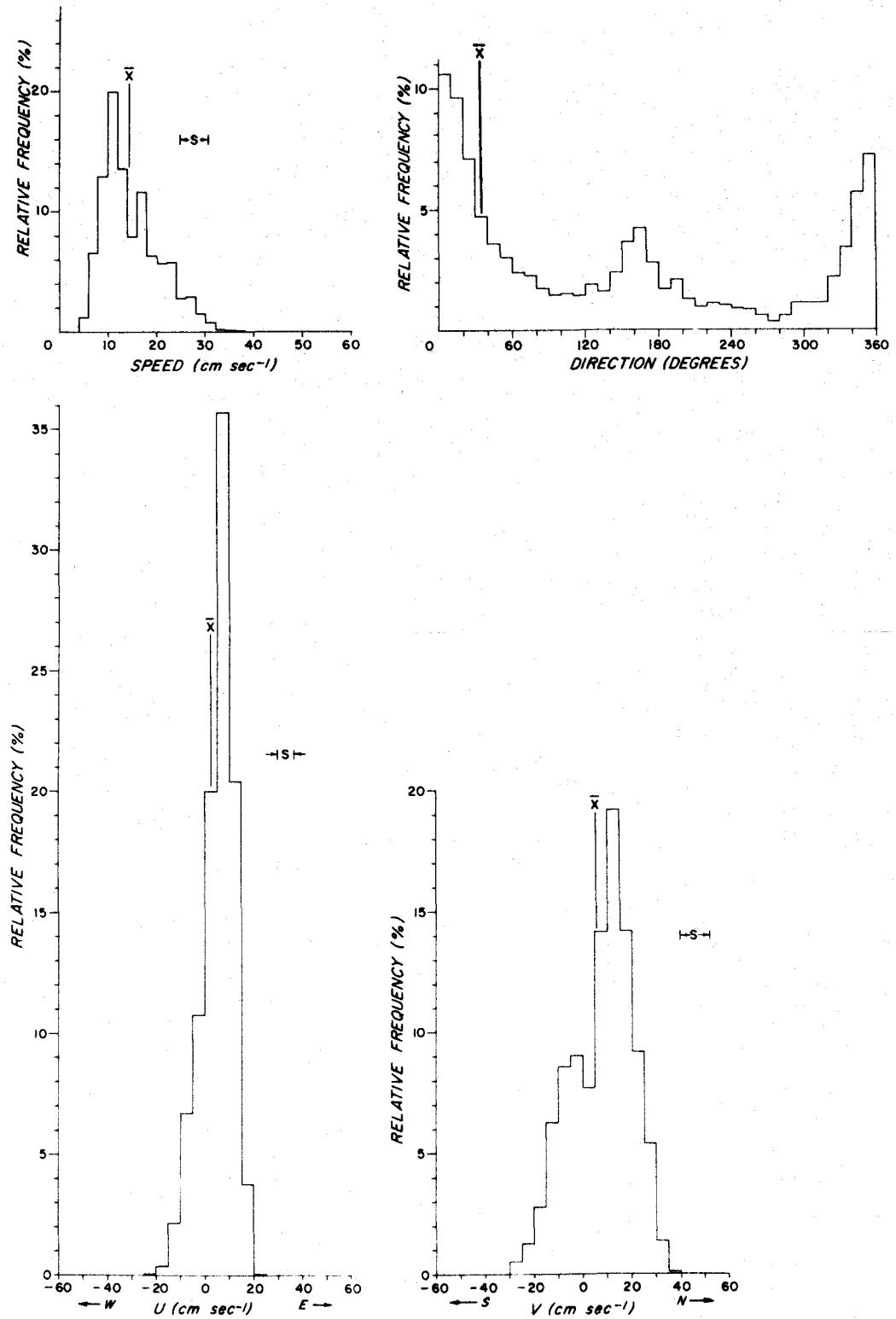

C

Figure 24c. Histograms of Speed, Direction, and Current Velocity Components, DB 5, 60 meters.

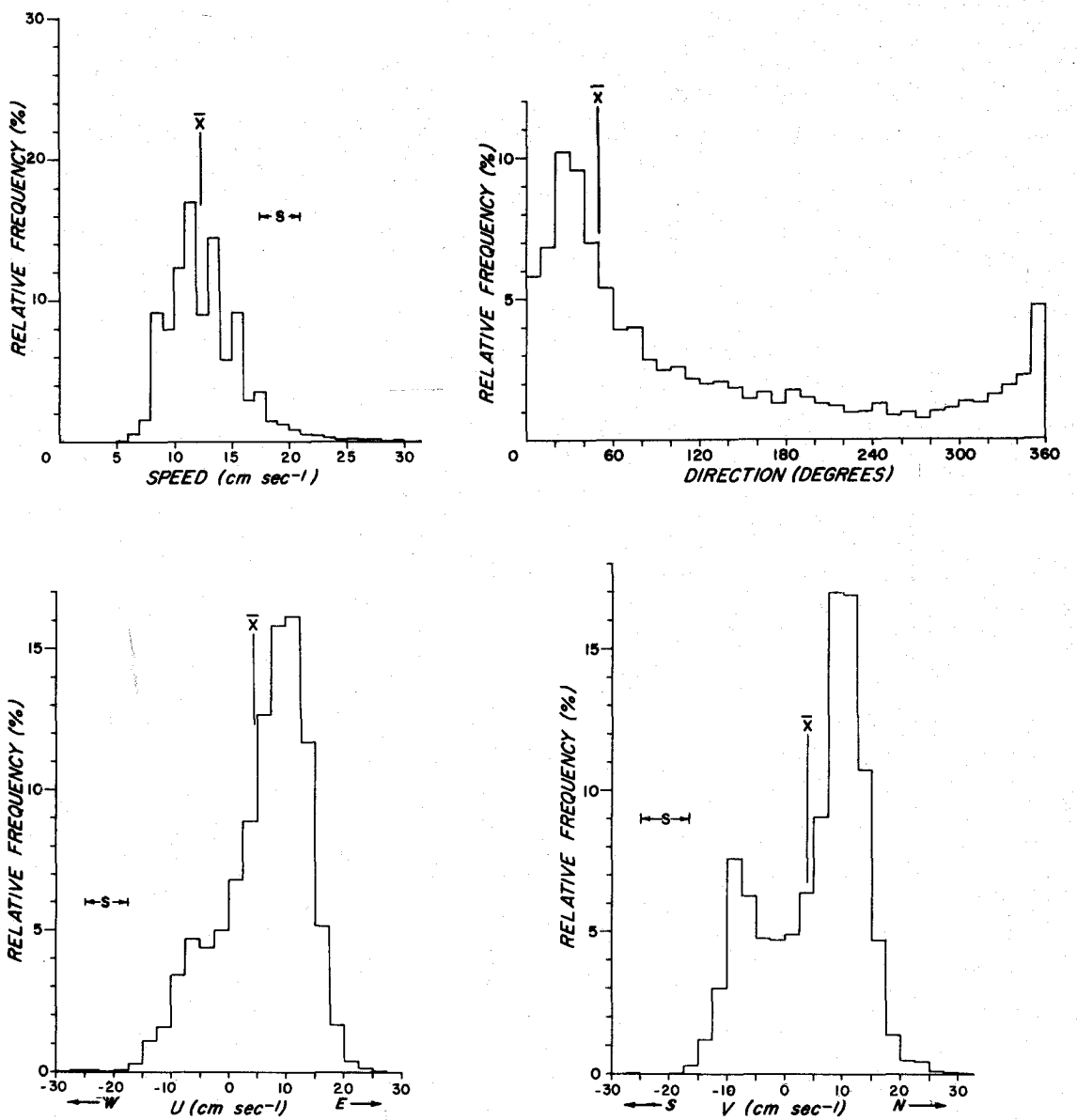

d

Figure 24d. Histograms of Speed, Direction, and Current Velocity Components, DB 15, 60 meters.

TABLE VIII

FIRST FOUR STATISTICAL MOMENTS OF SEVERAL VARIABLES

a. Current Statistics

Data Identification	Variable	No. of Samples	Mean	Variance	Skewness	Kurtosis
BRCM 1	Speed	2078	23.37	49.88	.63	3.10
DB 5, 20 m	U: Eastward		-2.09	129.44	.09	2.31
	V: Northward		-17.92	140.17	.65	3.53
	Direction Variability		27.73	308.06	3.85	26.90
	Tilt magnitude		2.13	1.40	.57	3.31
	Tilt direction		182.4			
	Mean Flow Direction*		187.2			
	Direction of Mean Flow		186.7			
BRCM 2	Speed	5229	14.26	33.94	.78	2.94
DB 5, 60 m	U: Eastward		2.68	44.83	-0.77	3.37
	V: Northward		5.05	159.78	-0.38	2.50
	Direction Variability		20.79	410.58	8.10	110.44
	Tilt magnitude		1.91	1.72	1.79	7.00
	Tilt direction		0.7			
	Mean flow direction*		185.6			
	Direction of mean flow		27.8			
BRCM 3	Speed	5337	18.40	39.81	1.11	4.64
DB 10, 20 m	U: Eastward		-0.77	120.75	.20	2.44
	V: Northward		-13.56	73.22	.20	4.24
	Direction Variability		40.71	575.69	3.74	28.64
	Tilt magnitude		.47	.35	.90	3.09
	Tilt direction		358.9			
	Mean flow direction*		36.8			
	Direction of mean flow		176.8			
BRCM 6	Speed	5734	12.46	11.29	1.29	6.04
DB 15, 60 m	U: Eastward		4.74	57.60	-0.76	3.21
	V: Northward		3.87	71.48	-0.53	2.35
	Direction Variability		89.25	4323.35	1.79	5.84
	Tilt magnitude		1.17	.44	.40	3.60
	Tilt direction		65.9			
	Mean flow direction*		49.9			
	Direction of mean flow		50.6			

*Mean flow direction computed in the same way as explained for mean tilt direction.

b. Wind Stress Statistics

Geostrophic Winds		241				
Aug.-Sept.	Tau X (Eastward)		0.6	1.0	-2.79	27.13
	Tau Y (Northward)		-0.9	4.0	.03	4.39
August	Tau X		0.7	1.0	.60	5.85
	Tau Y		-1.5	4.0	.45	5.50
September	Tau X		0.3	0.0	1.70	8.47
	Tau Y		-0.8	2.0	-0.71	6.70
Bluewater Winds		1464				
Aug.-Sept.	Tau X		0.3	1.0	-0.02	9.97
	Tau Y		-0.5	4.0	.06	5.15
August	Tau X		0.7	2.0	.70	3.50
	Tau Y		-1.0	4.0	.16	7.20
September	Tau X		0.4	0.0	1.75	6.86
	Tau Y		-0.5	2.0	-0.71	11.33

c. Temperature Statistics

BRT 1	5627	8.86	1.37	1.08	3.87
BRT 3	2894	10.71	2.35	.67	2.82
Hourly Temperature Differences (BRT 1 - BRT 3)	482	-2.37	3.49	-0.73	2.85

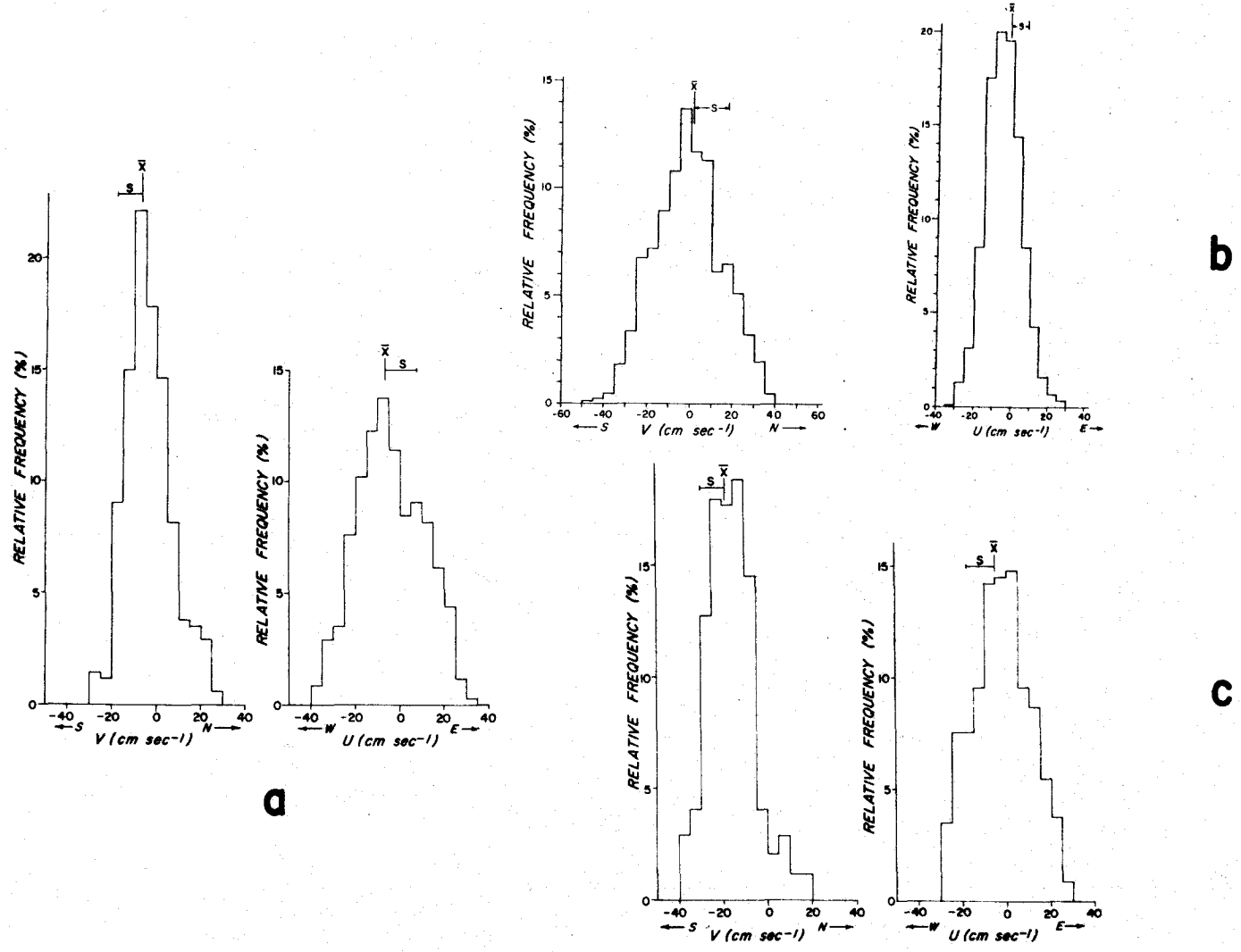

Figure 25. Histograms of Velocity Differences: a) DB 5-DB 10, 20 meters b) DB 5-DB 15, 60 meters c) DB 5, 20-60 meters.

TABLE IX

MEAN VELOCITY DIFFERENCES

(Based on Hourly Averages)

Sensor and Station Grouping	Mean ± Standard Deviation ΔU (cm/sec)	ΔV (cm/sec)	No. of Hourly Averages
DB 5, 20-60 meters	-5.0 ± 13.0	-18.6 ± 10.7	345
DB 5 - DB 10, 20 meters	-6.8 ± 14.6	- 5.7 ± 10.6	343
DB 5 - DB 15, 60 meters	-2.2 ± 9.5	+1.5 ± 15.8	860

Δ U: Eastward Velocity Difference

Δ V: Northward Velocity Difference

Figure 26 displays the histograms for temperature at the two thermograph sites; they are skewed towards high values. This skewness pattern is related to the fact that the thermographs were located near the base of the thermocline. The temperature extremes are indicative of rather large vertical oscillations, of the order of 10 to 20 meters, as can be estimated from the vertical profiles of temperature shown in Figure 8.

Figure 27 presents the histogram for the temperature difference between the two thermographs, viz DB 5, 20 meters, minus DB 15, 20 meters, based on hourly averages. On the average, it is 2 C° cooler at DB 5 than at DB 15, but extreme values of 8C° cooler and 3C° warmer occur.

Meter Tilt and Current Direction Variability

Figures 28 through 31 give the histograms of tilt direction and magnitude and current direction variability; further associated statistics are listed in Table VIII. These quantities are presented together as a measure of sensor string stability and meter performance. (In the tilt direction histograms, the direction was entered as 360° when tilt magnitude was zero. These values were ignored when the mean direction was computed by the formula $\bar{\theta} = \tan^{-1}(\Sigma_i M_i \mathrm{SIN}(\theta_i) / \Sigma_i M_i \mathrm{COS}(\theta_i))$, where θ_i is i^{th} tilt direction and M_i is i^{th} tilt magnitude.) In general, mean tilt direction corresponded with the direction of the mean flow. A notable exception is the value for DB 10, 20 meters, where mean tilt direction was northward (in opposition to the mean flow), which may somehow reflect strong northerly flow in the lower layer, or it may indicate that because the tilt magnitude was relatively small there, the mean tilt direction may have little significance. The mean tilt magnitude ranged from 0.5° to 2°; such tilt values are considered negligibly small for current meter calibrations and for concern over spurious accelerations due to mooring motions. The average direction variability ranged from 20° to 70°, and extreme values ranged from 180° to 240°. Two comments are appropriate based on the direction variability analysis:

i) There are probably motions of physical significance at time scales less than our sampling interval of 10 minutes.

ii) If we had wanted to study a variable flow, DB 15, 60 meters, would rate as an excellent site selection. (This remark is supported by the other current statistics for this location.)

Winds

Figure 32 depicts the histograms for the directly-measured and the geostrophic winds. Interestingly, though the PVD's for the two wind sets are notably different in detail, both the means and the standard deviations for the wind sets are quite similar. The wind speed was greater than or equal to the so-called critical value of 7 to 8 m/sec for about 46% of the directly-measured values and 70% of the geostrophic values. The greatest value of directly-measured wind speed was 21 m/sec and that of geostrophic wind speed was 23 m/sec. The histogram of the directly-measured wind is skewed to the north, and that of the geostrophic winds is skewed to the south, just as we would expect from the PVD's.

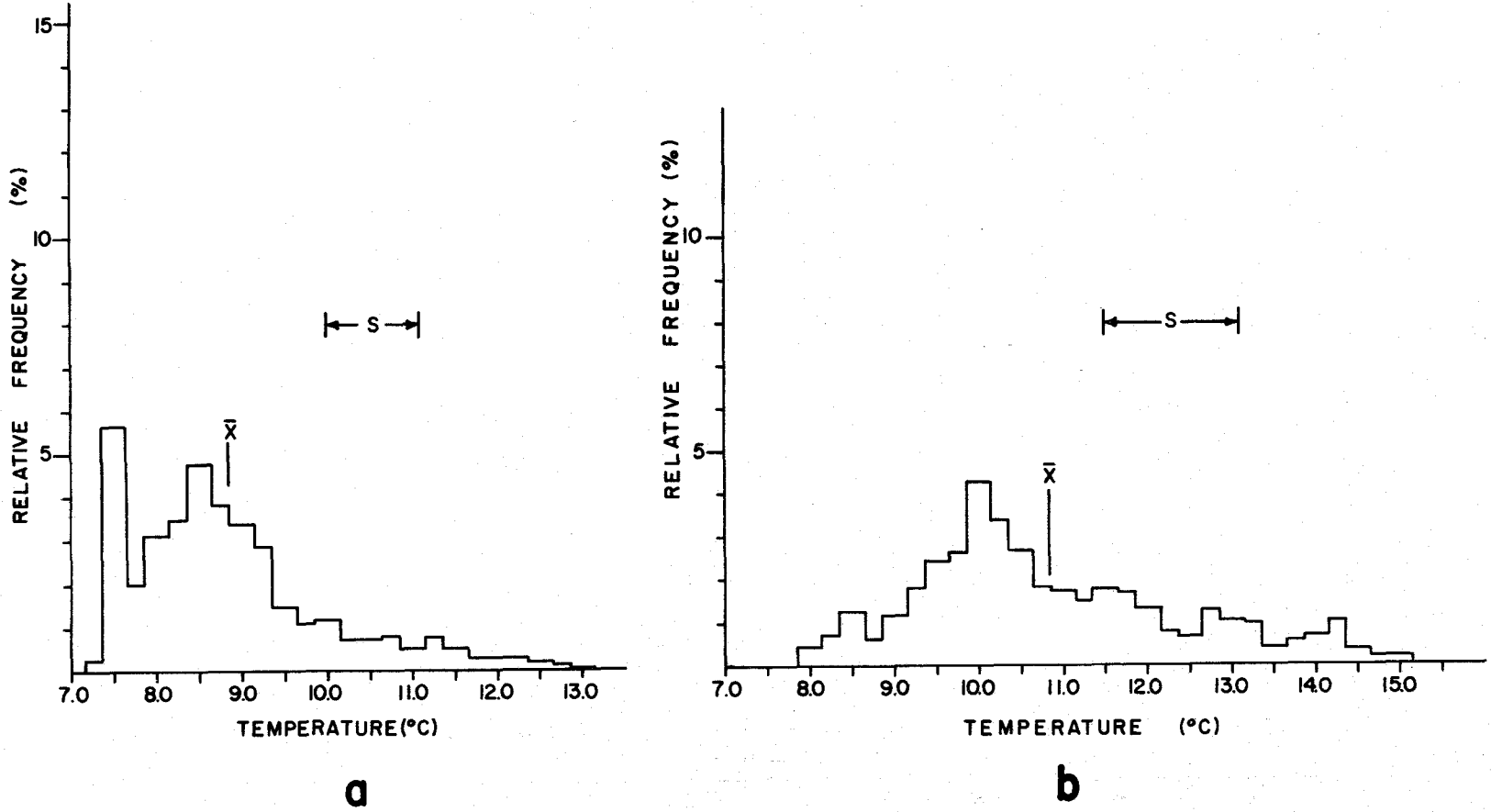

Figure 26. Histograms of Temperatures: a) DB 5, 20 meters b) DB 15, 20 meters.

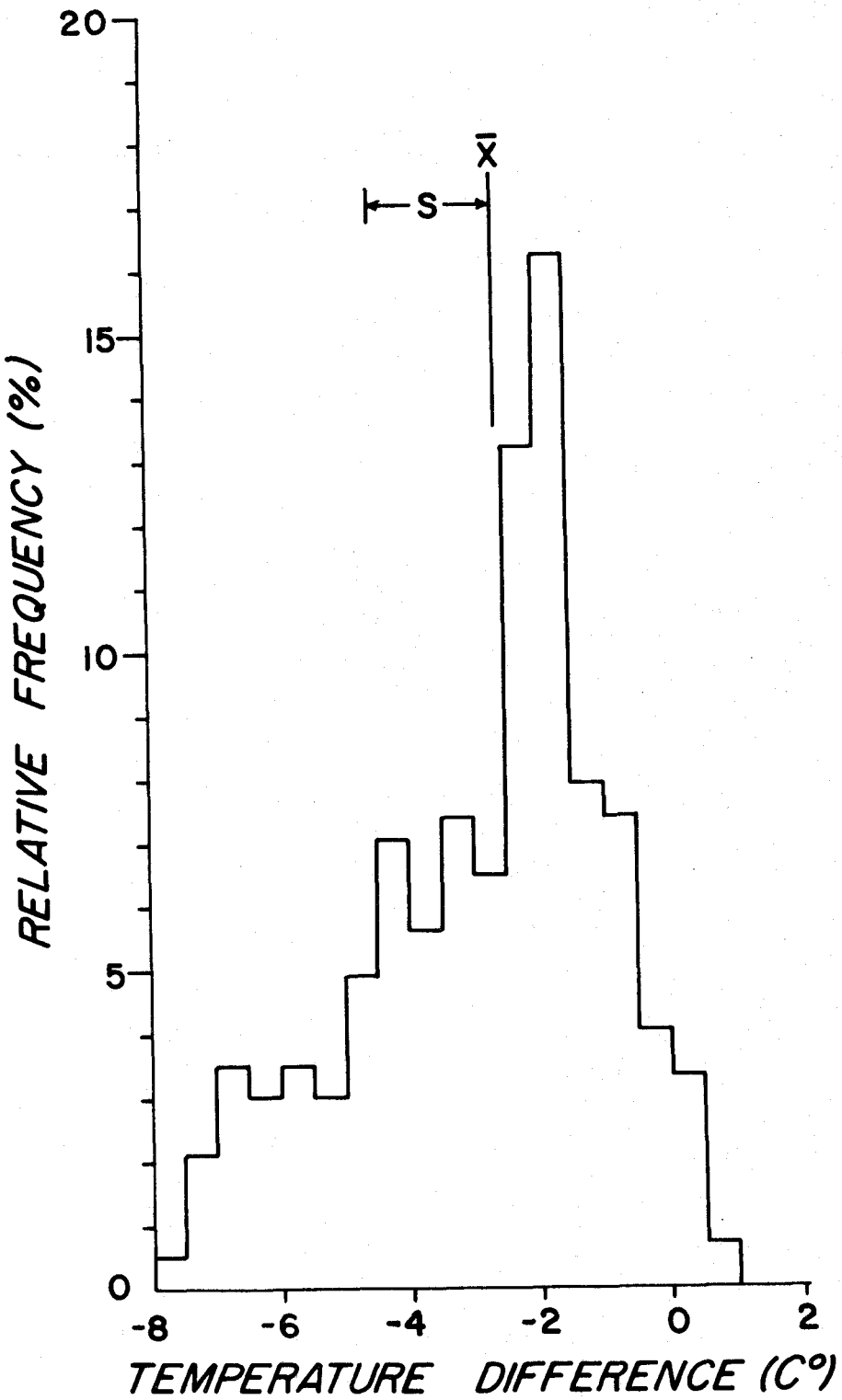

Figure 27. Histogram of Temperature Differences: a) DB 5-DB 10, 20 meters.

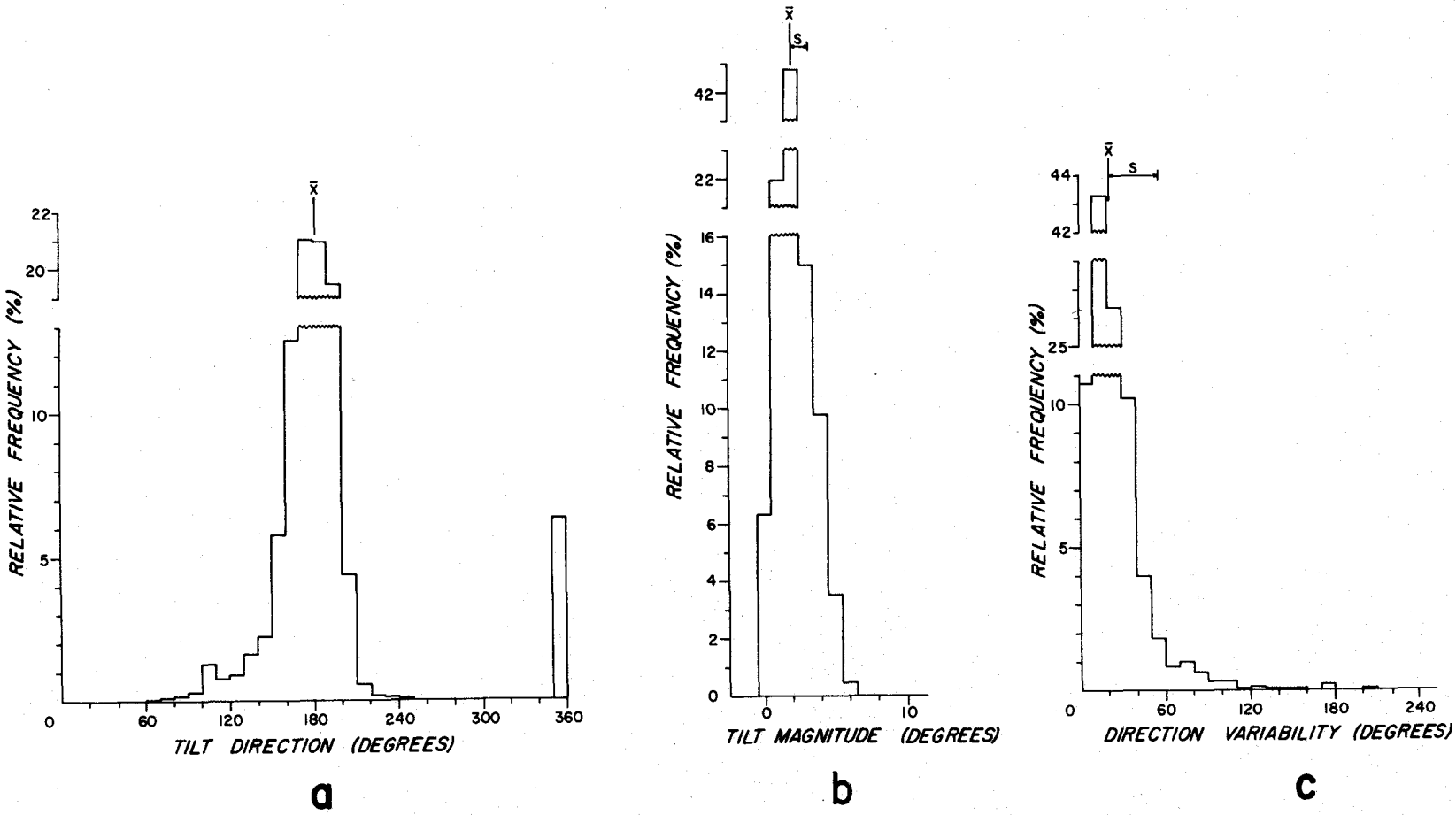

Figure 28. Histograms of Meter Tilt and Current Direction Variability, DB 5, 20 meters: a) Tilt direction b) Tilt magnitude c) Current direction variability.

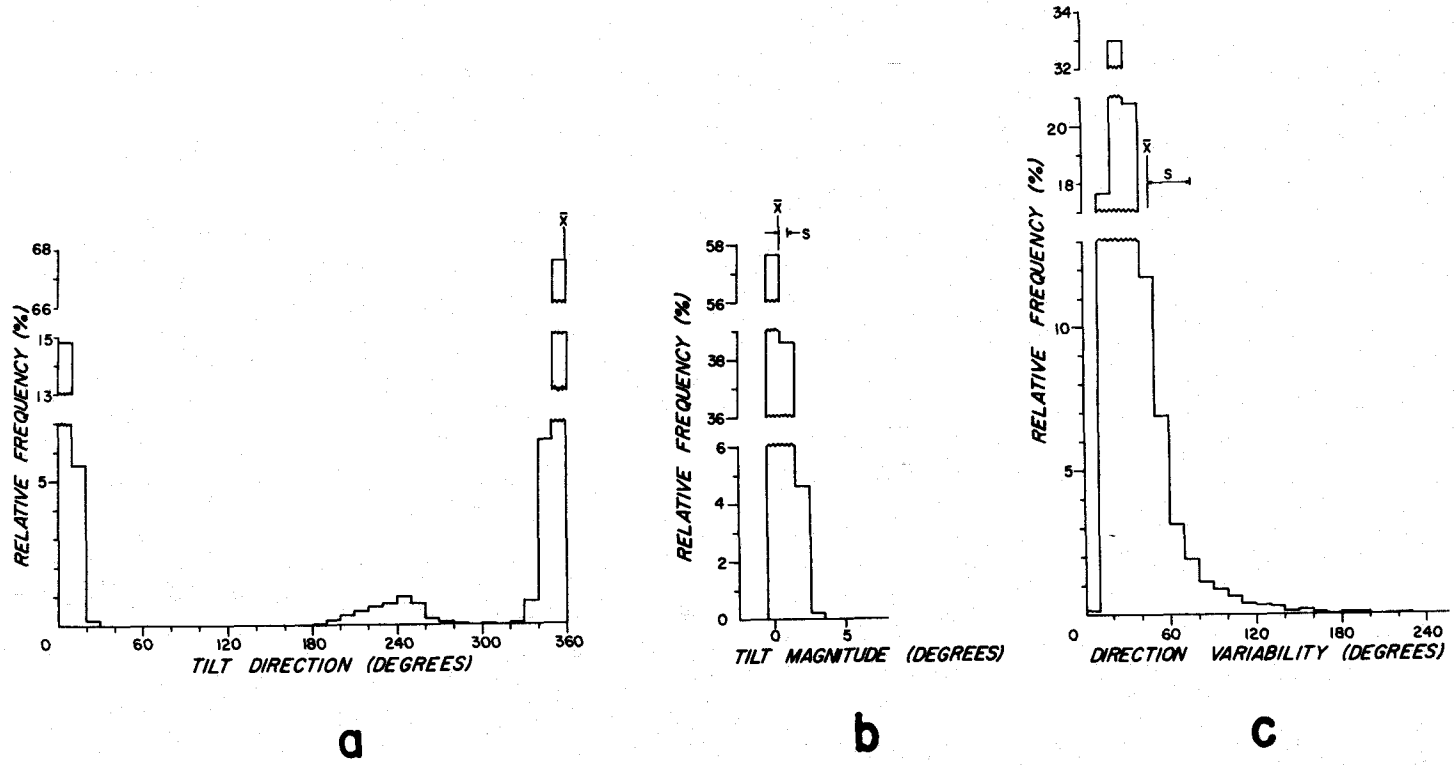

Figure 29. Histograms of Meter Tilt and Current Direction Variability, DB 10, 20 meters: a) Tilt direction b) Tilt magnitude c) Current direction variability.

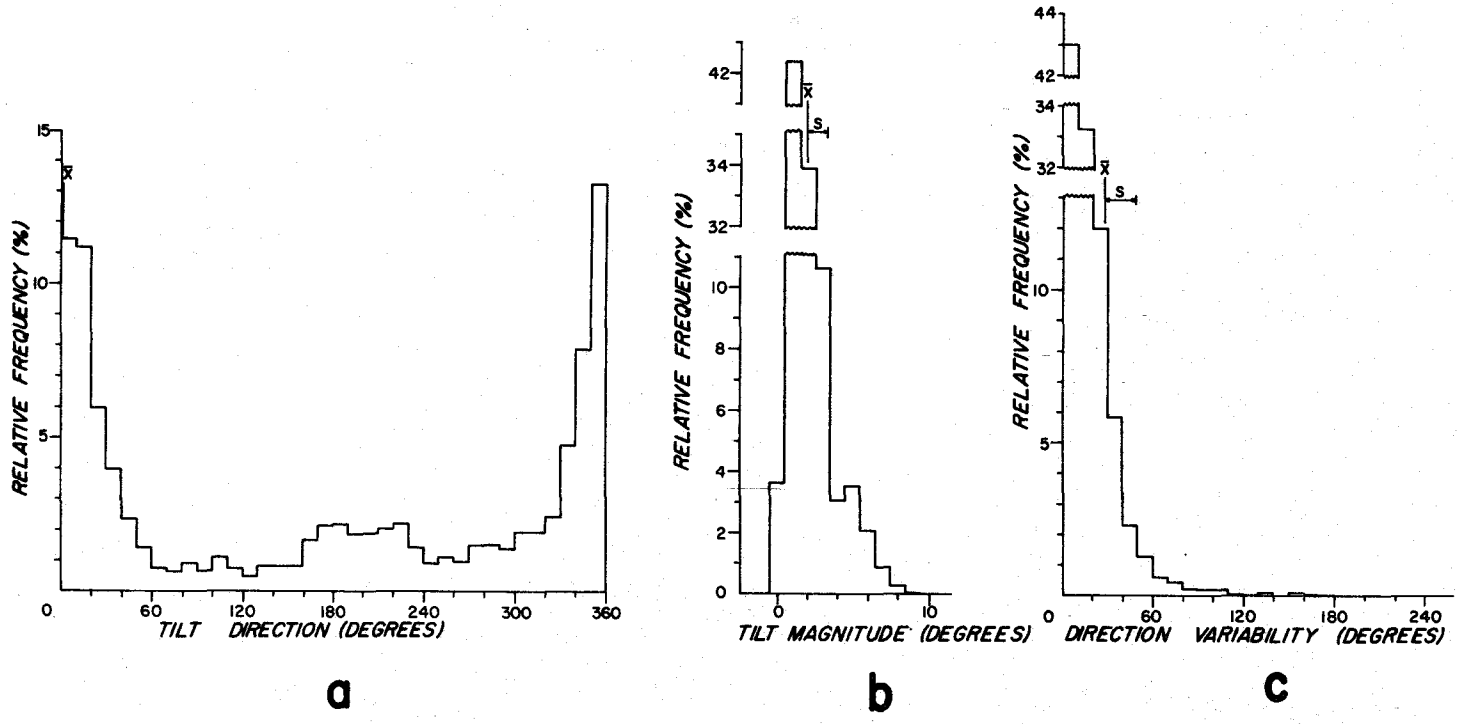

Figure 30. Histograms of Meter Tilt and Current Direction Variability, DB 5, 60 meters: a) Tilt direction b) Tilt magnitude c) Current direction variability.

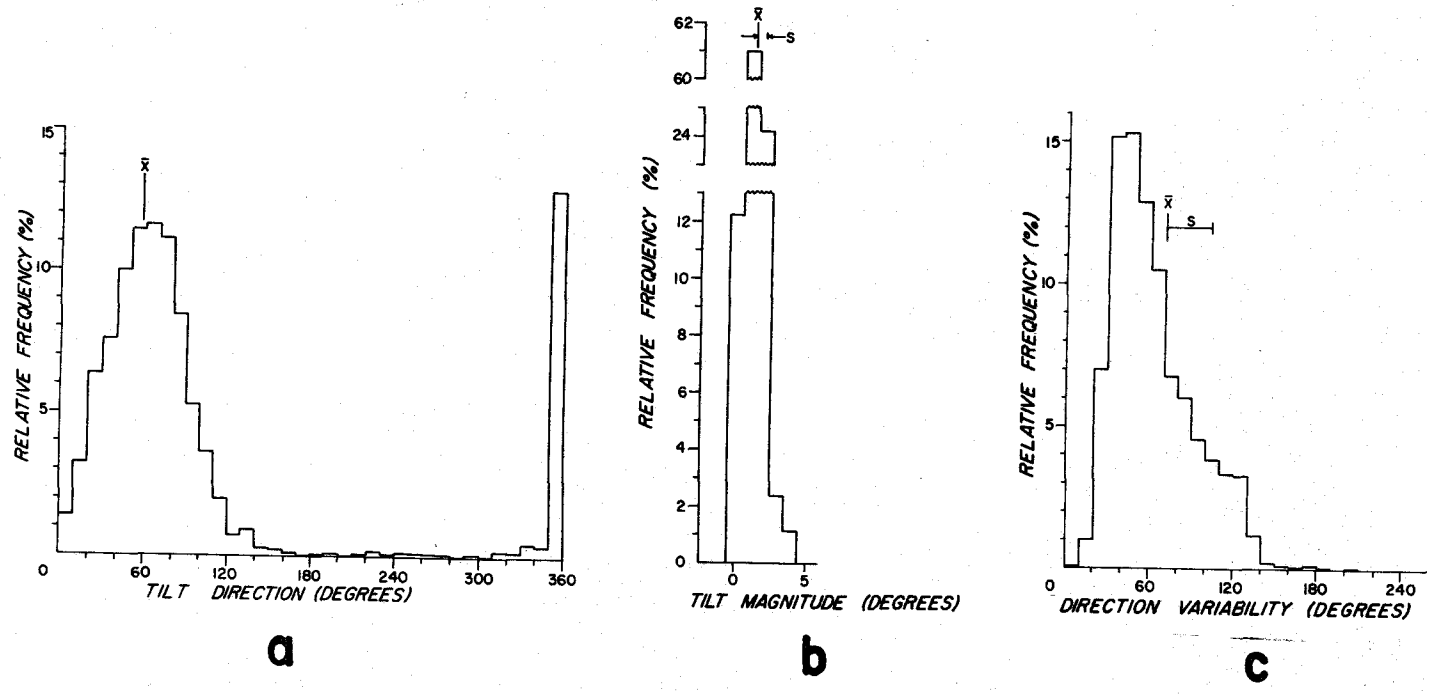

Figure 31. Histograms of Meter Tilt and Current Direction Variability, DB 15, 60 meters: a) Tilt direction b) Tilt magnitude c) Current direction variability.

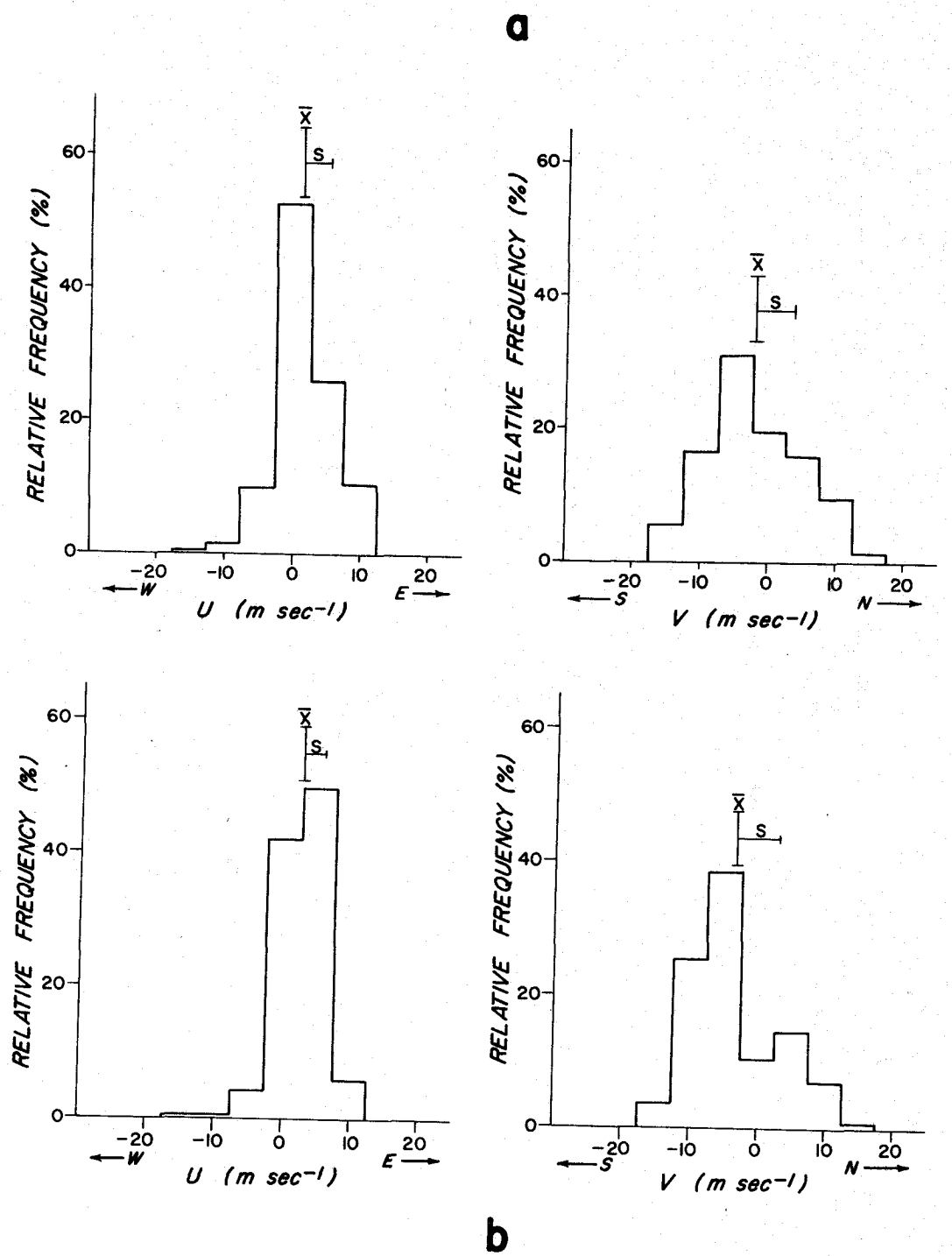

Figure 32. Histograms of Wind Velocity, Velocity Components: a) Directly Measured Winds b) Geostrophic Winds.

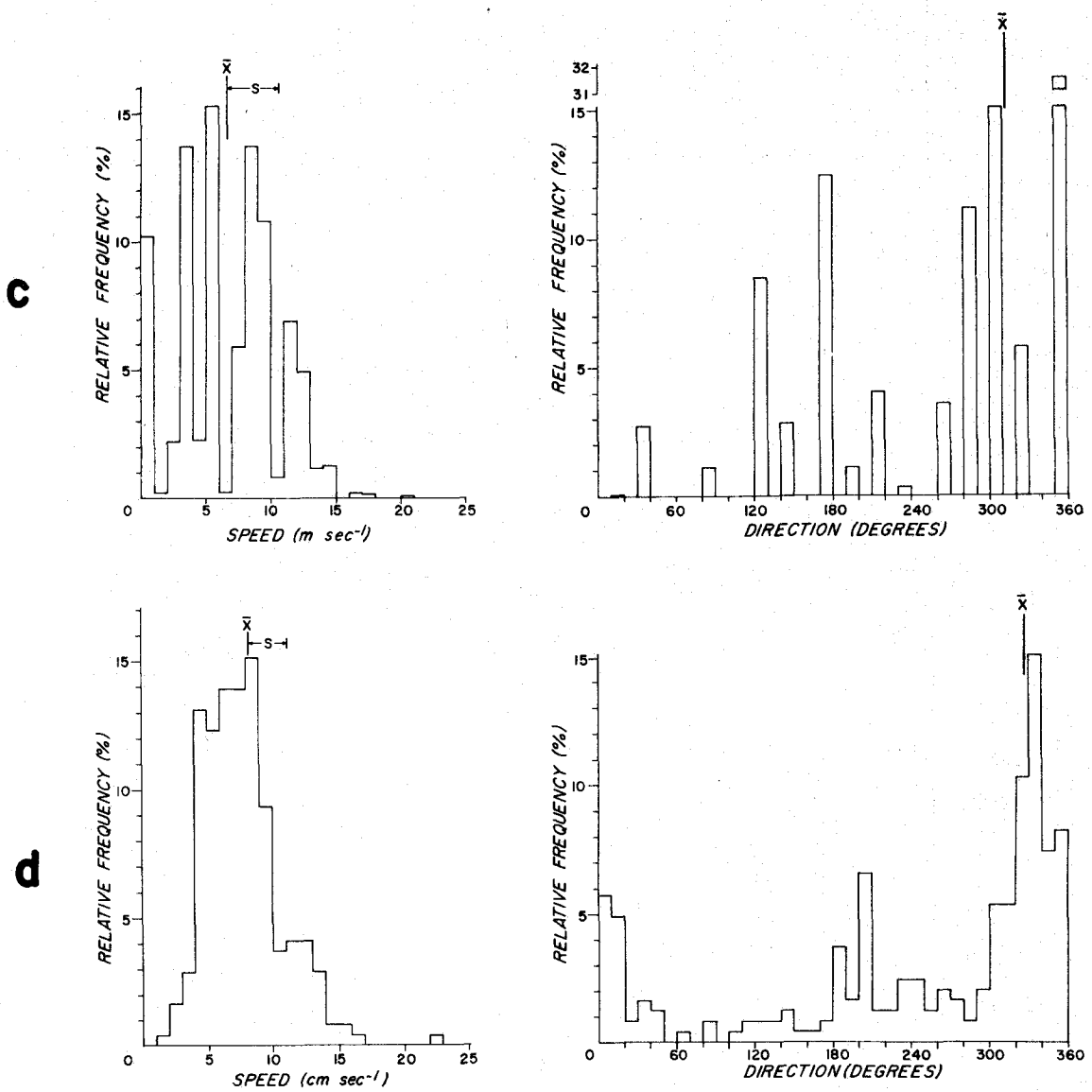

Figure 32. Histograms of Wind Velocity, Speed and Direction: c) Directly Measured Winds d) Geostrophic Winds.

Figure 33 shows wind stress for August and September, computed from geostrophic and directly-measured winds. The wind stress formula used is $\tau = \rho_a C |\vec{V}| \vec{V}$, where ρ_a is air denity (assumed equal to 1.2×10^{-3} c. g. s.), $C = 2.4 \times 10^{-3}$ is the dimensionless drag coefficient, and V is wind velocity in cm/sec. Since a high percentage of the wind speed values were greater than the so-called critical wind speed value of 7 to 8 m/sec (see Figure 33), we used the above value of C throughout the windstress calculations. It would have been a simple matter to have used the value of $C = 1.5 \times 10^{-3}$ for stress calculations at subcritical values of the wind speed, but we are inherently suspicious of any such refinement of the stress calculations which does not take due regard of the air column's static stability, the state of the sea surface, etc. The curves general agreement is rather good, especially in the northward component and when it is considered that the geostrophic winds are "regional winds" while the directly-measured winds are "local winds" which are complicated by coastal effects. The mean wind stress over the sample duration is quite small (see Table VIII), but there are appreciable magnitudes on a time-scale of roughly a week.

Daily Kinetic and Potential Energy and/or Variance

Figures 34a, b, c, and d show the daily total kinetic energy (KE) per unit mass, or one-half of the variance, for each of the current meters. Three curves have been plotted: the solid curve, KE1, corresponds to the average KE of the 10-minute samples; the long-dash curve, KE2, corresponds to the average KE of the hourly averages, and the short-dash curve, KE3, corresponds to the KE of the daily averages. The difference between KE1 and KE2 relates to energy at time scales of 10 to 60 minutes; the difference between KE2 and KE3 relates to energy at time scales of 1 to 24 hours. With a modest amount of imagination, the viewer can interpret the KE curves as indicators of the occurrence and the intensity of oceanographic storms and of epochs of relative quiescence. For instance, on the third and fourth days a storm occurred at all sensor sites; on the 20th day, a storm occurred at DB 5, 60 meters and DB 10, 20 meters, but not at DB 15, 60 meters. (Note: DB 5, 20 meters was inoperable by this date.) If the tidal flows were of uniform amplitude and were predominant, one might expect the difference between KE2 and KE3 to be constant; large variation in this difference may indicate the occurrence of large inertial motions. The difference between KE1 and KE2 is generally small, suggesting that there is not significant energy at time scales less than one hour in our data. These curves can be used to estimate the effective "decay rate": by visual inspection of the decay of large peaks, the "e-folding time" is of the order of a day, corresponding to an effective damping coefficient of the order of 10^{-5} sec^{-1}, which is a value commonly found in oceanographic data.

In Figures 35a, b, c, and d the kinetic energy per unit mass is resolved into northward and eastward components. Since KE1 minus KE2 was shown to be very small in the preceding figure, only KE2 and KE3 have been shown in this figure. One observation is that most of the storm energy is found in the northward component, with the exception of DB 15, 60 meters, perhaps because the mean flow is to the northeast at the latter site.

Figures 36a - f show the kinetic energy per unit mass for the velocity components of the directly-measured and the geostrophic wind fields, broken into the August and September sets. In this case, KE2 is the average kinetic energy for the hourly and six-hourly values of the winds for the directly-measured and the geostrophic winds, respectively. Again, these curves give

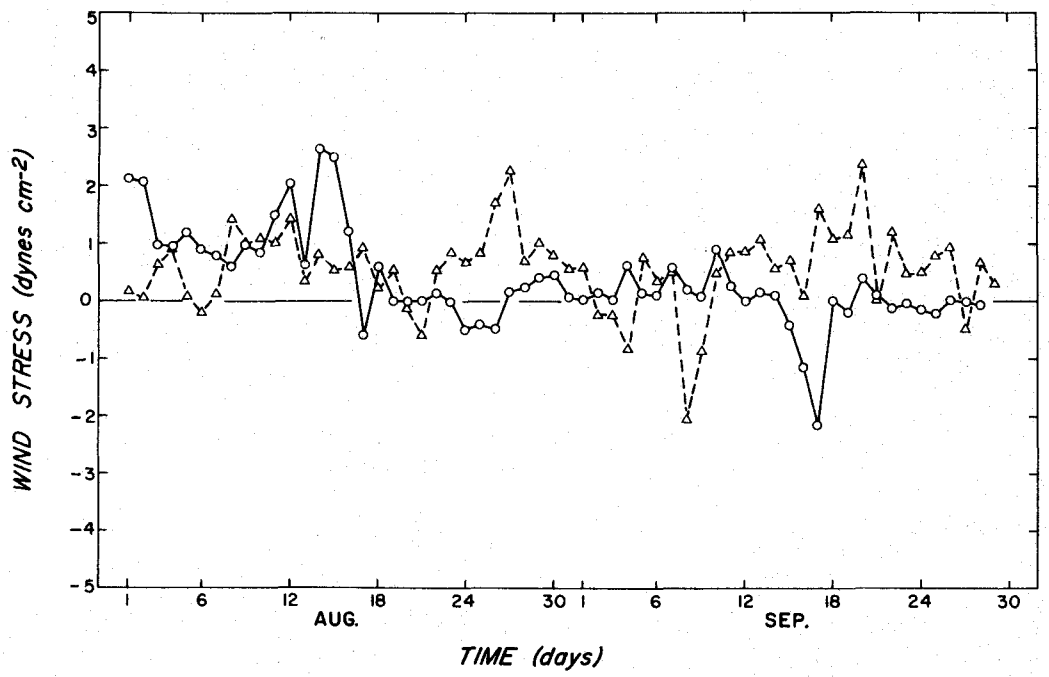

a

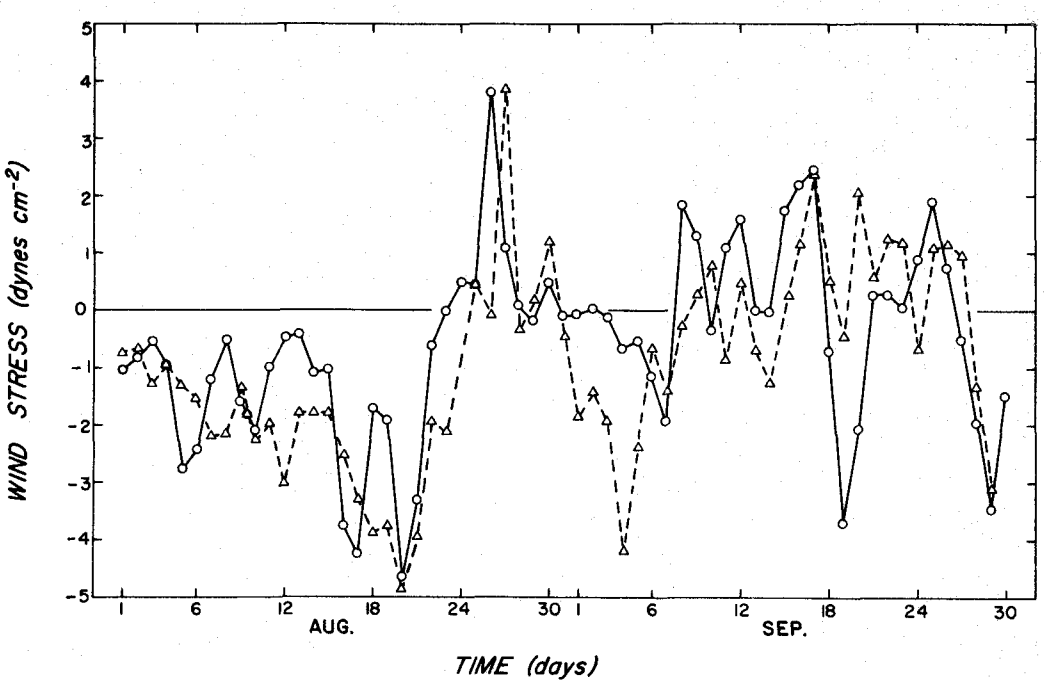

b

Figure 33. Daily Wind Stress, August and September: a) Eastward b) Northward.

O——O Directly Measured Δ– – –Δ Geostrophic

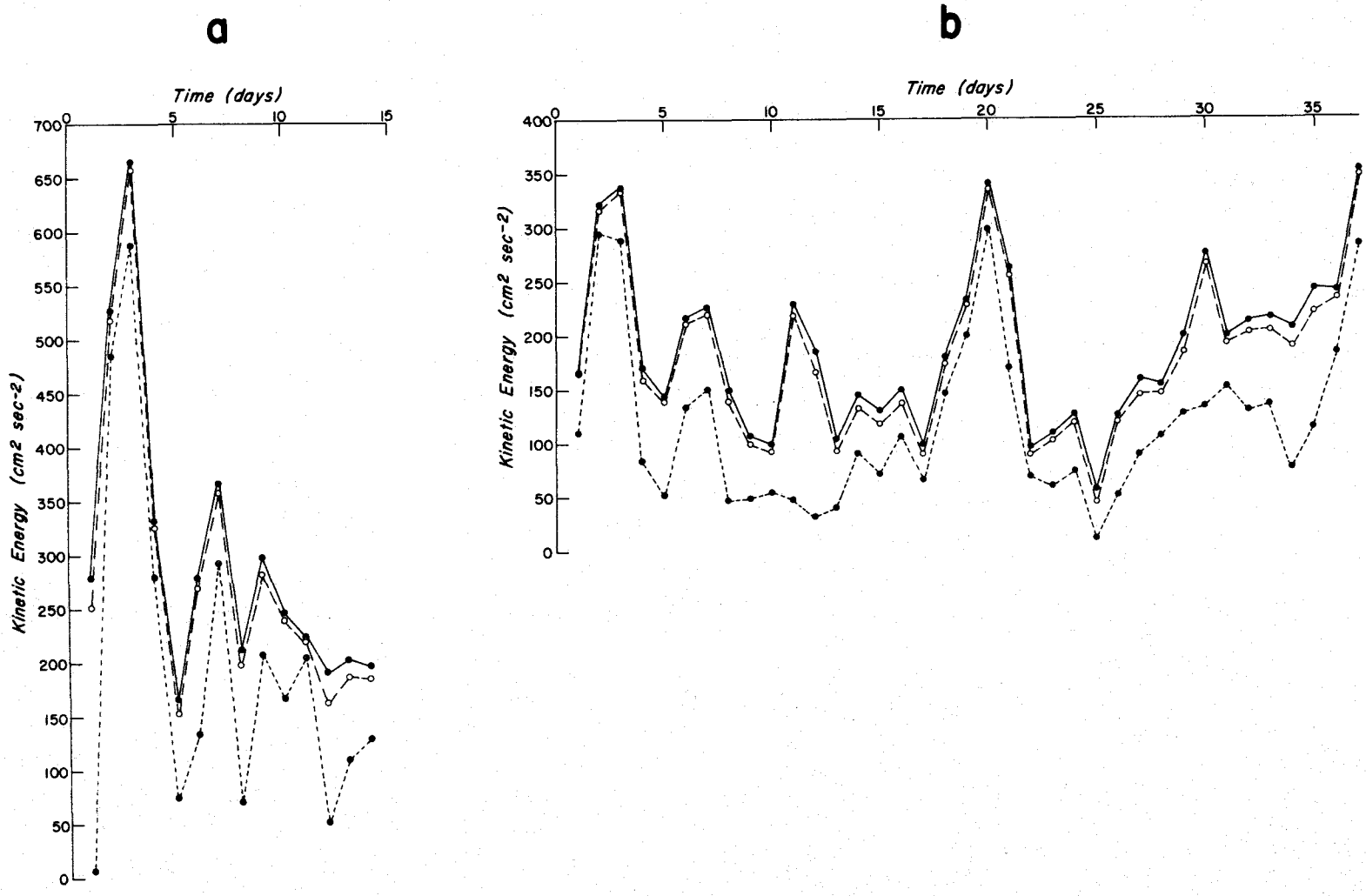

Figure 34. Daily Total Kinetic Energy of Currents Versus Time: a) DB 5, 20 meters b) DB 10, 20 meters.

KE 1 KE 2 KE 3

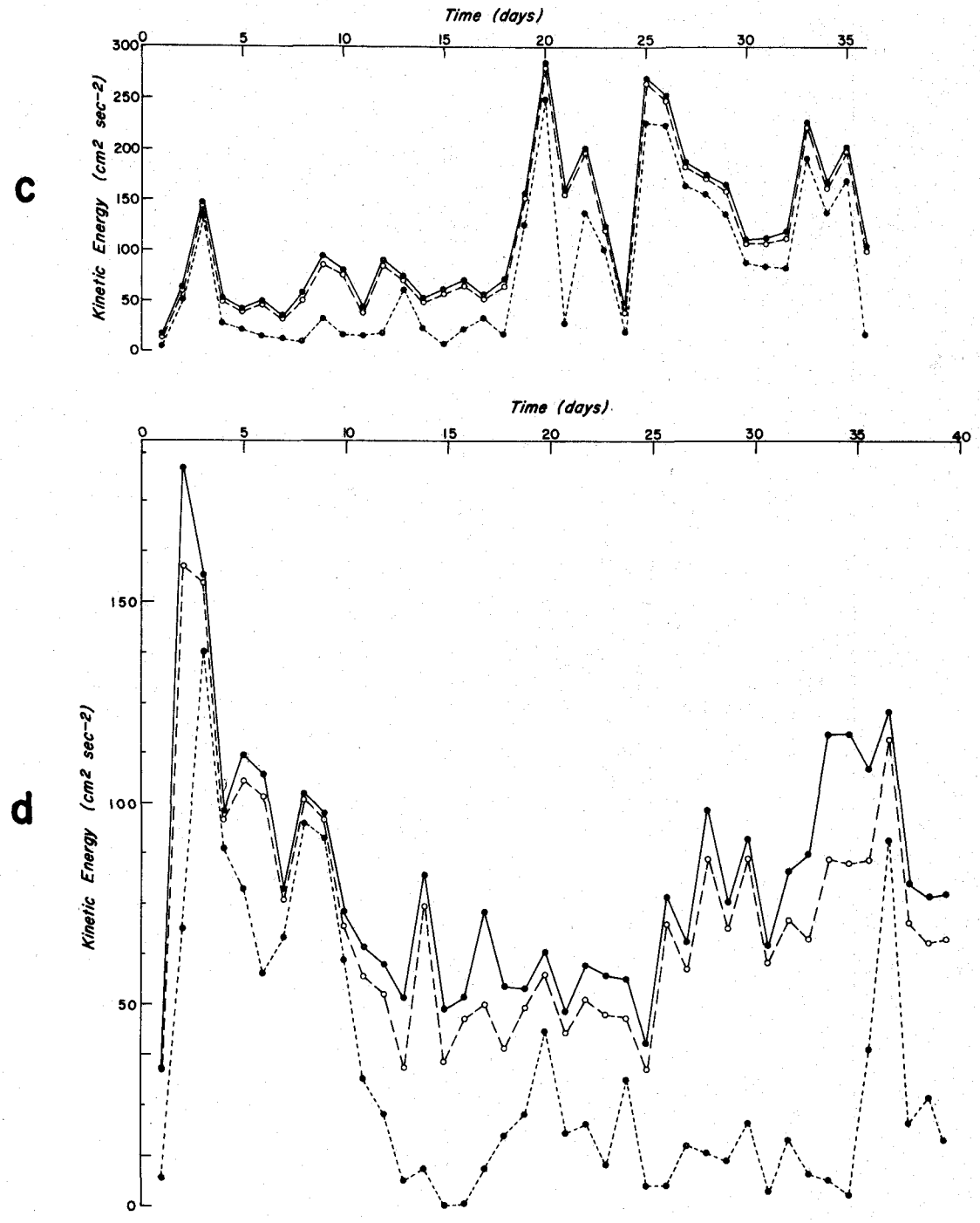

Figure 34. Daily Total Kinetic Energy of Currents Versus Time: c) DB 5, 60 meters d) DB 15, 60 meters.

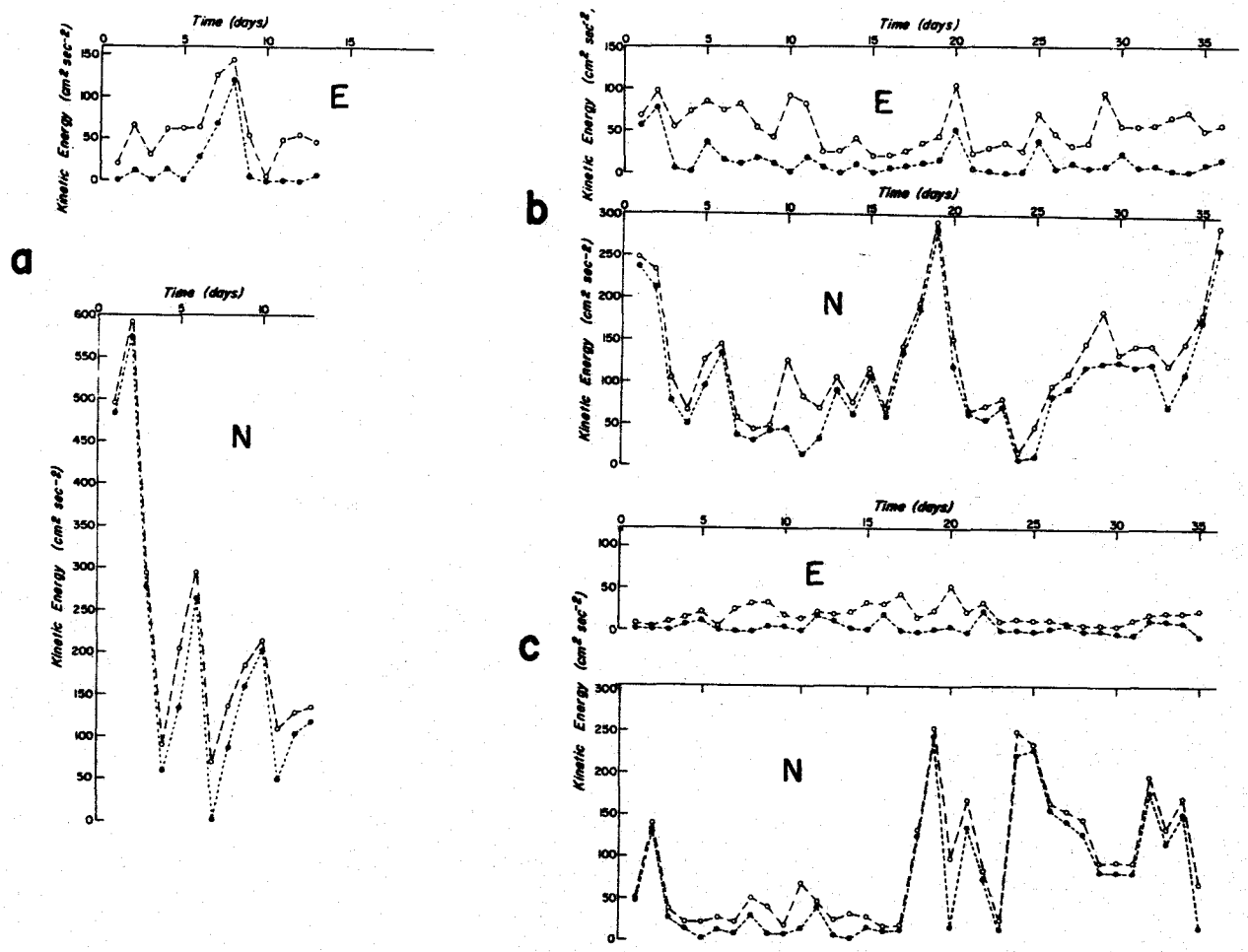

Figure 35. Daily Component Kinetic Energy of Currents Versus Time: a) DB 5, 20 meters, eastward, northward b) DB 10, 20 meters, eastward, northward c) DB 5, 60 meters, eastward (E), northward (N).

O— — —O KE 2 ●— — —● KE 3

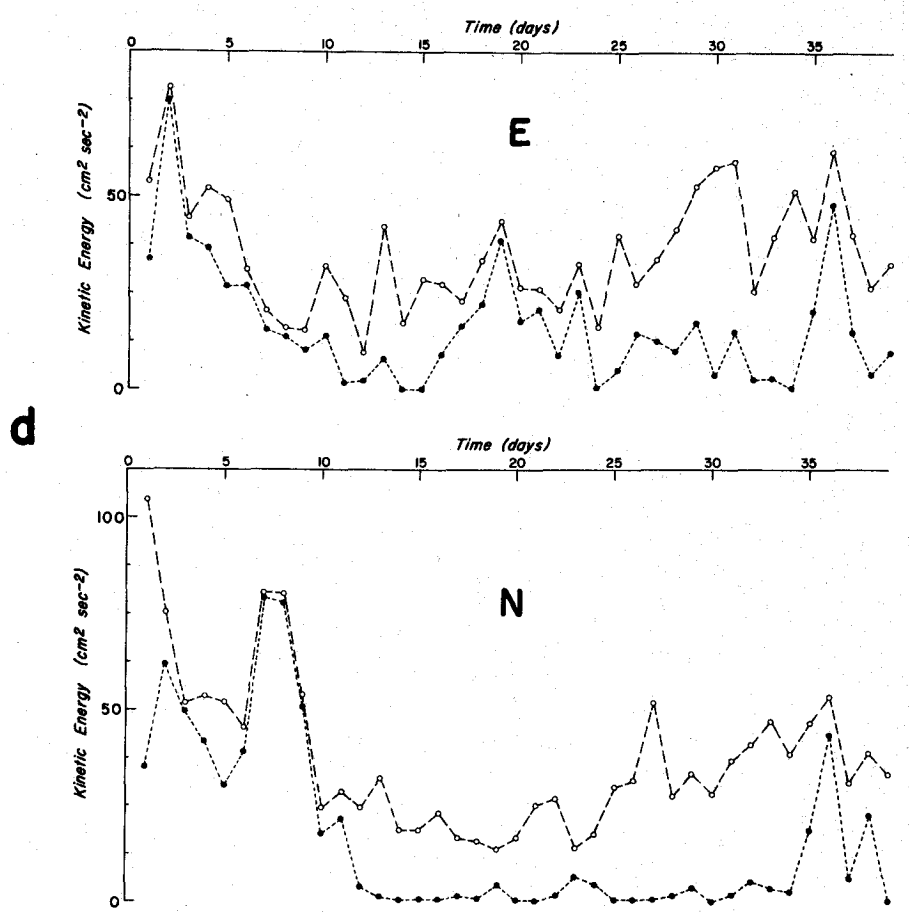

Figure 35d. Daily Component Kinetic Energy of Currents Versus Time, DB 15, 60 meters, eastward (E), northward (N).

O— — —O KE 2 ●— — —● KE 3

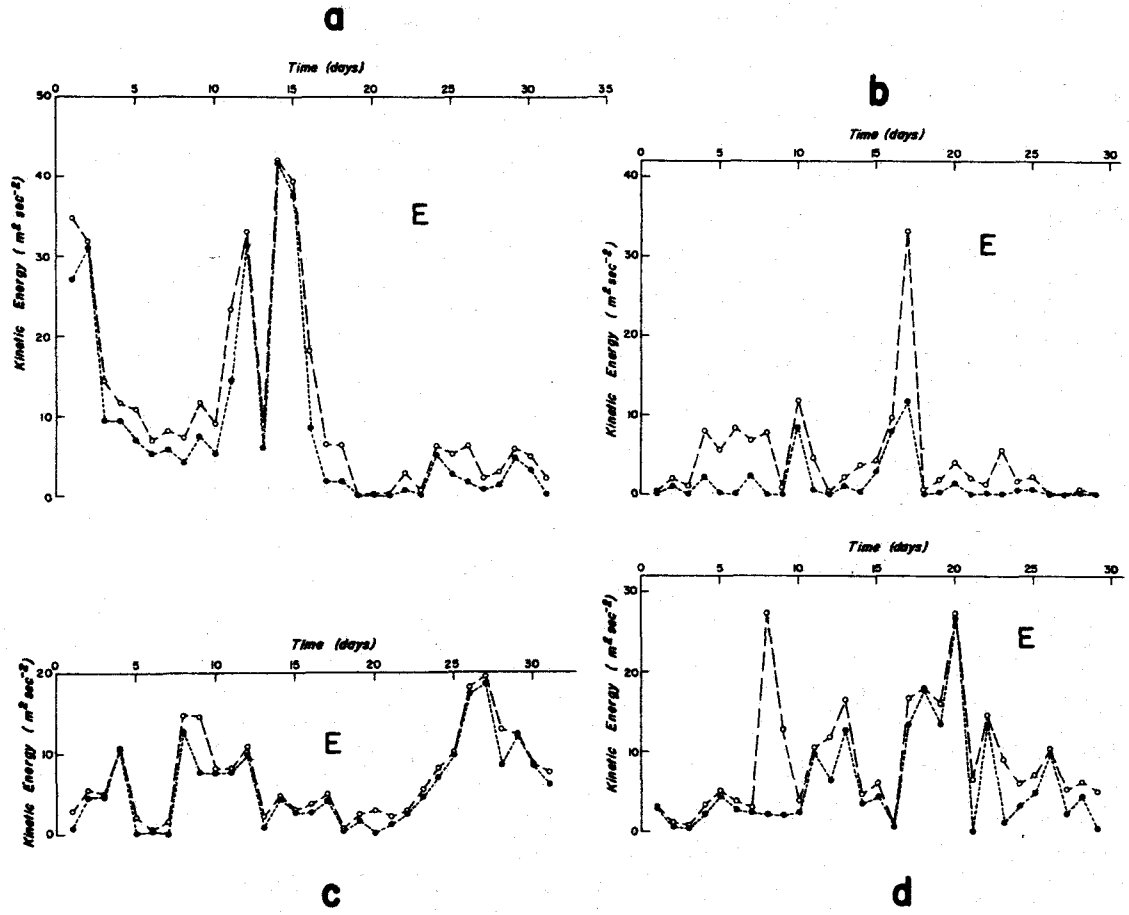

Figure 36. Daily Component Kinetic Energy of Winds Versus Time:
a) Eastward component, directly measured, August 1966
b) Eastward component, directly measured, September 1966
c) Eastward component, geostrophic, August 1966
d) Eastward component, geostrophic, September 1966.

O— — —O KE 2 ●— — —● KE 3

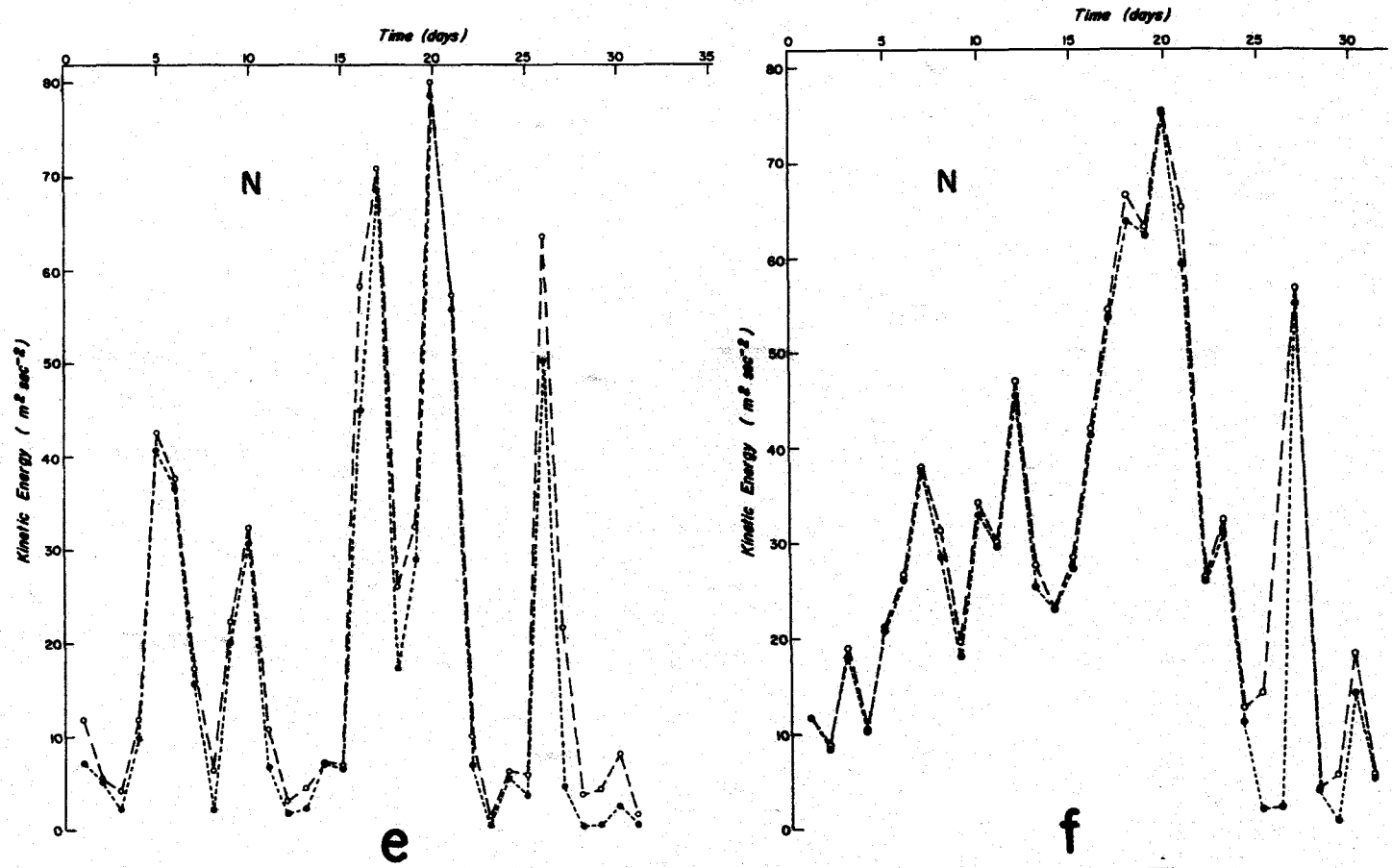

Figure 36. Daily Component Kinetic Energy of Winds Versus Time:
e) Northward component, directly measured, August 1966
f) Northward component, geostrophic, August 1966.

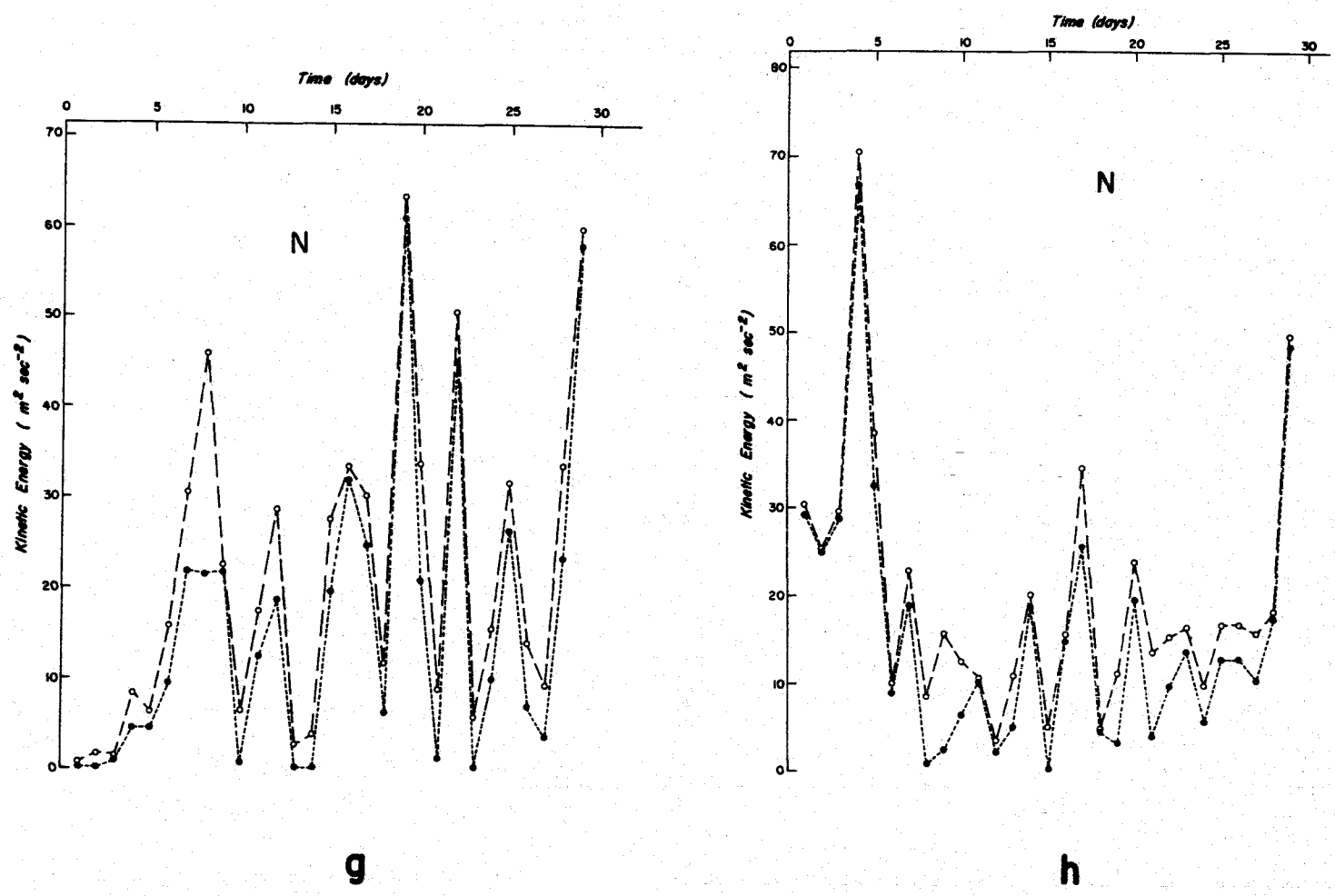

Figure 36. Daily Component Kinetic Energy of Winds Versus Time:
g) Northward component, directly measured, September 1966
h) Northward component, geostrophic, September 1966.

a measure of wind variability at time scales less than a day and of storms on a time-scale greater than a day. The difference between KE2 and KE3 is generally greatest for the eastward component of the directly measured wind which may be related to the "sea breeze" phenomenon. The atmospheric storm on the 20th of August (5th day of array measurements) corresponds to the previously noted oceanographic storm on that date. There are other correlations between wind and current variability to be seen by inspection. These curves are also a partial measure of the wind stress, without regard for sign.

Figures 37a and b show one-half the daily variance of temperature computed from the hourly averages of the two thermograph records; in a sense, this is a "pseudo-potential energy per unit mass" plot. If the daily mean temperature gradient was known and was uniform with depth, these curves could be readily converted to estimates of variations in potential energy per unit mass. The short-dashed curve is the average of the square of the hourly averages (the long-dashed line has been plotted for visual reference), and the solid curve is the difference between the average of the square of the hourly samples and the square of the daily mean. A simple observation is that an increase of temperature variability on time scales between one hour and one day accompanied the warming trend.

Figures 38a and b present the potential energy per unit mass computed from low-passed atmospheric pressure and sea level in the dashed curves. The solid curve is the residual PE2 minus PE3, whose small values imply little energy in the data at time scales less than a day. The curves for atmospheric pressure and sea level give additional measures of atmospheric and oceanographic storms; certainly September had more storms than August on this basis, but that is not in clear agreement with the wind or current results.

Statistical Effects of Numerical Tapers

Figures 39 and 40 are complementary; Figure 39 shows autocorrelation functions of representative current data which have been high-passed, intermediate-passed, and low-passed by the numerical taper of Appendix III, while Figure 40 shows energy spectra corresponding to the autocorrelation functions. These curves make the effect of the numerical taper graphically clear. The autocorrelation functions show the time scales of the "wiggles" which survive the numerical tapering. The spectral functions also show the frequency equivalent of this; further, they show where the half-power points occur on the equivalent numerical filters. The low-passed and the intermediate-passed curves intersect at a frequency corresponding to a period of about 40 hours; the intermediate-passed and the high-passed curves intersect at a frequency corresponding to a period of about 7 hours.

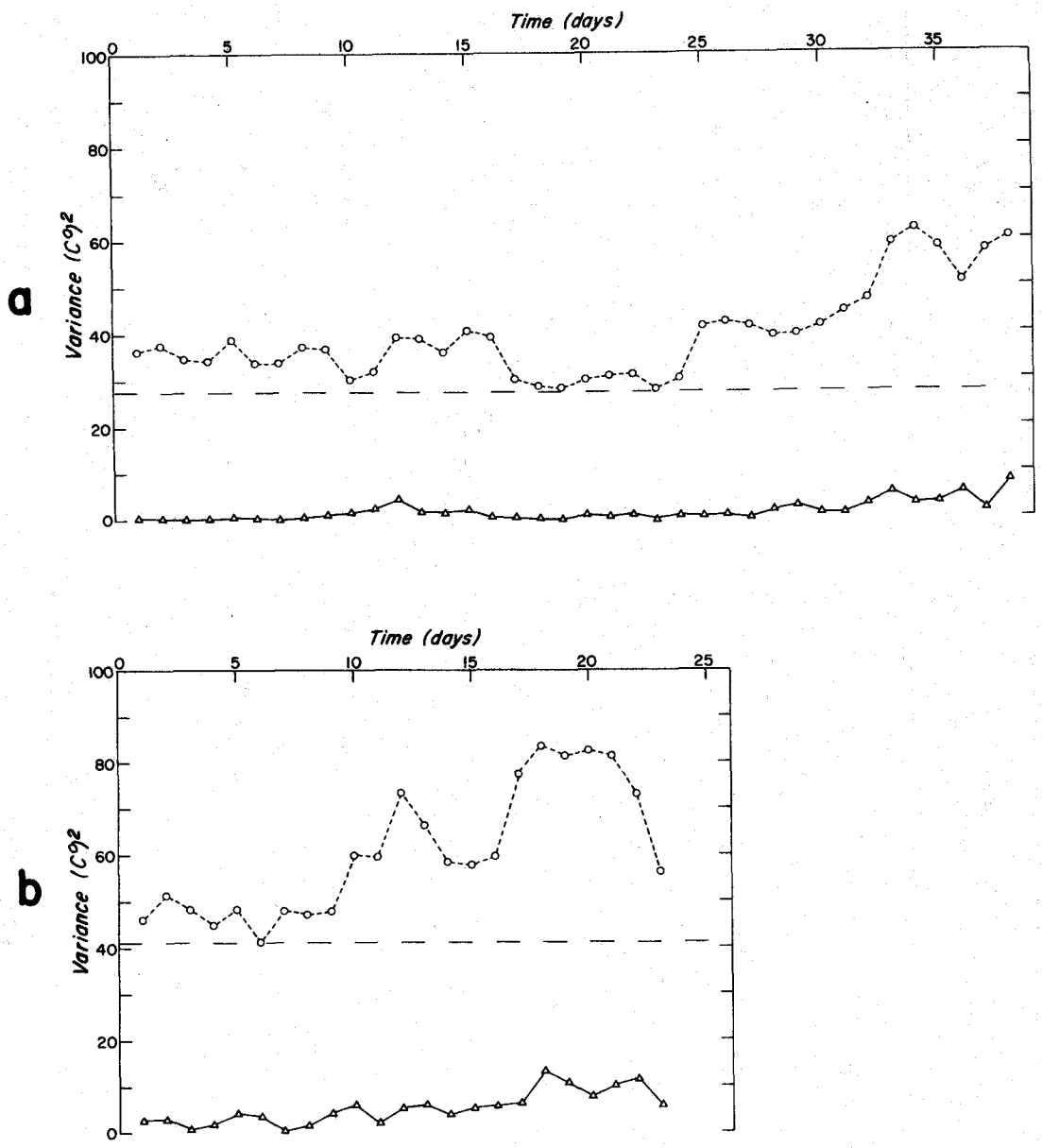

Figure 37. One-Half of Daily Variance of Hourly-Averaged Temperatures: a) DB 5, 20 meters b) DB 15, 20 meters.

O— — —O Daily Average of the Square of the Hourly Averages.
△——△ The Difference between the Daily Average of the Square of the Hourly Samples and the Square of the Daily Mean.

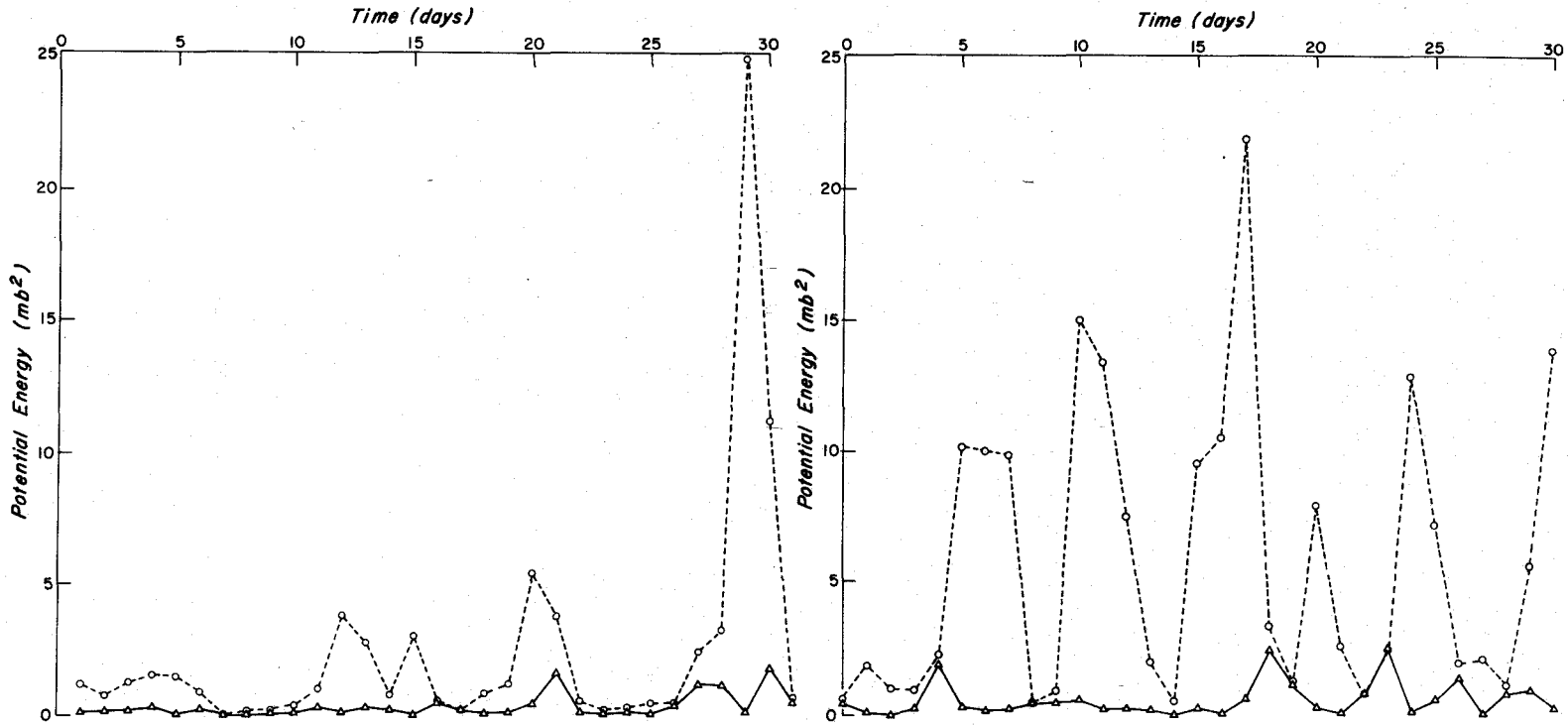

Figure 38a. Daily Potential Energy of Low-passed Atmospheric Pressure, August and September 1966.

O— — —O Daily Potential Energy of 6-Hourly Values.

▽——▽ The Difference between the Daily Potential Energy of 6-Hourly Values and the Potential Energy of the Daily Mean.

a

b

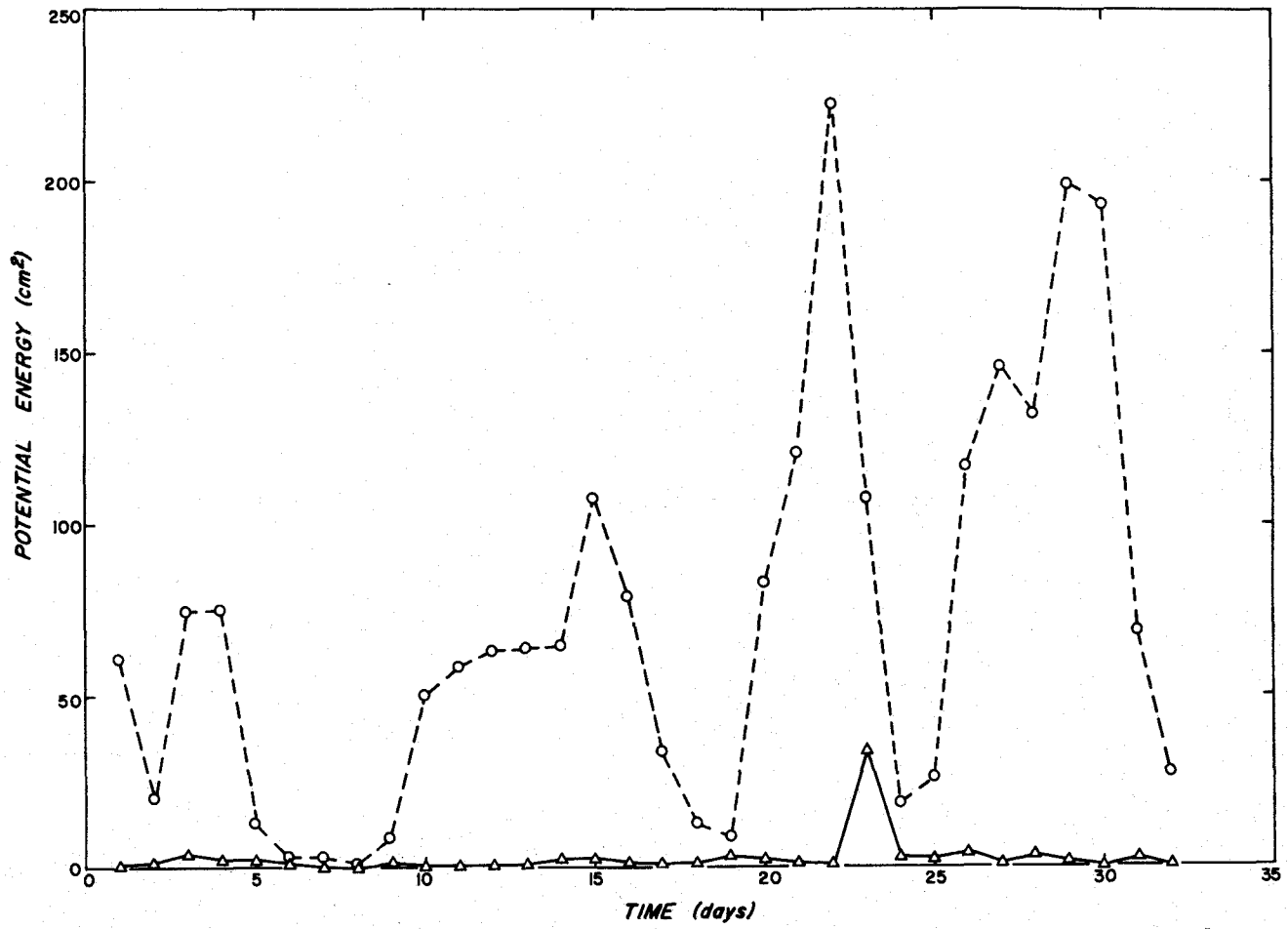

Figure 38b. Daily Potential Energy of Low-passed Mean Sea Level, 29 August to 30 September 1966.

O— — —O Daily Potential Energy of Hourly Values.

△——△ The Difference between the Daily Potential Energy of Hourly Values and the Potential Energy of the Daily Mean.

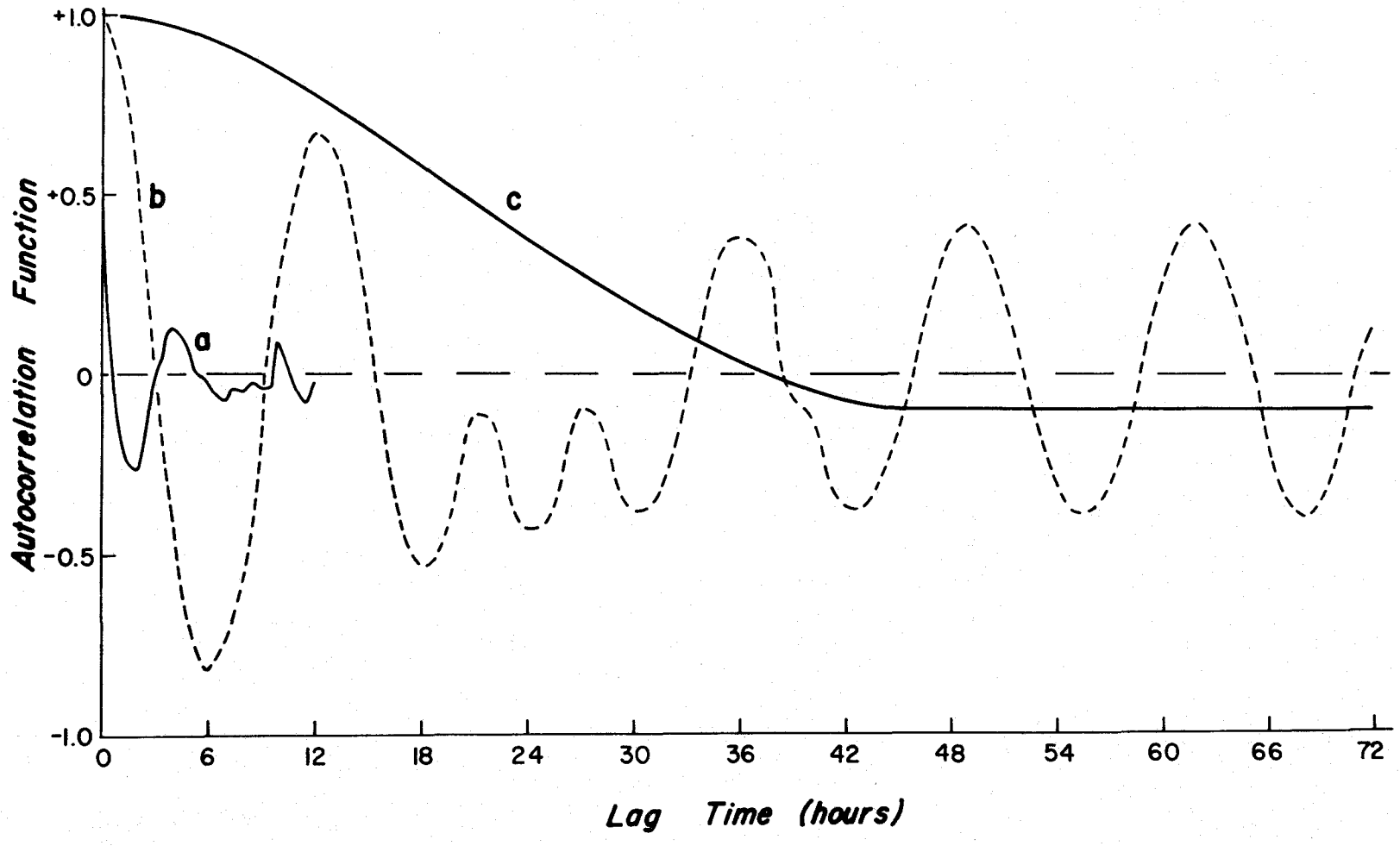

Figure 39. Sample Correlation Functions Based on Numerically-tapered Data (Eastward Component, DB 5, 60 meters): a) High-passed b) Band-passed c) Low-passed.

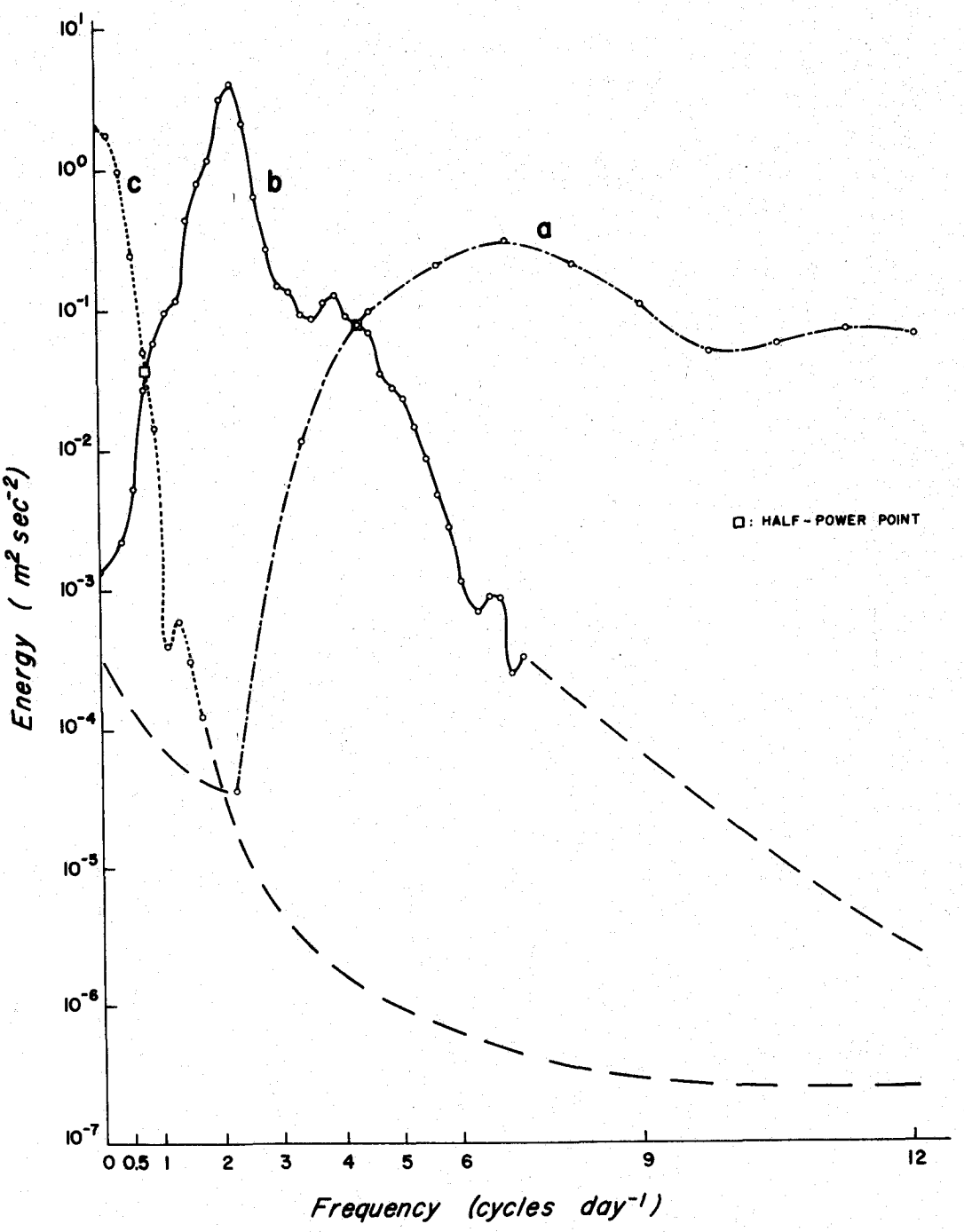

Figure 40. Sample Auto Spectral Functions Based on Numerically-tapered Data (Eastward Component, DB 5, 60 meters): a) High-passed b) Band-passed c) Low-passed.

RECOMMENDATIONS

At this stage of our work we can make a few general recommendations, in addition to those made within the main body of the text, applicable to our own future work and perhaps to that of other investigators.

The present investigation was initiated to fill-in some of the details of coastal upwelling (by direct current measurement) which were indeterminate by hydrographic methods. What has actually happened is that our "scientific appetite" for hydrographic data, to be used in the evaluation of direct current measurements, has been increasingly whetted! We have demonstrated the usefulness of atmospheric and sea level data, when available, for interpreting our oceanographic measurements; a need for more direct measurements of atmospheric variables in the coastal region has been at least implicitly indicated. With the strong baroclinic structure of the coastal region in the summer season, and with the highly variable winds and currents observed, the measurement of "mean sea level" in the coastal region with bottom-mounted pressure recorders promises to give further insight into the dynamics of the flow. We now realize that we need to occupy more anchor stations, especially on the continental shelf, and that the array site ought to be monitored hydrographically at least weekly. Float measurements in conjunction with our flow measurements can provide invaluable evidence for filling-in spatial detail in the flow field; this point is based on results not discussed in this data report. The use of STD instrumentation, and pairs of current meters, in the temperature inversion and in the highly variable flow regions, promises intriguing results. The nearly-uniform salinity gradient in the permanent pycnocline is a linear feature that has yet to be exploited with a recording salinograph. An attempt might be made to set meters along the mean position of isopycnals rather than at fixed levels for examination of the isentropic or nonisentropic nature of the flow. Future experiments will benefit from longer records, more sensors in a vertical sensor string, an alongshore array, extension of an offshore-onshore array both across the continental slope and into shallower water, and near-bottom measurements. Certainly it is unlikely that all of these objectives could be achieved simultaneously, but they could be achieved step-wise within several years. We must consider that we are still performing "pattern oceanography" rather than "precision oceanography" and will find it necessary to do so for the foreseeable future until a comprehensive, first-order picture of the many facets of coastal upwelling is developed. Fortunately, for our purposes, the "signal-to-noise ratio" has been large, with the proviso that one man's "signal" may be another man's "noise". Until we are ready for more sophisticated experiments, the present instrumentation seems reasonably adequate, though we would like to have some higher frequency samples to study stability oscillations.

We consider that we are far enough along in the technological and scientific aspects of our coastal oceanography study to begin to work with others on interdisciplinary problems, e.g. ecological, fisheries, pollution, sediment transport, and other studies.

We believe we have only "scratched the surface" in our approaches to "data massaging" and analysis. It may be useful to use coordinates oriented parallel and perpendicular to the bottom topography, rather than geographic coordinates for the current velocity analyses. We should make computation

of tidal constants and related quantities part of our basic reports. Further work should be done with the classical statistical structure of our data as well as modern time series analyses. A deeper study of the relationship between meter tilt and current velocity should be made to determine whether or not meter tilt can be reliably used when the speed or direction sensors fail. A spectral study of meter tilt should be made to determine more quantitatively whether or not a tidal, etc. correction for instrument string motion should be made to our velocity calculations.

Continued laboratory and field study of the meters' performance is a necessity. Documentation of procedures plays a particularly essential role in a project of this magnitude and complexity; it is the only solution to the continuity-of-effort problem in an academic environment. In every sense of the word, we cannot afford to re-learn past lessons. Many skills are required to perform this work and are non-uniformly distributed over the indigenous population; no single person can perform more than a fraction of the total effort. In brief, a project of this nature needs to provide for the fact that at least as much time is spent in training "new blood" as is available for research and for the fact that "scientific escalation" makes discontinuities in effort or skills prohibitively expensive. In this vein, we are attempting to reduce to a routine all phases of the operation which are amenable to such an approach; in particular, a comprehensive computer program system has become a painfully obvious necessity in order to make research time available for more advanced work.

The future work should concern itself increasingly with model building, using descriptive, analytical, numerical, and statistical-dynamical approaches. One aspect of upwelling which appears feasible to investigate is that of the time dependent divergence and vorticity fields, another is that of eddy flux calculations. Within our data fields, there is the potential of contributing to studies of the interaction of the tides with the continental slope and shelf. It also appears feasible to study inertial and continental shelf wave oscillations as a function of depth, distance offshore, and time, in conjunction with atmospheric and sea level time series.

PERSONNEL

Dr. June G. Pattullo is the principal investigator for this project, Dr. Robert L. Smith was chief scientist on the installation, recovery, and hydrographic cruises. Mr. R. Dale Pillsbury, aided by Mr. Robert George, was responsible for the instrument preparation and installation. Mr. Hugh Dobson is credited with much of the basic instrument string design, especially the ground line concept which has proven to be invaluable and successful. Mr. Christopher N. K. Mooers designed the array configuration and hydrographic sampling plans and has designed and supervised the data processing and analysis phases. Mr. David C. Cutchin has performed most of the post-calibration and instrument diagnostic work. Miss Lillie Bogert has been responsible for the numerous aspects of the data processing operation; she has been aided by Miss Laurabeth Drew, Miss Gloria Tipton, and others in film reading. Mr. Walter Pawley has provided computer programming advice and the PVD and Plot programs. Mr. Clayton Creech and Dr. Curtis A. Collins have given advice based upon their data processing experience. Mrs. Suzanne Butschun, Mr. Delmar Evans, and Miss Margaret Baldwin have plotted figures, made calculations, and assembled and edited this report. Mr. William Gilbert and Mr. Ronald Hill drafted most of the figures. Numerous other students have contributed to the field work to everyone's benefit.

Further data analyses are in progress; Mr. Mooers is performing them in consulation with Drs. Smith and Pattullo.

ACKNOWLEDGMENTS

Most of the work was conducted under Grant GA 331 from the National Science Foundation. Analysis of the data has continued under NSF Grant GA 1435 which has supported the final phases of the preparation of this data report. The National Science Foundation provided ship support for the R/V YAQUINA under Grant GA 295, and three full-time assistants: one, March through June 1967; one, June through August 1967; and one, January 1967 to the present. The Work-Study Program supported by the U.S. Department of Health, Education and Welfare and Oregon State University provided six part-time assistants during 1966 and 1967.

REFERENCES

Brainard, Edward C., II, 1964. 400 Day High Accuracy Recording Thermograph. Instrument Society of America Conference Reprint, 6 pp.

Braincon Corporation, 1965a. Type 316 Histogram Current Meter, Instruction Bulletin.

Braincon Corporation, 1965b. Type 146 Recording Thermograph, Data Sheet No. 19.

Collins, C. A., 1964. Structure and Kinematics of the Permanent Oceanic Front off the Oregon Coast. M.S. Thesis. Oregon State University.

Collins, C. A., 1968. A Description of Measurements of Current Velocity and Temperature over the Oregon Continental Shelf, July 1965-February 1966. Ph. D. Thesis. Oregon State University.

Collins, C. A., H. C. Creech, and June G. Pattullo, 1966. A Compilation of Observations from Moored Current Meters and Thermographs; Vol I; Oregon Continental Shelf July 1965-February 1966. Data Report #23, Dept. of Oceanography, Oregon State University.

Collins, C. A., C. N. K. Mooers, M. R. Stevenson, R. L. Smith, and J. G. Pattullo, (in preparation). The Dynamic Structure of a Frontal Zone in a Coastal Upwelling Region, Part 1. Direct Current Measurements.

Daugherty, F. M., Jr., 1966. Evaluation of Self-Recording Current Meter Arrays October 1962-March 1965, Navoceano, I. M. No. 66.7, 51 pp.

Davidson, Daniel R., and G. E. Birchfield, 1967. A Case Study of Coastal Currents in Lake Michigan. Dept. of Engineering Sciences, Technological Institute, Northwestern University, 31 pp.

Durham, Donald L., and Robert O. Reid, 1967. Analysis of Tidal Current Observations over the Northeastern Shelf of the Gulf of Mexico. Dept. of Oceanography, Texas A & M University, 110 pp.

Fofonoff, N. P., and Yucel Ercan, 1967. Response Characteristics of a Savonius Rotor Current Meter. Woods Hole Oceanographic Institution, Reference No. 67-33.

Gaul, R. D., J. M. Snodgrass, and D. F. Cretzler, 1963. Some Dynamical Properties of the Savonius Rotor Current Meter: Marine Science Instrumentation, Vol. 2, Plenum Press, N. Y., pp. 115-125.

Johnson, R. L., 1966. Laboratory Determination of Current Meter Performance. Technical Report No. 843-1, Division Hydraulic Laboratory, U. S. Army Engineer Division, North Pacific, Corps of Engineers, Bonneville, Oregon, 33 pp.

Maloney, William E., 1967. A Study of the Antilles Current Using Moored Current Meter Arrays. Naval Oceanographic Office, Washington, D. C., 142 pp.

Mooers, C. N. K., and R. L. Smith, 1967. Dynamical Structure in an Upwelling Frontal Zone. Trans. Am. Geophys. Un. 48: 125-126 (Abstract).

Mooers, C. N. K., C. A. Collins, R. L. Smith, and J. G. Pattullo (in preparation). The Dynamic Structure of a Frontal Zone in a Coastal Upwelling Region, Part 2. Dynamic Interpretation.

Sexton, R., 1964. Some Tow Tank Calibrations of the Savonius Rotor. Lamont Geological Observatory, Columbia University. Technical Report No. Cu-11-64 (Unpublished Manuscript).

Sunblad, Robert L., 1965. The Histogram Current Meter. Instrument Society of America Conference Reprint, 6 pp.

Webster, Ferris, 1964. Processing Moored Current Meter Data. Woods Hole Oceanographic Institution, Technical Report #64-555, 35 pp. (Unpublished Manuscript).

Webster, Ferris, and N. P. Fofonoff, 1965. A Compilation of Moored Current Meter Observations, Volume 1. Woods Hole Oceanographic Institution, Technical Report #65-44, 111 pp. (Unpublished Manuscript).

Webster, Ferris, and N. P. Fofonoff, 1967. A Compilation of Moored Current Meter Observations, Volume III. Woods Hole Oceanographic Institution, Reference No. 67-66, 105 pp.

APPENDIX I

DATA PROCESSING PROGRAMS

Program ERDET (Error Detection)

The general objective of the error detection program is that of a rational, automated search of reduced data records for high-frequency errors; e.g. film reading or key-punching errors. Any such erroneous data points could be fatal to further analyses. The basis for the error detection procedure is effectively a low-pass numerical filtering operation which is determined by a least-squares analysis, and is explained in Appendix II. (In addition to the computerized check, verification procedures are invoked at all steps and a visual inspection of machine plots of the reduced data is made.) If a data point appears erroneous by our criterion, we check the data record books and the films to locate the suspect data point. In the event an error appears in our test and the data record book or film appear to have been read or transcribed incorrectly, the correct value is used; if a suspicious data point appears to have been read, recorded, and transcribed satisfactorily, it is replaced with the predicted value (this case rarely occurs), because, even if the isolated data value were correct, it would appear as "noise" in our data due to the digital sampling.

The measured value is tested against the predicted value; if the absolute value of the difference exceeds a specified criterion, an error indication is made. Initially, a test value is inserted into the program; after twenty-five data values have been tested, enough data have been entered to justify computing a standard deviation which, when multiplied by a variable factor, becomes the test criterion. A running criterion is computed on the previous twenty-five values; thus, this criterion takes explicit account of low and high variability sections of the data. The test is repeated until 1% of the data is "culled-out" for error checking; on each repetition the variable factor is reduced by 0.2 (from an initial value of 2.0). Individual versions of the basic program have been written for scalar and vector data; in the latter case, the scalar components are individually tested. These tests have been run on our temperature, atmospheric pressure, sea level, and wind and current velocity data.

Program CUMSAD (Current Meter Speed and Direction)

Program CUMSAD makes several necessary conversions of raw data and calculates several first-order statistics. The program reads month, day, year, time, tilt magnitude, tilt direction, clockwise limit of the direction arc, modal direction, counterclockwise limit of the direction arc, and speed in degrees of arc. It then performs the following conversions on each observation: changes speed to cm/sec, corrects speed for instrument tilt in the event it is necessary, changes magnetic direction to true direction, finds direction variability from the limits of the direction arc, and resolves velocity into eastward (U) and northward (V) components. These processed observations are written on magnetic tape in a card image format, sample mean and standard deviation are printed for speed, U, V, tilt magnitude, and direction variability. Hourly and daily averages for speed, U, V, and

direction are printed. The total daily kinetic energy is computed from one-half of the square of the speed of the daily mean (KE3), of the sum of the squares of the hourly average speeds (KE2), and of the sum of the squares of the observed speeds (KE1). Similar kinetic energy calculations are performed on the velocity components. Potential energy for scalar variables is computed in a similar fashion. The output magnetic tape is used as input for subsequent calculations performed locally and data card preparation for calculations performed at off-campus computer installations.

Program HISTO (Histogram)

Program HISTO prints tables of values from which histograms may be plotted; it computes the frequency of occurrence of each value, the relative frequency (%) of each value, and a class relative frequency.

Two basic versions of this program have been used: one for temperature data and one for current data. The temperature data version uses values to the nearest tenth, but temperature classes are x.4, x.5, and x.6 in one class, x.7 and x.8 in another class, and x.9, x.0, and x.1 in another class. These class intervals were chosen to overcome the natural bias of the film reader to call more readings x.0 than x.1 or x.9 and x.5 than x.4 or x.6. The current data version uses speed, U and V in tenths of a cm/sec, and direction to the nearest degree. Other first-order statistics (mean, standard deviation, skewness, and kurtosis) are also computed for speed, U, V, and direction. Other scalar and vector time series are processed in a similar manner.

APPENDIX II

DERIVATION OF ERROR DETECTION FORMULA

The general objective is to produce a predicted value for each element of a time series in an optimum fashion and to compare the difference between the two with a reasonable criterion. If the difference exceeds the criterion, the element under examination is labeled suspect and requires manual checking.

First we assume any time series can be represented as

$$x(t) = \sum_i a_i \cos (\sigma_i t + \theta_i), \quad (i = 1, 2, \ldots).$$

Second we decide to form a predicted series from the three preceding and the three succeeding values: i.e.,

$$x'(t) = \sum_{j=1}^{3} [b_{-j} \; x (t - j) + b_j \, x (t+j)] \; .$$

The problem is then to determine the coefficients b_j, $(j = -3, -2, -1, 1, 2, 3)$ in an optimum fashion. One approach is to substitute the assumed form of $x(t)$ into the formula of $x'(t)$ and consider the results:

$$x'(t) = \sum_i a_i \left\{ \sum_{j=1}^{3} [(b_{-j} + b_j) \cos (j\sigma_i)] \cdot \cos (\sigma_i t + \theta_i) \right.$$

$$\left. + \sum_{j=1}^{3} [(b_{-j} - b_j) \sin (j\sigma_i)] \cdot \sin (\sigma_i t + \theta_i) \right\} \; .$$

Since it is undesirable to cause a phase shift in the harmonic constituents of $x'(t)$ as compared to $x(t)$, it is sufficient to force the b_j's to be symmetric; i.e., $b_1 = b_{-1}$, $b_2 = b_{-2}$, and $b_3 = b_{-3}$ so that all of the $\sin (\sigma_i t + \theta_i)$ terms vanish. We then have

$$x'(t) = \sum_i F (\sigma_i) \; a_i \cos (\sigma_i t + \theta_i),$$

where

$$F(\sigma_i) = 2 \sum_{j=1}^{3} b_j \cos (j\sigma_i).$$

Another logical constraint is to require $F(\sigma_i)$ to be normalized in the sense that it equals unity at zero frequency; i.e.,

$$F(0) = 1 \; = 2 \, (b_1 + b_2 + b_3).$$

Now, two degrees of freedom remain. Next, we assume that errors will naturally appear as high frequency noise so that the predicted series ought to suppress high frequencies in preference for low frequencies; i.e., $F(\sigma_i)$ should be as "flat" as possible at the origin, $\sigma = 0$.

Logically, this is achieved when

$$\frac{d^2F}{d\sigma^2} = 0 \qquad \text{and} \qquad \frac{d^4F}{d\sigma^4} = 0 \quad \text{at } \sigma = 0.$$

(Note that odd-order derivatives equal zero by the even symmetry of $F(\sigma_i)$.) In other words, (setting $\sigma_i = \sigma$, i.e., σ continuous):

i) $$\left.\frac{dF}{d\sigma}\right|_{\sigma = 0} = 2\left[-b_1 \sin(\sigma), -2 b_2 \sin(2\sigma) - 3 b_3 \sin(3\sigma)\right]_{\sigma = 0}$$

$$= -2 \sin(\sigma)\left[b_1 + 4 b_2 \cos(\sigma) + 3b_3 (4 \cos^2(\sigma) - 1)\right]_{\sigma = 0}$$

$$= 0$$

ii) $$\left.\frac{d^2F}{d\sigma^2}\right|_{\sigma = 0} \overset{(\text{set})}{=} 0 = -2 \cos(\sigma)\left[b_1 + 4b_2 \cos(\sigma) + 3b_3(4 \cos^2(\sigma) - 1)\right] - 2 \sin(\sigma)\left[-4b_2 \sin(\sigma) - 24b_3 \sin(\sigma) \cos(\sigma)\right]_{\sigma = 0}$$

or, $b_1 + 4b_2 + 9b_3 = 0$

iii) $$\left.\frac{d^3F}{d\sigma^3}\right|_{\sigma = 0} = \Big\{ 2 \sin(\sigma)\left[b_1 + 4b_2 \cos(\sigma) + 3b_3 (4 \cos^2(\sigma) - 1)\right] - 4 \cos(\sigma)\left[-4b_2 \sin(\sigma) - 24b_3 \sin(\sigma) \cos(\sigma)\right] - 2 \sin(\sigma)\left[-4b_2 \cos(\sigma) - 24 b_3 \cos(2\sigma)\right]\Big\}_{\sigma = 0}$$

$$= 0$$

iv) $$\left.\frac{d^4F}{d\sigma^4}\right|_{\sigma = 0} \overset{(\text{set})}{=} 0 = \Big\{ 2 \cos(\sigma)\left[b_1 + 4b_2 \cos(\sigma) + 3b_3 (4 \cos^2(\sigma) - 1)\right] + 6 \sin(\sigma)\left[-4b_2 \sin(\sigma) - 24b_3 \cos(\sigma) \sin(\sigma)\right] + 6 \cos(\sigma)\left[-4b_2 \cos(\sigma) - 24b_3 \cos(2\sigma)\right] - 2 \sin(\sigma)\left[4b_2 \sin(\sigma) + 48b_3 \sin(2\sigma)\right]\Big\}_{\sigma = 0}$$

$$= 2\left[b_1 + 4b_2 + 9b_3\right] + 24\left[b_2 + 6b_3\right]$$

or, $b_2 + 6b_3 = 0.$

Finally, we must solve the third-order, linear inhomogeneous algebraic system of equations for b_1, b_2, and b_3:

$$b_1 + b_2 + b_3 = 1/2$$

$$b_1 + 4b_2 + 9b_3 = 0$$

$$0 \cdot b_1 + b_2 + 6b_3 = 0.$$

Solving: $b_1 = 0.75$, $b_2 = -0.30$, $b_3 = 0.05$, so

$$\begin{aligned} x'(t) = \; & 0.75 \, [\, x(t-1) + x(t+1)] \\ & - 0.30 \, [\, x(t-2) + x(t+2)] \\ & + 0.05 \, [\, x(t-3) + x(t+3)] \end{aligned}$$

and

$$F(\sigma) = 0.75 \cos(\sigma) - 0.30 \cos(2\sigma) + 0.05 \cos(3\sigma).$$

This is the formula used in our error detection program; it could be readily generalized to include higher order coefficients but this would, of course, increase the expense of computer implementation. To demonstrate the efficacy of $F(\sigma)$ in its designed task, $F(\sigma)$ is evaluated at several periods for a record sampled digitally at 10-minute intervals:

F	$T = \frac{2\pi}{\sigma}$ (minutes)
1.00	∞
1.00	120
0.95	60
0.74	50
0.60	40
-0.35	30
-1.60	24
-3.20	20

Thus isolated, individual errors are greatly exaggerated: the difference $x(t) - x'(t)$ squared is of the order $(3.2)^2$, or ten times magnified. (Note: another practical consequence of this procedure is that a genuine error generally produces a cluster of suspect data points in the test, making bona fide errors easy to find in the center of a cluster.)

APPENDIX III

COSINE-LANCZOS TAPER AND FILTER CHARACTERISTICS USED FOR DATA SMOOTHING AND BAND SEPARATION

The Cosine-Lanczos Taper is the Fourier transform of the product of a cosine and a Lanczos filter, or the Cosine-Lanczos Filter. The Cosine-Lanczos Filter is a low-pass filter with a rapid "roll-off" and is thus very effective in separating sections of the energy spectrum of a time series.

The principal quantities of the taper and the filter (as we use it) are tabulated below:

x_i: observed value

y_i: tapered value

Symbol: C-L 121

Taper Operation: $y_i = \frac{1}{G}\left(x_i + \sum_{m=1}^{60} f(m)\,(x(i-m)+x(i+m))\right)$

Weighting Factor: $f(m) = \frac{1}{2}\left[\frac{1 + \cos(\pi m/60)\sin(0.7\pi m/12)}{0.7\pi m/12}\right]$

Normalizing Factor: $G = 1 + 2\sum_{m=1}^{60} f(m) = 17.05$

Filter Function: $F(\sigma) = \left[1 + 2\sum_{m=1}^{60} f(m)\cos(m\sigma)\right] / G$

Half-Power Point:

a) 10-minute sampling rate: 6.7 hours

b) 1-hour sampling rate: 40 hours

The weighting factors are listed below:

m	f(m)	m	f(m)	m	f(m)	m	f(m)	m	f(m)	m	f(m)
1	0.989	11	0.409	21	-0.122	31	-0.0471	41	0.0284	51	0.000452
2	0.970	12	0.331	22	-0.135	32	-0.0309	42	0.0263	52	-0.000468
3	0.943	13	0.256	23	-0.141	33	-0.0163	43	0.0235	53	-0.000961
4	0.900	14	0.184	24	-0.141	34	-0.00329	44	0.0200	54	-0.00112
5	0.847	15	0.118	25	-0.136	35	0.00747	45	0.0163	55	-0.00102
6	0.787	16	0.0589	26	-0.126	36	0.0162	46	0.0128	56	-0.000793
7	0.719	17	0.00676	27	-0.113	37	0.0225	47	0.00935	57	-0.000487
8	0.648	18	-0.0374	28	-0.0981	38	0.0266	48	0.00634	58	-0.000219
9	0.570	19	-0.0738	29	-0.0810	39	0.0288	49	0.00385	59	-0.0000452
10	0.490	20	-0.102	30	-0.0643	40	0.0295	50	0.00189	60	0.0

The filter function is evaluated below for several periods ($T = \frac{2\pi}{\sigma}$: units of hours); it is evaluated for a sampling rate of once per hour. For any other sampling rate, it is a simple matter of scaling the time units of T to obtain the proper filter function.

T (Hours)	F (σ)	T	F (σ)	T	F (σ)	T	F (σ)
100.	1.004279	32.	.376798	24.066	.012338	12.192	-.000132
80.	1.006590	30.	.263081	23.934	.009995	12.	-.000028
60.	.989450	29.	.207416	22.306	-.005725	11.967	-.000010
50.	.931550	28.	.154763	20.	-.001245	11.755	.000094
45.	.861464	27.	.107036	15.	-.000119	8.280	.000047
42.	.795247	26.868	.101208	12.905	-.000202	6.	-.000001
40.	.737569	26.	.066166	12.872	-.000214	5.	-.000000
38.	.667192	25.819	.059641	12.658	-.000256	4.	-.000000
36.	.583084	25.	.033841	12.626	-.000257	3.	-.000000
34.	.485460	24.833	.029364	12.421	-.000225	2.	-.000000

It should be recalled when applying a numerical taper that the corresponding filter function operates in the amplitude vs. frequency domain, while its square operates in the energy vs. frequency domain.

You will note that each tapered value consists of a symmetric, weighted average of the observed value and its 60 preceding and 60 succeeding values. Usually, when we taper a series to "low-pass" it, we also obtain the "high-passed" series; where y (t) is the "low-passed" value, then 1 -y (t) is the "high-passed"value. Our procedure has been to "low- and high-pass" the error-detected/corrected data sampled at 10-minute intervals, and to then "thin" (or, "sub-sample" or "decimate") the "low-passed" data to 1-hour intervals and repeat the tapering procedure. The resultant is three tapered time series:

a) "High-passed," 10-minute intervals, half-power point at T≈ 6.7 hours; symbol: HP

b) "Low-low-passed," 1-hour intervals, half-power point at T≈40 hours; symbol: LP

c) "High-low-passed" (or, "intermediate-passed"), 1-hour intervals, half-power points at T ≈ 6.7 hours and 40 hours; symbol: IP

Thus, a complex problem of oceanographic analysis has been broken into three simpler problems:

a) HP: for the study of stability oscillations, etc.

b) LP: for the study of continental shelf waves, etc.

c) IP: for the study of tidal and inertial motions, etc.

An example demonstrating that the C-L 121 Taper/Filter in fact accomplishes this objective is given in Figures 39 and 40.

DISTRIBUTION LIST (INITIAL)

Gross

YAQUINA (5 copies)
OSU Computer Center (5 copies)
OSU Oceanography:
- Biologists (5 copies)
- Chemists (5 copies)
- Geologists (5 copies)
- Geophysicists (5 copies)
- Physical (20 copies)

Internal to OSU

Baldwin, Margaret, Miss
Baughman, Joanne, Mrs.
Barstow, Dennis, Mr.
Beardsley, George, Dr.
Bernick, Paul, Mr.
Bogert, Lillie, Miss
Bottero, Joseph, Mr.
Bourke, Robert, Mr.
Butschun, Suzanne, Mrs.
Curtin, Thomas, Mr.
Cutchin, David, Mr.
De Rycke, Dick, Lt.
Donally, James F., Mr.
Drew, Laurabeth, Miss
Eagle, Rodney, Mr.
Enfield, David, Mr.
Evans, Delmar, Mr.
Fisher, Carl, Lt.
George, Robert, Mr.
Gilbert, William, Mr.
Hewson, E. W., Prof.
Johnson, Ronald E., Mr.
Jorgensen, Raymond, Mr.
Keith, Nathan, Mr.
Kowalik, Zygmunt, Dr.
Lee, Henry, Mr.
Longuet-Higgens, Michael S., Prof.
Marine Science Center (Weather Bureau)
Matthews, John, Mr.
Mesecar, Roderick, Dr.
McKeel, Daniel, Mr.
Mysak, Lawrence, Dr.
Nelson, Tom, Mr.
Neshyba, S. N., Dr.
Pattullo, June G., Dr.
Pawley, Walter, Mr.
Pearcy, William, Dr.
Pillsbury, Dale, Mr.
Pond, Steven, Dr.

Pittock, Henry, Lt.
Quinn, William, Dr.
Sakou, Toshitsugu, Dr.
Shidler, Carl, Mr.
Slotta, Larry S., Dr.
Small, Larry F., Dr.
Smith, Robert, Dr.
Spigai, Joel, Lt.
Still, Robert, Mr.
Swanson, Larry F., LCDR
Tipper, Ron, Lt.
Tucker, Stevens, Mr.
Tipton, Gloria, Miss
Trump, Cliff, Mr.
Wyatt, Bruce, Mr.
Yao, George, LCDR
Zaneveld, Ronald, Mr.

External to OSU

Birchfield, Daniel, R., Dr., Northwestern Univ., Evanston, Ill.
Bourke, Benjamin, Mr., Calif. Research Corp., La Habra, Calif.
Bowden, K. F., Prof., Univ. of Liverpool, Liverpool, England
Brainerd, E., Mr., Braincon Corp., Watham, Mass.
Cartwright, D. E., Mr., NIO, Wormley, Godalming, England
Collins, Curtis A., Dr., Pacific Oceano. Group, Nanaimo, B. C., Canada
Cox, Charles S., Prof., SIO, La Jolla, Calif.
Creech, Clayton, Sp. 4, 1605 Tenth Street, Tillamook, Oregon 97141
Csanady, C. S., Dr., Univ. of Waterloo, Waterloo, Canada
Denner, Warren, Mr., USNPGS, Monterey, Calif.
Dobson, Hugh, Mr., 2309 Samuel Drive, Ottawa, Ontario, Canada
Dodimead, A. J., Dr., Pacific Oceano. Group, Nanaimo, B. C., Canada
Dowling, G. B., Dr., NMDL, Panama City, Fla.
Duxbury, A., Dr., Dept. of Oceanography , Univ. of Wash., Seattle, Wash.
Fofonoff, N. P., Dr., WHOI, Woods Hole, Mass.
Green, Thomas, Dr., USNPGS, Monterey, Calif.
Griswold, Gale M., LCDR., USNPGS, Monterey, Calif.
Hopkins, Thomas, Mr., Dept. of Oceanography, Univ. of Wash., Seattle.
Laurs, Michael R., Dr., Bur. Comm. Fish., Tuna Resources Lab., Calif.
Maloney, William, Mr., NAVOCEANO, Suitland, Maryland
Morse, Betty-Ann, Miss, Dept. of Oceanography, Univ. of Wash., Seattle.
Mortimer, C. H., Prof., Great Lakes Research Institute, Univ. of Wisconsin (Milwaukee Extension), Milwaukee, Wisconsin.
O'Brien, James J., Dr., NCAR, Boulder, Colo.
Peck, R. E., Mr., 26 Broadway, New York, New York
Reid, R. D., Prof., Dept. of Oceanography and Meteor., Texas A&M, College Station, Texas
Stevenson, Merrit R., Dr., Inter-American Tropical Tuna Comm., SIO, Calif.
Stewart, R. W. Prof., Pacific Oceano. Group, Nanaimo, B. C., Canada
Waldichuck, Michael, Mr., Pacific Oceano. Group, Nanaimo, B. C., Canada

Webster, Ferris, Dr., WHOI, Woods Hole, Mass.
Woodruff, Roger, Mr., ESSA, Miami, Fla.
WDPC, UCLA, Los Angeles, Calif.
NSF
ONR
Themis-Computer Center (3 copies)

UNCLASSIFIED TECHNICAL REPORTS DISTRIBUTION LIST
FOR OCEANOGRAPHIC CONTRACTORS
OF THE OCEAN SCIENCE & TECHNOLOGY GROUP
OF THE OFFICE OF NAVAL RESEARCH
(Revised April 1967)

DEPARTMENT OF DEFENSE

Director of Defense Research and Engineering
Office of the Secretary of Defense
Washington, D. C. 20301
1 Attn: Office, Assistant Director (Research)

Navy

2 Office of Naval Research
Ocean Science & Technology Group
Department of the Navy
Washington, D. C. 20360
1 Attn: Surface & Amphibious Programs (Code 463)
1 Attn: Undersea Programs (Code 466)
1 Attn: Field Projects (Code 418)
1 Attn: Geography Branch (Code 414)

1 Commanding Officer
Office of Naval Research Branch Office
495 Summer Street
Boston, Massachusetts 02210

1 Commanding Officer
Office of Naval Research Branch Office
219 South Dearborn Street
Chicago, Illinois 60604

1 Commanding Officer
Office of Naval Research Branch Office
1030 East Green Street
Pasadena, California 91101

5 Commanding Officer
Office of Naval Research Branch Office
Navy #100, Fleet Post Office
New York, New York 09510

6 Director
Naval Research Laboratory
Washington, D. C. 20390
Attn: Code 5500

2 Commander
U. S. Naval Oceanographic Office
Washington, D. C. 20390
1 Attn: Code 1640 (Library)
1 Attn: Code 031
1 Attn: Code 70
1 Attn: Code 90

1 West Coast Support Group
U. S. Naval Oceanographic Office
c/o U. S. Navy Electronics Laboratory
San Diego, California 92152

1 U. S. Naval Oceanographic Office
Liaison Officer (Code 332)
Anti-Submarine Warfare Force
U. S. Atlantic Fleet
Norfolk, Virginia 23511

1 U. S. Naval Oceanographic Office
Liaison Officer
Anti-Submarine Warfare Force Pacific
Fleet Post Office
San Francisco, California 96610

1 Commander-in-Chief
Submarine Force Pacific Fleet
Fleet Post Office
San Francisco, California 96610

1 Commander-in-Chief
Pacific Fleet
Fleet Post Office
San Francisco, California 96610

1 Chief
Naval Ordnance Systems Command
Department of the Navy
Washington, D. C. 20360

1 Chief
Naval Air Systems Command
Department of the Navy
Washington, D. C. 20360
1 Attn: AIR 370E

1 Office of the U. S. Naval Weather Service
Washington Navy Yard
Washington, D. C. 20390

1 Chief
Naval Facilities Engineering Command
Department of the Navy
Washington, D. C. 20390
1 Attn: Code 70

U. S. Navy Electronics Laboratory
San Diego, California 92152
1 Attn: Code 3102
1 Attn: Code 3060C

1 Commanding Officer and Director
U. S. Naval Civil Engineering Laboratory
Hueneme, California 93041

1 Commanding Officer
Pacific Missile Range
Pt. Mugu, Hueneme, California 93041

1 Commander, Naval Ordnance Laboratory
White Oak
Silver Spring, Maryland 20910

1 Commanding Officer
Naval Ordnance Test Station
China Lake, California 93557

1 Commanding Officer
Naval Radiological Defense Laboratory
San Francisco, California 94135

1 Commanding Officer
U. S. Naval Underwater Ordnance Station
Newport, Rhode Island 02884

1 Chief
Naval Ship Systems Command
Department of the Navy
Washington, D. C. 20360
1 Attn: Code 1622B

1 Officer-in-Charge
U. S. Navy Weather Research Facility
Naval Air Station, Bldg. R-48
Norfolk, Virginia 23511

1 Commanding Officer
U. S. Navy Air Development Center
Warminster, Pennsylvania 18974
1 Attn: NADC Library

1 U. S. Fleet Weather Central
Joint Typhoon Warning Center
COMNAVMARIANAS Box 12
San Francisco, California 94101

1 Superintendent
U. S. Naval Academy
Annapolis, Maryland 21402

2 Department of Meteorology and Oceanography
U. S Naval Postgraduate School
Monterey, California 93940

1 Commanding Officer
U. S. Navy Mine Defense Laboratory
Panama City, Florida 32404

1 Commanding Officer
U. S. Naval Underwater Sound Laboratory
New London, Connecticut 06321

1 Officer-in-Charge
U. S. Fleet Numerical Weather Facility
U. S. Naval Postgraduate School
Monterey, California 93940

Air Force

1 Headquarters, Air Weather Service (AWSS/TIPD)
U. S. Air Force
Scott Air Force Base,
Illinois 62225

1 AFCRL (CRZF)
L. G. Hanscom Field
Bedford, Massachusetts 01730

Army

1 Coastal Engineering Research Center
Corps of Engineers
Department of the Army
Washington, D. C. 20310

1 U. S. Army Beach Erosion Board
5201 Little Falls Road, N. W.
Washington, D. C. 20016

1 Army Research Office
Office of the Chief of R&D
Department of the Army
Washington, D. C. 20310

1 Director
U. S. Army Engineers Waterways Experiment Station
Vicksburg, Mississippi 49097
1 Attn: Research Center Library

OTHER GOVERNMENT AGENCIES

20 Defense Documentation Center
Cameron Station
Alexandria, Virginia 20305

2 National Research Council
2101 Constitution Avenue, N. W.
Washington, D. C. 20418
Attn: Committee on Undersea Warfare
Attn: Committee on Oceanography

1 Laboratory Director
California Current Resources Laboratory
Bureau of Commercial Fisheries
P. O. Box 271
La Jolla, California 92038

1 Director
Coast & Geodetic Survey - U. S. ESSA
Attn: Office of Hydrography and Oceanography
Washington Science Center
Rockville, Maryland 20852

1 Director
Atlantic Marine Center
Coast & Geodetic Survey - U. S. ESSA
439 West York Street
Norfolk, Virginia 23510

1 Director
Institute for Oceanography
U. S. ESSA
Gramax Building
Silver Spring, Maryland 20910

1 U. S. ESSA
Geophysical Sciences Library (AD 712)
Washington Science Center
Rockville, Maryland 20852

1 Commanding Officer
Coast Guard Oceanographic Unit
Bldg. 159, Navy Yard Annex
Washington, D. C. 20390

1 Chief, Office of Marine Geology and Hydrology
U. S. Geological Survey
Menlo Park, California 94025

1 Director
Pacific Marine Center
Coast & Geodetic Survey - U. S. ESSA
1801 Fairview Avenue, East
Seattle, Washington 98102

1 Geological Division
Marine Geology Unit
U. S. Geological Survey
Washington, D. C. 20240

1 National Science Foundation
Office of Sea Grant Programs
1800 G Street, N. W.
Washington, D. C. 20550

1 Laboratory Director
Bureau of Commercial Fisheries
Biological Laboratory
451-B Jordan Hall
Stanford, California 94035

1 Bureau of Commercial Fisheries
U. S. Fish & Wildlife Service
P. O. Box 3830
Honolulu, Hawaii 96812

1 Laboratory Director
Biological Laboratory
Bureau of Commercial Fisheries
P. O. Box 3098, Fort Crockett
Galveston, Texas 77552

1 Laboratory Director
Biological Laboratory
Bureau of Commercial Fisheries
P. O. Box 1155
Juneau, Alaska 99801

1 Laboratory Director
Biological Laboratory
Bureau of Commercial Fisheries
P. O. Box 6
Woods Hole, Massachusetts 02543

1 Laboratory Director
Biological Laboratory
Bureau of Commercial Fisheries
P. O. Box 280
Brunswick, Georgia 31521

1 Laboratory Director
Tuna Resources Laboratory
Bureau of Commercial Fisheries
P. O. Box 271
La Jolla, California 92038

1 Bureau of Commercial Fisheries and Wildlife
U. S. Fish & Wildlife Service
Librarian
Sandy Hook Marine Laboratory
P. O. Box 428
Highlands, New Jersey 07732

1 Director
National Oceanographic Data Center
Washington, D. C. 20390

1 Laboratory Director
Biological Laboratory
Bureau of Commercial Fisheries
#75 Virginia Beach Drive
Miami, Florida 33149

1 Director, Bureau of Commercial Fisheries
U.S. Fish & Wildlife Service
Department of the Interior
Washington, D. C. 20240

1 Bureau of Commercial Fisheries
Biological Laboratory, Oceanography
2725 Montlake Boulevard, East
Seattle, Washington 98102

1 Dr. Gene A. Rusnak
U. S. Geological Survey
Marine Geology & Hydrology
345 Middlefield Road
Menlo Park, California 94025

1 Assistant Director
Oceanography Museum of Natural History
Smithsonian Institution
Washington, D. C. 20560

1 Advanced Research Projects Agency
The Pentagon
Washington, D. C. 20310
Attn: Nuclear Test Detection Office

RESEARCH LABORATORIES

2 Director
Woods Hole Oceanographic Institution
Woods Hole, Massachusetts 02543

1 Director
Narragansett Marine Laboratory
University of Rhode Island
Kingston, Rhode Island 02881

1 Gulf Coast Research Laboratory
Ocean Springs, Mississippi 39564
Attn: Librarian

1 Chairman, Department of Meteorology and Oceanography
New York University
New York, New York 10453

1 Director
Lamont Geological Observatory
Columbia University
Palisades, New York 10964

1 Director
Hudson Laboratories
145 Palisade Street
Dobbs Ferry, New York 10522

1 Great Lakes Research Division
Institute of Science & Technology
University of Michigan
Ann Arbor, Michigan 48105

1 Department of Physics
Northern Michigan University
Marquette, Michigan 49855

1 Director
Chesapeake Bay Institute
Johns Hopkins University
Baltimore, Maryland 21218

Department of Geology
Yale University
New Haven, Connecticut 06520

1 Director, Marine Laboratory
University of Miami
#1 Rickenbacker Causeway
Miami, Florida 33149

2 Head, Department of Oceanography and Meteorology
Texas A&M University
College Station, Texas 77843

1 Director
Scripps Institution of Oceanography
P. O. Box 109
La Jolla, California 92038

1 Allan Hancock Foundation
University Park
Los Angeles, California 90007

1 Chairman, Department of Oceanography
Oregon State University
Corvallis, Oregon 97331

1 Director, Arctic Research Laboratory
Pt. Barrow, Alaska 99723

1 Head, Department of Oceanography
University of Washington
Seattle, Washington 98105

1 Director Institute of Marine Science
University of Alaska
College, Alaska 99735

1 Director
Bermuda Biological Station for Research
St. Georges, Bermuda

1 Director
Hawaiian Marine Laboratory
University of Hawaii
Honolulu, Hawaii 96825

1 President
Osservatorio Geofisico Sperimentale
Trieste, Italy

1 Department of Engineering
University of California
Berkeley, California 94720

1 Applied Physics Laboratory
University of Washington
1013 N. E. Fortieth Street
Seattle, Washington 98105

1 Physical Oceanographic Laboratory
Nova University
1786 S. E. Fifteenth Avenue
Fot Lauderdale, Florida 33316

1 Director
Ocean Research Institute
University of Tokyo
Tokyo, Japan

1 Marine Biological Association of the United Kingdom
The Laboratory
Citadel Hill
Plymouth, England

Westinghouse Electric Corporation
1625 K Street, N. W.
Washington, D. C. 20006

1 Serials Department
University of Illinois Library
Urbana, Illinois 61801

1 New Zealand Oceanographic Institute
Department of Scientific and Industrial Research
P. O. Box 8009
Wellington, New Zealand
Attn: Librarian

1 Director
Instituto Nacional de Oceanographia
Rivadavia 1917-R25
Buenos Aires, Argentina

1 Lieutenant Nestor C. L. Granelli
Head, Geophysics Branch
Montevideo 459, 4° "A"
Buenos Aires, Argentina

1 Oceanographische Forschungsantalt der Bundeswehr
Lornsenstrasse 7
Kiel, Federal Republic of Germany

1 Underwater Warfare Division
of the Norwegian Defense Research Establishment
Karljohansvern, Horten, Norway

1 Department of Geodesy and Geophysics
Cambridge University
Cambridge, England

1 Institute of Oceanography
University of British Columbia
Vancouver, B.C., Canada

1 Dept. of the Geophysical Sciences
University of Chicago
Chicago, Illinois 60637

1 Coastal Engineering Laboratory
University of Florida
Gainesville, Florida 32601

1 Marine Science Center
Lehigh University
Bethlehem, Pennsylvania 18015

1 Institute of Geophysics
University of Hawaii
Honolulu, Hawaii 96825

1 Mr. J. A. Gast
Wildlife Building
Humboldt State College
Arcata, California 95521

1 Department of Geology and Geophysics
Massachusetts Institute of Technology
Cambridge, Massachusetts 02139

1 Division of Engineering and Applied Physics
Harvard University
Cambridge, Massachusetts 02138